ELECTROSPUN CELLULOSE AS A MODEL SUBSTRATE FOR ENZYMATIC HYDROLYSIS

A Thesis

Presented to the Faculty of the Graduate School

of Cornell University

in Partial Fulfillment of the Requirements for the Degree of

Masters of Science

by

Heidi Jeeho Park

January 2009

ABSTRACT

Biomass is a potential feedstock for fuels and chemicals, but is primarily composed of cellulose, which is resistant to hydrolysis. It has been hypothesized that the microstructure of cellulose plays an important role in the hydrolysis process; however, current cellulose substrates do not have easily controllable microstructure.

The microstructure of cellulose can be controlled by electrospinning nonwoven mats of pure cellulose fibers from solution. The degree of polymerization, degree of crystallinity, and diameter of the fibers can be controlled by varying the binary solvent and processing conditions for eletrospinning. Cellulose with degrees of polymerization (DP) 210, 550, and 1140 were electrospun with two different binary solvents. Fibers electrospun from solutions of cellulose in N-methlymorpholine-N-oxide (NMMO)/water at elevated temperature had mid to high crystallinities ($\sim$50 - 80%), whereas solutions of lithium chloride (LiCl)/ dimethylacetamide (DMAc) at room temperature gave less crystalline ($\sim$30%) cellulose fibers. Varying the infusion rate of the solution or the distance between the nozzle and the collector allowed for varying the fiber diameters, producing submicron- through micron-scale fibers with superficial surface areas on the order of $\sim 10\ \mathrm{m}^2/\mathrm{g}$.

Some preliminary results for hydrolysis of electrospun cellulose (ESC) fibers with cellulase enzymes are reported, and demonstrated the potential for kinetics studies with ESC to provide insight into how the microstructure affects the rates of hydrolysis. The conversion and product profiles demonstrate that ESC is hydrolyzed similarly to other insoluble cellulose substrates. However, the

results of these preliminary hydrolysis studies with monoaxial ESC revealed interesting effects on the fibers; specifically, loss of long-range fiber connectivity and residual insoluble fractions that consisted of primarily $\sim 10\ \mu\mathrm{m}$ fragments at the end of hydrolysis.

Coaxial cellulose fibers were investigated to address issues seen during monoaxial electrospinning and hydrolysis. First, fibers with a cellulose core made from low DP cellulose/LiCl/DMAc solutions were electrospun with well-spinnable solutions on the shell, as the low DP cellulose/LiCl/DMAc solutions did not electrospin monoaxially. Solutions of cellulose acetate (CA) were able to entrain the cellulose solutions in the core of the fibers; however, upon chemical removal of the CA shell the fiber morphology was largely lost. While this demonstrated that coaxial electrospinning can be utilized to form fibers from non-spinnable solutions, further work must be done to retain fiber morphology once the non-cellulose shell is removed.

Coaxial electrospinning was also used to form fibers with a cellulose shell and a non-hydrolysable core, to prevent fragmentation and loss of long-range fiber connectivity during hydrolysis. Initial studies used cellulose/LiCl/DMAc solutions as the shell and CA as the core. Though transmission electron microscopy (TEM) showed that these fibers have some coaxial nature, hydrolysis produced no soluble products. Scanning electron microscopy (SEM) of the hydrolyzed pellets showed interesting pitting and surface roughening, indicating the potential for coaxial ESC to provide insights into cellulose degradation.

Cellulose/NMMO/water solutions were also investigated as the shell in coaxial electrospinning. Due to the heating required for electrospinning the cellulose/NMMO/water solutions, polyacrylonitrile (PAN) was found to be the most suitable core material. Preliminary hydrolysis of cellulose-PAN fibers

showed reasonable degradation, and SEM analysis showed evidence of fiber stripping, peeling, and thinning. These things were not seen in previous ESC hydrolysis with monoaxially spun cellulose, and further demonstrate the potential for coaxial ESC to provide new insights into cellulose hydrolysis mechanisms. However, the conditions required for varying the important microstructural features of the cellulose shell must be investigated, and fiber uniformity still needs to be optimized for coaxial ESC. Once this is achieved, ESC and coaxial ESC may reveal novel details of the evolution of the degradation of cellulose by cellulases and the effects of microstructure on this process.

BIOGRAPHICAL SKETCH

Heidi Park was born and raised in Niles, IL. She received her undergraduate degree in Chemical Engineering from Rose-Hulman Institute of Technology in Terre Haute, IN in 2005. Heidi began graduate school at Cornell University in 2005, and received her Masters of Science degree in January, 2009.

This document is dedicated my parents, Chung Hyeong and Zoon Hoon Park.

ACKNOWLEDGEMENTS

I would like to thank my advisors, Drs. Yong Lak Joo and Alan Brad Anton in Chemical Engineering for their support and encouragement. I would also like to thank Dr. David Wilson for allowing the use of his laboratory for the hydrolysis experiments, his help in the preparation of this manuscript, and for serving as Dr. Anton's proxy for my final examination; John Dingee (Cornell University, Chemical Engineering PhD, 2009) for his extensive help in the hydrolysis experiments of this work; and undergraduate students Sean Fitzgibbon and Carly Anderson for their help with the electrospinning. This work was funded in part by an US Department of Education GAANN Fellowship, the Cornell Center for Sustainability, and the Arthur Synder Graduate Scholarship. This work also made use of the Cornell Center for Materials Research Facilities supported by the National Science Foundation under Award Number DMR-0520404.

I also thank my family and friends for all the emotional support they have given me during my time at Cornell. Special thanks to Jennifer Jasko for the proof-reading of my manuscript.

TABLE OF CONTENTS

LIST OF TABLES

LIST OF FIGURES

CHAPTER 1

INTRODUCTION

1.1 Cellulose

Plant biomass is composed primarily of cellulose (∼50% by mass), which is an abundant and renewable polymer that is getting increased attention as new sources for fuels and chemicals are sought [1, 2]. Cellulose has the potential to be a renewable feedstock for the production of these commodities, but current conversion of cellulose is slow and costly. However, a fundamental understanding of how various pretreatment processes will accelerate the hydrolysis process will be instrumental in making cellulose hydrolysis economically feasible [3].

As of 2006, all of the industrial-scale production of ethanol in the United States came from fermentable sugars derived from corn starch [4]. However, the economic and energetic benefits derived from producing ethanol from starch have been highly debated [4–7]. Starch-based ethanol has the additional complication of direct competition with food resources [6]. The absence of industrial-scale conversion of cellulose to fermentable sugars is due primarily to the fact that the enzymatic hydrolysis of cellulose is about 100 times slower than that of starch. This requires large reactors, high concentrations of expensive cellulase enzymes, and long contact times. The slow overall hydrolysis rate of cellulose is likely due to the unusual microstructure of cellulose and its effect on enzyme binding, as the turnover rates (k_{cat}, hydrolysis rate per bound enzyme) for amylases bound to starch and cellulases bound to cellulose are actually comparable [3].

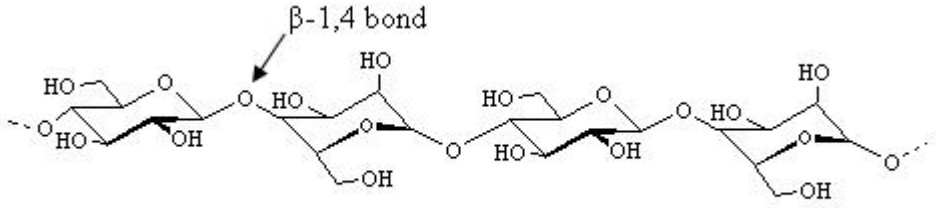

(a)

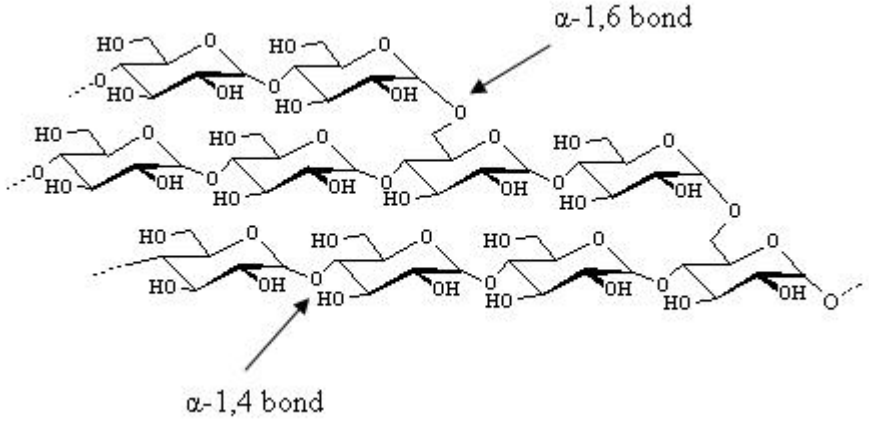

(b)

Figure 1.1: Cellulose and starch molecular structure. (a) Cellulose with β-1,4 glycosidic bonds; (b) Starch with α-1,4 and α-1,6 glycosidic bonds

Cellulose and starch are both natural polymers of anhydroglucopyranose units. Cellulose is a linear polymer of anhydroglucopyranose joined by β-1,4 glycosidic bonds with alternating glucose units rotated 180° about the plane of the glucopyranose rings, giving a repeating monomer unit of anhydrocellobiose. Adjacent chains of cellulose are joined by hydrogen bonds and van der Waals forces, resulting in straight, stable fibers of high tensile strength and crystallinity. Starch is composed of monomers connected via α-1,4 and α-1,6 glycosidic bonds and has extensive branching, preventing strong intermolecular forces and resulting in a water-soluble polymer. Figure 1.1 shows the dif-

ference in molecular structure between cellulose and starch. The more "open" microstructure of starch facilitates its easy degradation by amylase enzymes, so it has been proposed that the hydrolysis of cellulose depends critically on the substrate properties [3] but the relationship between cellulose structure and the rate of enzymatic hydrolysis is still poorly understood [3, 8–16].

1.2 Cellulase Enzymes

Cellulase enzymes are functionally categorized by how they degrade their substrates as endocellulases or exocellulases [17]. The two enzyme classes are very similar in structure aside from the shape of their active sites. Endocellulases have an active site cleft, cleave randomly in the middle of accessible cellulose chains, and rapidly decrease the chain's degree of polymerization. Because the product of endocellulase activity is broken glycosidic bonds, the observed products during insoluble cellulose hydrolysis by endocellulases are soluble cellulose oligosaccharides that are resistant to further homogenous hydrolysis, such as glucose (G1), cellobiose (G2), and cellotriose (G3). Exocellulases, also called cellobiohydrolyases (CBH), have active site tunnels and cleave cellobiose from the ends of accessible cellulose chains, gradually reducing their degree of polymerization. Exocellulases and some endocellulases are processive. They can bind to and move along cellulose chains causing sequential bond cleavage before unbinding, with the direction of movement being dependent on the cellulose polarity. Figure 1.2 shows the determined structure of the catalytic domains of an endocellulase known as E2 from *Thermobifidia fusca* [18] and an exocellulase known as CBH II from *Trichoderma reesei* [19] with the side chains of the catalytic residues shown. The open-cleft and closed-tunnel natures of the active

sites can be seen in these images, with the main difference being the presence or absence of additional loops across the active site, either closing it off or leaving it open.

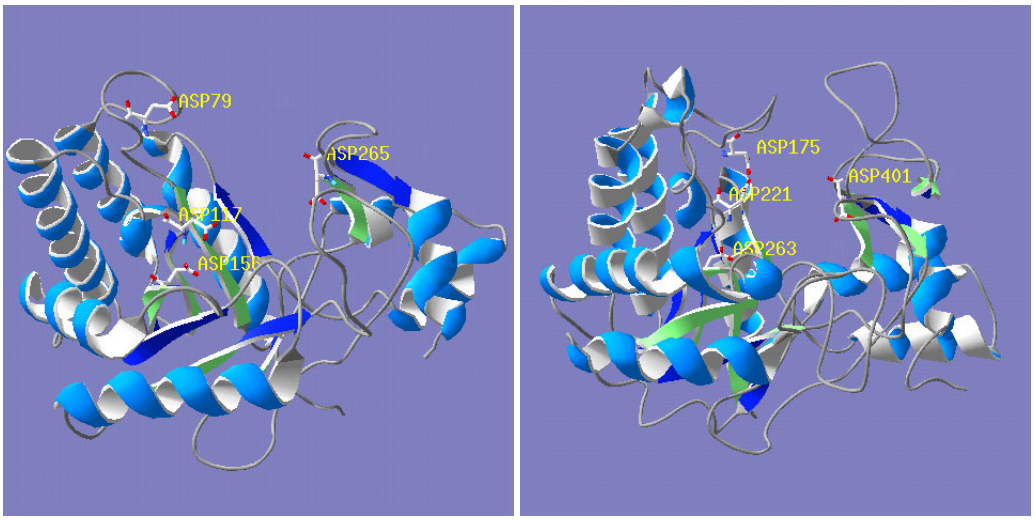

(a) (b)

Figure 1.2: Cellulose catalytic domain structure. Catalytic residues are labeled. (a) Catalytic domain of endocellulase E2 from *Thermobifidia fusca* (generated from PDB file 1TML, [18]); (b) Catalytic domain of exocellulase CBHII from *Trichoderma reesei* (generated from PDB file 1QK0, [19])

β-Glucosidase is often quoted as being part of the cellulase system but it is not a true cellulase; it is an accessory glycosyl hydrolase that assists cellulases in the complete decomposition of cellulose. β-Glucosidase cleaves the β-1,4 glycosidic bonds of soluble oligosaccharides, including the main product of cellulose hydrolysis, cellobiose, and produces glucose that can then proceed to fermentation to produce fuels and chemicals.

Although some substrates such as bacterial microcrystalline cellulose (BMCC) can be completely hydrolyzed by a single cellulase enzyme, more re-

calcitrant cellulose substrates require a set of functionally different cellulase enzymes with a range of activities for their complete conversion. A typical "cellulase system" has historically consisted of endocellulases, exocellulases, and β-glucosidase. A more specific cellulase system would include at least one non-reducing end specific exocellulase, one reducing end specific exocellulase, one processive endocellulase, and a handful of endocellulases with a range of activity on crystalline and amorphous cellulose. Natural biomass is even more complex, consisting of cellulose, hemicellulose, and lignin. These lignocellulosic materials require analogous enzyme systems in addition to the cellulase system, which target other cell wall polymers such as lignin and xylan for their complete conversion [10].

1.3 Microstructural effects on cellulose hydrolysis

Mechanistic studies of enzymatic hydrolysis have used various forms of pure cellulose, including cotton batting, filter paper, Avicel (a commercial wood pulp), and bacterial microcrystalline cellulose (BMCC). All have been defined as "model substrates". Much is known about their microstructure, and they are uniform insofar that widely available samples of each material have the same properties. Substrate characteristics that have been considered important in the enzymatic hydrolysis of cellulose include degree of crystallinity (also called crystallinity index, CrI), accessible surface area, and degree of polymerization (DP) [10]. These sources have degree of crystallinity ranging from 0 (completely amorphous) to 95% (highly crystalline), specific surface areas of 20 - $240\ \mathrm{m}^2/\mathrm{g}$, and degree of polymerization from 100 to 3000 [3]. Much of the confusion in determining which microstructural features actually influence enzymatic hy-

drolysis arises from the use of a limited set of model cellulose substrates with microstructures and physical properties that vary widely, but not systematically.

Originally, it was thought that crystallinity played a significant role in hydrolysis, with amorphous cellulose being degraded much more quickly than crystalline cellulose. Many researchers saw the degree of crystallinity increase as hydrolysis proceeded [9, 15, 16, 20, 21], supporting this theory. While it is likely that accessible amorphous cellulose is degraded before crystalline cellulose, a given insoluble cellulose sample will not have physically separated amorphous and crystalline regions. Some researchers, however, have seen the crystallinity of a substrate decrease as hydrolysis proceeds [8, 12, 14], and still others have shown that the crystallinity of different substrates remains essentially constant [8, 12, 22]. It has also been suggested that the higher reactivity of amorphous cellulose may depend on the enzyme system used [23]. It was pointed out that many of the pretreatments that decrease crystallinity also increase particle surface area and decrease DP, so it is possible that the importance of crystallinity has been overstated [8, 11].

Accessible surface area has been considered an important factor because cellulase enzymes must adsorb to the cellulose surface before hydrolysis can take place. Typical cellulase enzymes from *Trichchoderma reesei* or *Thermobifida fusca* have a catalytic core of approximately 60Å by 50Å by 40Å [24], and are considerably larger than glucose residues or glycosidic bonds and must cover many glucose residues when binding to the cellulose surface [3]. Hydrolysis rates have been shown to increase with increasing pore volume [25], because larger pore volumes allow the enzymes to diffuse into the cellulose matrix, exposing more area for hydrolysis. Thompson *et al.* [26] looked at the effects of degree

of crystallinity and lignin content along with available surface area and found surface area to be the most significant factor. However, their study looked at a much larger range of surface area than either crystallinity or lignin content. Still a third study found no effect of particle size on hydrolysis rates [27].

An important consideration when looking at accessible surface area is how the cellulose sample has been treated. There has been evidence that drying a cellulose sample reduces the pore size, and therefore reduces the accessible surface area [28–30]. This has been reported to be caused by pore collapse as the fibers dry, and it has been found that it is the larger pores that collapse first [30]. When amorphous cellulose was oven dried at high temperature, it was found to be almost as recalcitrant to hydrolysis as microcrystalline cellulose, despite the drastic difference in crystallinity. However, freeze-dried or solvent-exchanged amorphous cellulose still retained a fair amount of accessibility to the enzymes [28]. It was found that the intensity of drying correlates strongly to the percentage of large pores to small ones [29]. However, many researchers have not taken drying into consideration when discussing the effects of substrate accessibility, which may have skewed the conclusions that have been drawn.

The relative importance of the degree of polymerization has also been under much debate. Cellulose samples can range in DP from less than 100 to over 15,000 [3]. Changes in DP distribution during hydrolysis depend on the types of enzymes being used, since exoglucanases decrease DP incrementally as they act on chain ends only, while endoglucanases decrease DP rapidly [27]. Chang *et al.* [22] found that for native cellulose, DP less than 1000 was typically not hydrolyzed, but for swollen and regenerated cellulose, hydrolysis stopped at a DP of about 300. It was suggested that this is the length of a typical crystalline

region. As cellulases can hydrolyze cellulose of all degrees of polymerization, it is possible that Chang *et al.* had a particularly recalcitrant form of cellulose, or required other functionalities of cellulase to achieve complete hydrolysis. It is unclear whether the degree of polymerization itself is a limiting factor to cellulose hydrolysis, or if it is closely associated with other factors [31].

Pretreatments of cellulose substrates to vary the above characteristics have been unable to change them independently of each other, making it difficult to come to definite conclusions about how each microstructural characteristic affects hydrolysis. An ideal set of experiments would utilize a cellulose substrate that can vary microstructural characteristics such as degree of polymerization, degree of crystallinity, and accessible surface area *independently* of one another.

1.4 Electrospinning

Electrospinning is a process by which submicron scale fibers can be formed using electrostatic forces. Fibers produced by this electrostatic spinning process can be several orders of magnitude smaller than those produced by conventional fiber-spinning methods [32–34]. Although electrospinning has gained increasing attention in recent years as a method of producing uniform submicron fibers from a variety of polymeric materials, the process dates as far back as 1934 [35]. The advantages of electrospinning include a simple setup and small quantities of solution required to produce a fiber product with relatively large specific surface areas. The main drawback is a low production rate [36].

In electrospinning, the polymer solution or melt is charged by placing it in a reservoir and connecting it to a high voltage supply. As the electric force

increases, the droplet at the capillary tip is deformed and elongated, leading to the formation of a Taylor cone. When the electrical forces overcome the surface tension of the polymeric fluid, a charged jet is ejected [32]. Figure 1.3(a) shows a general setup for electrospinning. The charged jet first extends along a straight line in the stable jet region. The electrohydrodynamic instability of the jet causes a bending instability that thins the jet by a vigorous whippping motion. As the jet travels between the capillary tip and the grounded collector plate, the solvent evaporates or the solution or melt solidifies and a randomly-oriented non-woven mat of dry fibers is usually collected. This non-woven mat can have a high surface area to mass ratio ($10 \sim 1000\,\mathrm{m}^2/\mathrm{g}$). Insufficient solvent removal or jet solidification can lead to a web or film structure rather than a non-woven mat [34].

Electrospinning can also be used to create fibers with a core/shell microstructure via a process known as coaxial electrospinning [33, 37–40]. In coaxial electrospinning, two coaxially placed spinnerets are utilized to separate the core and shell polymer solutions. The two solutions are electrospun together, creating fibers with a core-shell structure in a single step. Coaxial electrospinning has been used to easily make hollow nanofibers by using mineral oil as the inner jet, followed by thermal treatment. It has also been used to form core-shell nanofibers with a core that is not spinnable on its own, and to effectively functionalize just the surface of the fiber by the coating of the shell layer. Figure 1.3(b) shows a typical syringe and needle assembly for coaxial electrospinning, which would take the place of the single syringe in Figure 1.3(a).

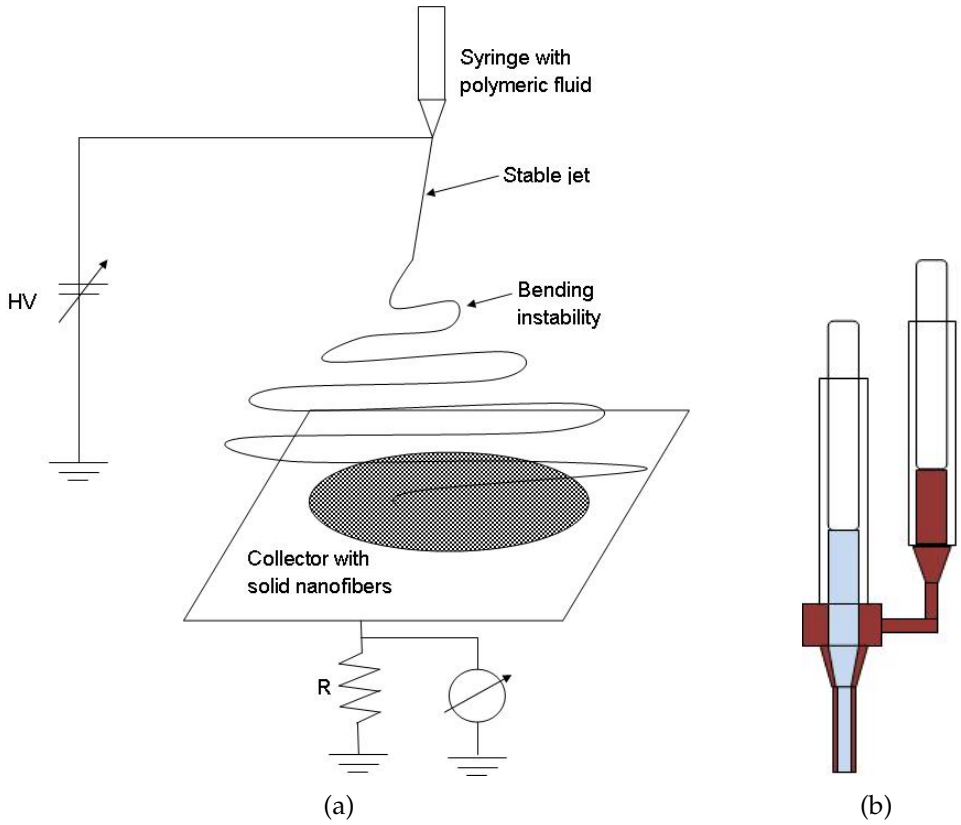

Figure 1.3: Electrospinning setups. (a) General setup for electrospinning; (b) Needle assembly for coaxial setup

1.5 Cellulose dissolution and fiber formation

Cellulose does not dissolve readily in most solvents due to such properties as complex crystalline and amorphous structure, considerable hydrogen bonding, and very high molecular weight [41]. The theoretical melting point of cellulose is higher than its thermal degradation temperature [42], so melting is not physically observed. The glass transition temperature of cellulose is in the range of 70 to $105\ ^{\circ}\mathrm{C}$ and cellulose undergoes thermal degradation from 250 to $300\ ^{\circ}\mathrm{C}$ [43].

Traditionally, cellulose fibers have been made from the viscose process. The

viscose process was developed in the late 1800s and involves derivatizing the cellulose chain. The cellulose derivative is dissolved and extruded, then regenerated back to the original cellulose. Another method of producing cellulose fibers involves cuprammonium, a mixture of copper and ammonia. The cellulose forms a complex with the cuprammonium ions, and the cellulose solution is spun into a coagulant/regenerating bath to form stable fibers. These processes are difficult, expensive, and often result in toxic byproducts and pollutants [41, 42].

Cellulose will directly dissolve in a few binary solvents. Of particular interest are lithium chloride and dimethylacetamide (LiCl/DMAc) and N-methylmorpholine-N-oxide and water (NMMO/water), as it has been demonstrated that solutions of cellulose in these solvents can be successfully electrospun [36, 44–47].

LiCl/DMAc will dissolve cellulose without reacting with or degrading it. It is believed that the mechanism of dissolution occurs through the formation of complexes between the solvent and the cellulose hydroxyl groups, and the best method of dissolving cellulose involves pretreating the cellulose with DMAc [41]. Water must be excluded from the system as both LiCl and DMAc are highly hydroscopic and the presence of water will prevent complex formation of the solvent with cellulose. Permissible water content is generally below 3 wt%, and depends on the amount of LiCl and the amount and DP of cellulose present in the mixture [48]. Methods of pretreating the cellulose vary, but in general involve polar medium swelling, activation with hot DMAc, or a combination thereof. Polar medium swelling involves soaking the cellulose in water to allow water to swell and open the cellulose structure as inter- and intra- molecular hy-

drogen bonds are replaced by hydrogen bonds with water. A solvent exchange process is then implemented, either directly exchanging the water with DMAc or going through several other polar solvent intermediates (such as acetone or methanol). The pretreated cellulose is typically dried under vacuum, and then combined with the LiCl/DMAc solvent [48–51]. In the hot DMAc activation method, DMAc is refluxed through the cellulose near its boiling point ($\sim$165 °C). The vapor pressure of DMAc near its boiling point is sufficiently high to penetrate the cellulose and swell it. The mixture is then cooled and LiCl is added while stirring [41, 49]. A disadvantage of the hot DMAc activation method is the risk of cellulose degradation if it is exposed to the high temperatures for too long. This is visually apparent by a brown discoloration of the solutions [52, 53]. The amount of LiCl required for complete dissolution depends on the concentration and degree of polymerization of the cellulose. However, the maximum solubility of LiCl in DMAc is only about 9 wt%, depending on the water content [48].

Dissolving cellulose in NMMO/water is much simpler, but requires heating to above $\sim$110 °C to obtain isotropic solutions. The dissolution mechanism is believed to involve hydrogen bonding of the N—O appendage of NMMO with the hydroxyl groups of cellulose. A high water content will prevent complete dissolution as water will compete with cellulose for the hydrogen bonds with NMMO, but the absence of water requires dissolution temperatures that are near the degradation temperature of NMMO [54]. Two methods can be used to make the solutions: the evaporation method or the direct method [55–57]. In the evaporation method, cellulose is combined with an NMMO hydrate with water molar ratio (n, moles water per moles anhydrous NMMO) $\approx$1.65 (78 wt% NMMO) to swell the cellulose. The excess water is then evaporated off, as n

must be near 1 in order for the cellulose to dissolve. In the direct method, cellulose is directly combined with NMMO of $n \approx 1$ and heated to dissolve the cellulose. N-propyl gallate is typically added as an anti-oxidant to prevent thermal degradation of the cellulose. Spinning conventional fibers from the NMMO/water system has been commercialized by Courtaulds and are known as Lyocell fibers [41].

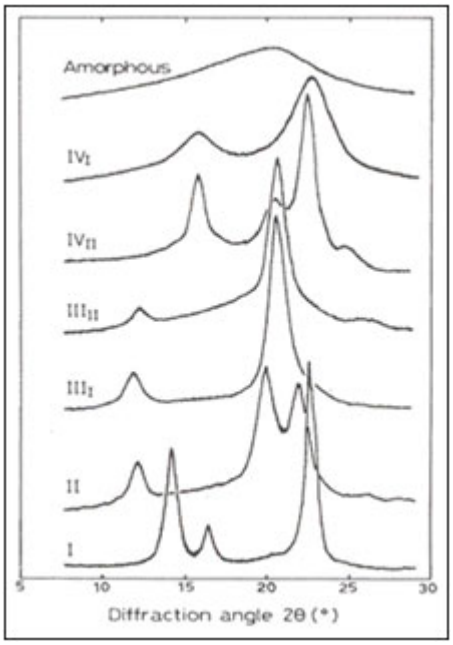

Figure 1.4: X-ray diffraction spectra of cellulose crystal polymorphs. Subscripts I and II refer to the original type of cellulose that was converted to either Type III or Type IV. Adopted from reference [41]

A consequence of regeneration of cellulose after derivitization or after direct dissolution is a change in the cellulose crystal structure. Cellulose can have several distinct crystal structures, shown in Figure 1.4. Native cellulose has a crystal structure identified as Type I, where the cellulose chains are arranged in layered sheets. The chains within each sheet are arranged parallel to one an-

other, and the glucopyranose rings are parallel to the ab plane of the crystal, seen in Figure 1.5(a). Type I cellulose can be modified to other crystal types by chemical or heat treatments. Type I can be converted to Type II by treatment with alkali solution. Type II cellulose is also found in cellulose regenerated from the viscose process or cellulose precipitated after direct dissolution and is a "swollen" form of cellulose, where the chains are now rotated 30° from parallel to the ab plane (Figure 1.5(b)) [17]. When cellulose is dissolved, a highly polar solvent is required to screen the strong hydrogen bonds that are present in native cellulose. When that polar solvent is removed, the cellulose chains rearrange to re-form the hydrogen bonds and both parallel and anti-parallel chains are present. Early researchers found that the anti-parallel configuration (Type II crystal structure) is slightly energetically favored over the parallel configuration (Type I), and thus far there has been no evidence that Type II cellulose can be reconverted to Type I [41]. There is a potential issue with utilizing Type II cellulose as a hydrolysis substrate, as the hydrolysis kinetics of regenerated cellulose may differ from the kinetics of native cellulose. Other cellulose crystal types include Type III and Type IV, which are only accessible in unusual circumstances and are not relevant to this work; Type III occurs by treating either Type I or Type II with liquid ammonia then washing with water, and Type IV occurs when the other types of cellulose are heated between $140\ ^{\circ}\mathrm{C}$ and $300\ ^{\circ}\mathrm{C}$ under pressure in glycerol or water, or in formamide [41, 42].

1.6 Research objectives

The main goal of this research is to utilize the process of electrospinning to develop a model cellulose substrate with a well defined and controllable mi-

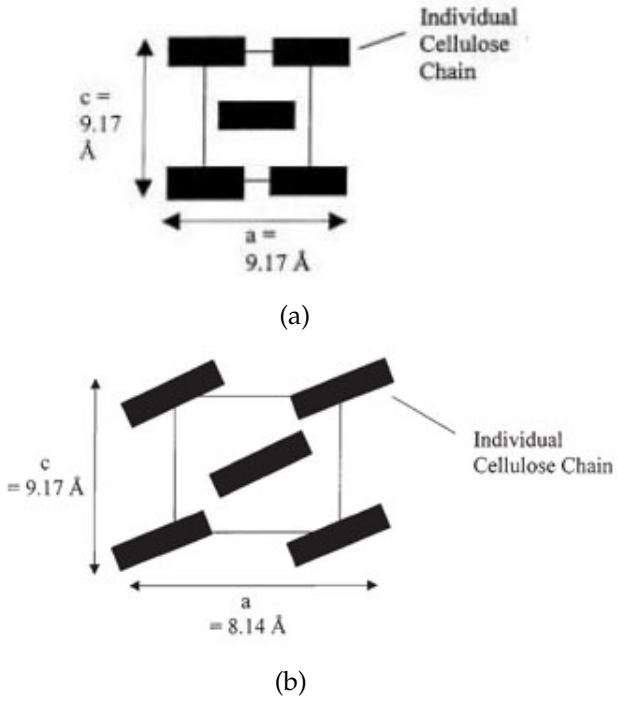

Figure 1.5: ac plane of cellulose crystals: (a)Type I; (b)Type II. Adopted from reference [17]

crostructure. Specifically, means of *independently varying* the microstructural characteristics of degree of polymerization, degree of crystallinity, and accessible surface area will be investigated. In order to achieve this, previous work on two well-studied binary solvents of cellulose (LiCl/DMAc and NMMO/ water) will be extended to determine the electrospinning parameters necessary to achieve the desired cellulose microstructure. The viability of using these carefully designed cellulose fibers in hydrolysis studies will be investigated, and results from preliminary hydrolysis studies will guide the next stages of the work associated with coaxially electrospun cellulose . In addition to elucidating how microstructure affects cellulose hydrolysis by cellulase enzymes, this work hopes to gain some insight into the mechanism of macroscopic cellulose degradation by the enzymes.

CHAPTER 2

CONTROL OF CELLULOSE MICROSTRUCTURE IN MONAXIAL FIBERS

2.1 Introduction

In this study, the processing conditions under which the cellulose microstructure can be controlled via electrospinning are presented, showing the potential to vary independently the substrate characteristics that are most suspected to affect enzymatic hydrolysis rates. Conditions required to vary the degree of polymerization, crystallinity, and diameter (and therefore surface area) of the fibers are considered. Previous work has already demonstrated the possibility of utilizing electrospinning to control the desired microstructural characteristics of cellulose [36, 44–47].

The degree of polymerization of the fibers is controlled by the cellulose substrate used to make the polymeric solutions for electrospinning, as the degree of polymerization of cellulose is not significantly affected during electrospinning [36, 45, 46].

The degree of crystallinity of the fibers can be controlled by both the solvent used for electrospinning and the processing conditions. Two binary solvents were utilized for this study, lithium chloride (LiCl)/dimethylacetamide (DMAc) and N-methylmorpholine-N-oxide (NMMO)/water. Previous work found that the LiCl/DMAc system produces fibers of low crystallinity (nearly amorphous) while the NMMO/water system produces fibers of moderate to high crystallinity ($40 \sim 60\%$), depending on such processing conditions as nozzle temperature and needle-to-collector distance [36, 45, 46]. Effects of other

processing conditions such as coagulation schemes will also be investigated in this study.

Previous work on electrospinning cellulose focused on obtaining submicron-scaled fibers [36, 44–47]. Here, it was desirable to create both submicron- and micron- scaled fibers in order to have a range of accessible surface area for the cellulase enzymes. It is generally known that the fiber diameters can be varied to a certain extent with electrospinning by changing the voltage applied at the capillary tip, which alters the electric field strength, or increasing the flowrate of the polymeric fluid, which will decrease the flight time of the polymer. Altering the needle-to-collector distance will also change the electric field strength and the flight time of the polymer, and thus also affect the fiber diameter [33].

This study builds on the previous work and attempts to pinpoint the electrospinning processing conditions required to control the degree of polymerization (DP), degree of crystallinity (CrI), and diameter of the cellulose fibers that are electrospun. Electrospinning conditions taken into consideration include solvent used, solution concentration, solution infusion rate, needle-to-collector distance, voltage applied at the needle tip, temperature and environment at the collector, and coagulation conditions. It is demonstrated that both submicron- and micron- scale electrospun fibers with a wide range of crystallinity (low, intermediate, and high crystallinity) can be obtained for three different DP cellulose sources (DP = 210, 550 and 1140). The fibers produced by electrospinning are used in preliminary hydrolysis studies to validate the use of these specially designed fibers in enzymatic hydrolysis studies.

2.2 Experimental Proceedure

2.2.1 Materials

Three cellulose sources with different degrees of polymerization were used for this study. DP 1140 (surgical cotton batting), DP 550 (BMCC), and DP 210 (Whatman fibrous cellulose, CF-11 powder) were used to provide a wide range of DP. While specific particle size was not particularly important, the substrates needed to be in powder form to facilitate complete dissolution. The DP 1140 substrate was ground in a Wiley mill to 20 mesh and the DP 550 substrate was washed, dried, and ground in a Wiley mill to 60 mesh, while the DP 210 substrate was used as is. All other chemicals used in this study were analytical grade from commercial sources. Anhydrous dimethylacetimide (Sigma-Aldrich) and high-performance liquid chromatography water (Mallinckrodt) were used without further purification. Lithium chloride was obtained from Mallinckrodt, while 97% NMMO powder, 50% aqueous NMMO solution, and n-propyl gallate were obtained from Sigma-Aldrich.

2.2.2 Solution Preparation

Solution preparation methods of Kim *et al.* [45, 46] were followed for this study. For the NMMO/water system, cellulose was placed with appropriate amounts of 97% NMMO powder in a vial and mixed vigorously before adding 50% aqueous NMMO solution slowly to achieve the desired solution composition. N-propyl gallate, an antioxidant that slows the thermal degradation of cellulose, was added at 0.5-1% mass proportion to that of cellulose. A solvent composition

of 85% NMMO and 15% water (by mass) was used here. Samples were heated at $100\,^{\circ}\mathrm{C}$ for about 1 hr until the cellulose was completely dissolved and were manually stirred every 15 - 20 min. Solution compositions used in this study were 2 wt% of DP 1140, 5 wt% of DP 550, and 9 wt% of DP 210. These compositions were used because they gave solution viscosities that were acceptable for electrospinning and allowed for the formation of a continuous jet. The rheological properties of NMMO/water/cellulose solutions are detailed by Kim *et al.* [45, 46]

For the LiCl/DMAc system, the conditioning of cellulose was critical for complete dissolution, as the presence of residual water within the cellulose sample greatly inhibits cellulose dissolution. A combination of polar medium swelling and hot DMAc activation was used to pretreat the cellulose. A solvent exchange from water to DMAc was necessary to activate the cellulose, which was required to ensure complete dissolution. The cellulose was first pretreated by soaking in water overnight at $\sim 20\,^{\circ}\mathrm{C}$, then was filtered and dried under vacuum at $\sim 60\,^{\circ}\mathrm{C}$. The dried cellulose was soaked in DMAc for 1 hr and filtered two consecutive times, and then dried again under vacuum. The cellulose was dissolved in LiCl/DMAc with constant stirring at $50 - 60\,^{\circ}\mathrm{C}$ for 2 hrs. The solutions were further mixed at room temperature for a minimum of 12 hrs to allow for complete dissolution. In this study, cellulose concentrations of 1–3 wt% of DP 1140 and 3–5 wt% of DP 550 cellulose were dissolved in 8/92% LiCl/DMAc (w/w). Again, these compositions gave solution viscosities that were suitable for electrospinning and formation of a continuous jet; the rheological properties of the LiCl/DMAc/cellulose solutions have been detailed by Kim *et al.* [45]

DP 210 cellulose was also dissolved in LiCl/DMAc, at concentrations of 4–6

wt%, but these solutions formed droplets when electrospun and did not form continuous jets. The lower molecular weight of this cellulose sample may require higher concentrations for electrospinning to increase the polymer chain entanglements that will prevent the breakup of the jet [33]. It has been difficult to completely dissolve cellulose in concentrations higher than 6 wt%, and further work is necessary to determine whether the LiCl/DMAc binary solvent is suitable for dissolving higher concentrations of low-DP cellulose. It is expected that a higher cellulose concentration will allow for electrospinning of the DP 210 substrate.

2.2.3 Electrospinning Setup

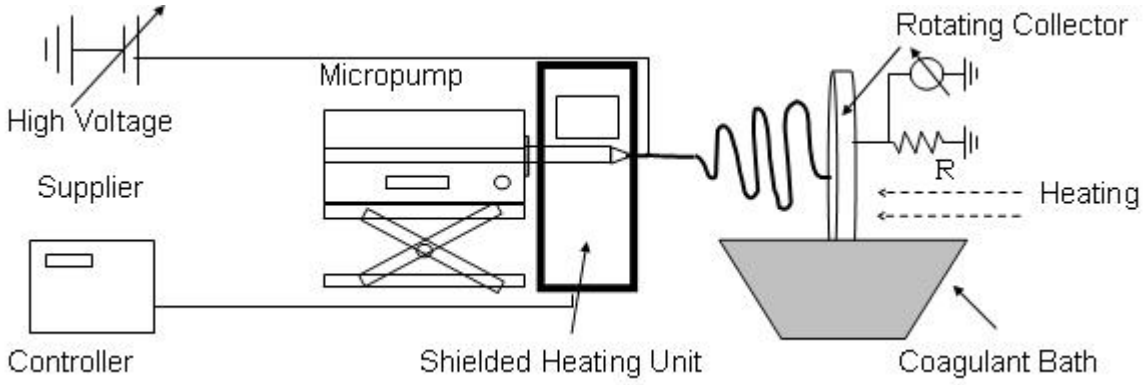

Figure 2.1: Electrospinning setup used for microstructure Study. With syringe heater, rotating collector, and coagulation bath

Figure 2.1 shows the electrospinning setup used for these experiments. Solutions were electrospun as prepared without additional filtration. The syringe chamber was fabricated from ceramic insulating material and had a heating coil inside. Table 2.1 summarizes the different processing conditions between the

Table 2.1: Electrospinning conditions of the two binary solvents

Binary Solvent	**Solution Temperature**	**Collector Temperature**	**Coagulation Temperature**
NMMO/water	$100\,^{\circ}\mathrm{C}$	RT	$\sim 10\,^{\circ}\mathrm{C}$
LiCl/DMAc	RT	$\sim$90-$110\,^{\circ}\mathrm{C}$	RT
	Electric Field	**Typical Infusion rates**	
NMMO/water	15–17 kV/15 cm	$< 0.01\ \mathrm{ml/min}$	
LiCl/DMAc	22–25 kV/12 cm	$< 0.05\ \mathrm{ml/min}$	

two binary solvents. For the NMMO/water system, the syringe chamber was kept at $100\,^{\circ}\mathrm{C}$, and the needle was heated to $50 - 70\,^{\circ}\mathrm{C}$. Needle temperatures were controlled with a heat gun fitted with a glass nozzle. The LiCl/DMAc system was electrospun at room temperature. A flat aluminum plate or mesh was used as the rotating collector and placed 10–20 cm from the needle tip to collect the fibers under varying conditions. The electric field was varied from about $1 - 2\,\mathrm{kV/cm}$ by changing either the voltage applied at the needle tip or the distance from the collector. Infusion rates were typically under $0.05\ \mathrm{ml/min}$, corresponding to cellulose production rates on the order of $0.05\ \mathrm{g/h}$ or less. The NMMO/water system utilized a cold water bath at the collector ($\sim 9 - 10\,^{\circ}\mathrm{C}$) for faster solidification of the fibers and solvent removal, while for the LiCl/ DMAc system the collector was heated to remove the solvent. The coagulation of the LiCl/DMAc system was done at room temperature as a post-spinning treatment rather than *in situ*. All samples were typically coagulated in water overnight before being dried.

2.2.4 Structural Characterization of Electrospun Cellulose

The degree of polymerization of all three samples was measured with a Cannon capillary viscometer (size 150, No. C573) according to ASTM D4243 [58]. The morphology of the fibers was observed with a scanning electron microscope (LEICA 440 SEM). Wide angle X-ray scattering (WAXS, Scintag, Inc. Theta-Theta Diffractometer) was used to determine the crystal structure and degree of crystallinity of the samples. The degree of crystallinity was obtained by taking the area ratio of the crystalline phase to the sum of the crystalline plus amorphous phases, which was obtained after deconvolution of each peak in the WAXS patterns [46].

2.3 Results and Discussion

2.3.1 Degree of Polymerization

The degree of polymerization of the electrospun cellulose (ESC) fibers can be varied by using starting materials of different DP. Previous work had shown that both the DP 210 and DP 1140 substrates could be successfully electrospun with the NMMO/water system [46], and that the DP 1140 substrate could also be electrospun with the LiCl/DMAc system [45]. The DP 550 substrate (*i.e.* BMCC) had not been used as the cellulose substrate in previous electrospinning studies.

Figure 2.2 shows the electrospun fibers from the NMMO/water system, as well as the morphology of BMCC before electrospinning. Cellulose concentra-

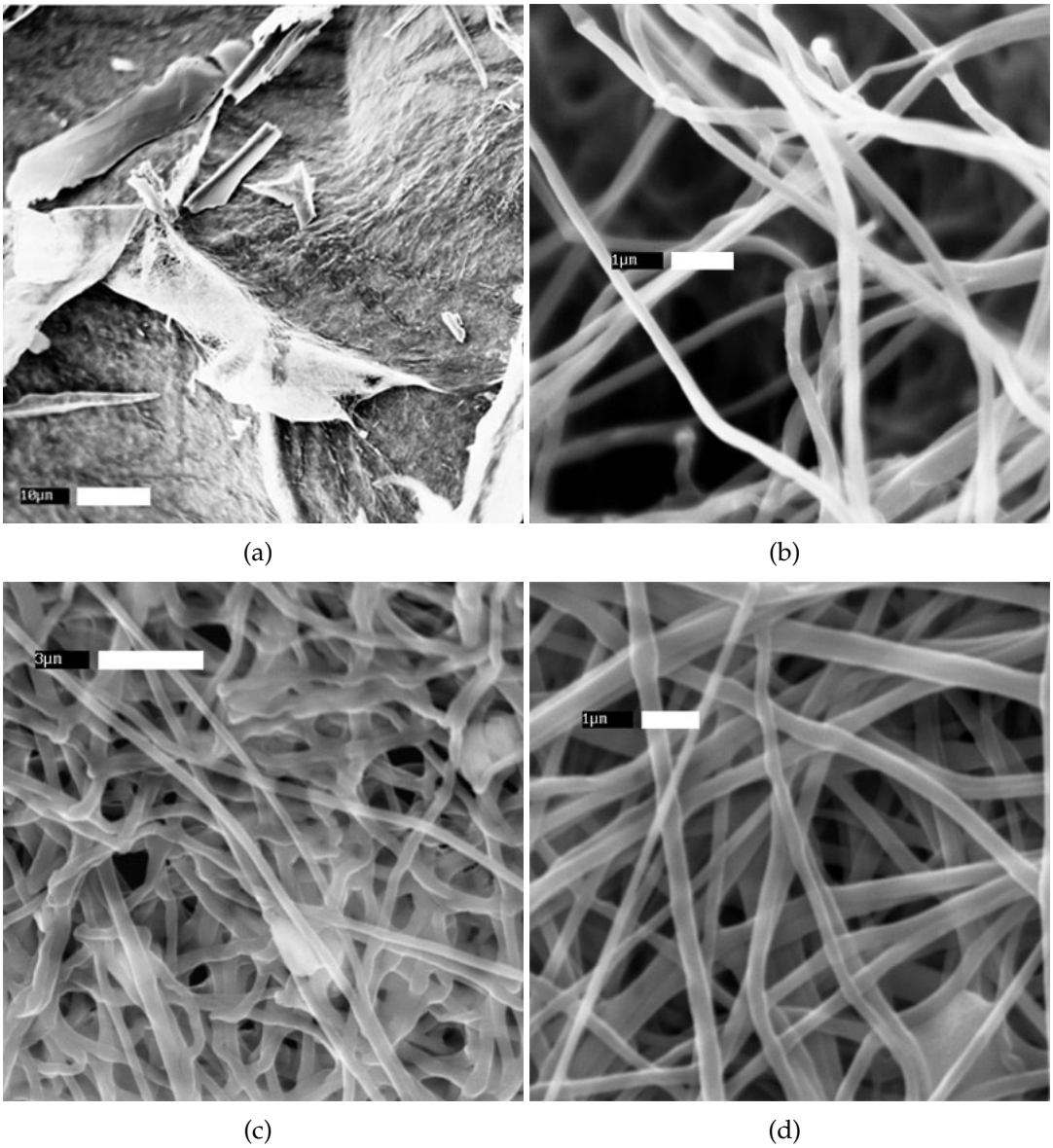

(a) (b)

(c) (d)

Figure 2.2: SEM images of: (a) as recieved BMCC (DP 550) before electrospinning (scale bar = $10\ \mu m$); electrospun fibers from (b) 2 wt% DP 1140 in NMMO/water (scale bar = $1\ \mu m$); (c) 5 wt% DP 550 in NMMO/water (scale bar = $3\ \mu m$); (d) 9 wt% DP 210 in NMMO/water (scale bar = $1\ \mu m$).

tions were 9 wt% for DP 210, 5 wt% for DP 550, and 2 wt% for DP 1140. The weight fraction that was necessary to make a solution suitable for electrospinning decreased as degree of polymerization increased. Higher DP substrates required lower cellulose concentrations to have viscosities suitable for electrospinning [33], but the fiber diameters were on the same order of magnitude, $0.3\pm\ 0.1\ \mu\mathrm{m}$ (DP 210, DP 1140) or $0.4\pm\ 0.1\ \mu\mathrm{m}$ (DP 550). These fibers were generally very uniform, but the electrospinning process also tends to create nonuniformities such as "plates", films, and merged fibers that are not seen in the particular SEM images shown in Figure 2.2.

Electrospun cellulose fibers of DP 1140 and DP 550 were also produced from the LiCl/DMAc binary solvent, using 1–3 wt% and 3–5 wt% cellulose, respectively. Figure 2.3 shows the morphology of the fibers spun from LiCl/DMAc solutions of DP 1140 and DP 550 cellulose. These fibers are less uniform than the fibers formed by the NMMO/water system, with fiber diameters of $0.6\pm$ $0.5\ \mu\mathrm{m}$. The ions present in the LiCl/DMAc solution result in a less stable jet during electrospinning, similar to the results found by Frenot *et al.* [44], forming thick fibers that must be removed from the collector during spinning. It should be noted that the coagulation of the LiCl/DMAc system was done as a post-spinning treatment rather than *in situ*, which resulted in an increase in the degree of crystallinity of electrospun fibers. As discussed in an earlier work on electrospun fibers from LiCl/DMAc [45], nonuniform fiber morphology may be attributable to delayed coagulation, while *in situ* coagulation gives rise to amorphous cellulose fibers. The following section will show that delayed coagulation offers a means to obtain cellulose fibers with low degree of crystallinity from the LiCl/DMAc solvent.

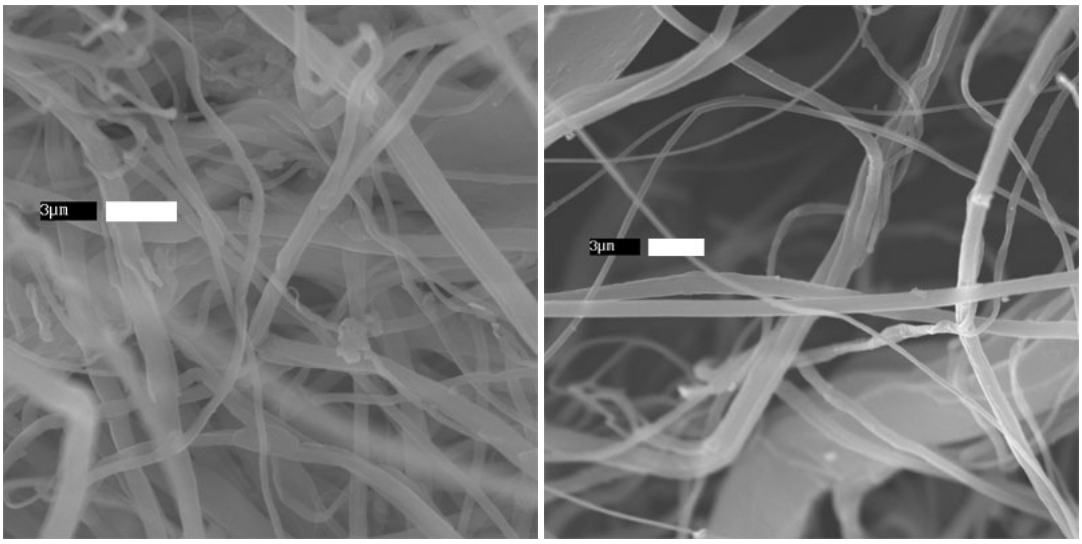

(a) (b)

Figure 2.3: SEM images of electrospun fibers from LiCl/DMAc: (a) 3 wt% DP 1140 cellulose and (b) 4 wt% DP 550 cellulose. Scale bars are $3\ \mu\mathrm{m}$.

2.3.2 Crystallinity

Cellulose Fibers from NMMO/water

Table 2.2 shows the degree of crystallinity (crystallinity index- CrI) of the various DP samples shown in Figure 2.2 along with the conditions under which they were electrospun. These samples were more crystalline than those previously obtained. The infusion rates used here were very low, $0.005 - 0.001\ \mathrm{ml/min}$. Lower infusion rates give the fibers more time to crystallize, as the time it takes for the polymer jet to reach the collector increases due to the lower velocity of the fiber[34]. This results in higher crystallinities (70 - 80%). These higher crystallinities are similar to the crystallinity of native cellulose, although the cellulose polymorph is different.

Table 2.2: Degree of Crystallinity for NMMO/water/cellulose solutions of varying DP

Cellulose Source (DP)	**CrI**	**Electrospinning Conditions**	**Fiber Diameter (μm)**	**Figure 2.2**
Surgical Cotton Batting (1140) 2 wt%	81%	$100\,^{\circ}$C Chamber $55\,^{\circ}$C Needle 17 kV 15 cm collector distance ~ 0.005ml/min infusion rate $\sim$10 $^{\circ}$C water bath	0.3 ± 0.1	(b)
BMCC (550) 5 wt%	69%	$100\,^{\circ}$C Chamber $88\,^{\circ}$C Needle 17 kV 15 cm collector distance ~ 0.005ml/min infusion rate $\sim$10 $^{\circ}$C water bath	0.4 ± 0.1	(c)
Whatman CF-11 powder (210) 9 wt%	78%	$100\,^{\circ}$C Chamber $78\,^{\circ}$C Needle 17 kV 20 cm collector distance ~ 0.005ml/min infusion rate $\sim$10 $^{\circ}$C water bath	0.3 ± 0.1	(d)

The NMMO/water binary solvent produced Type II crystal structure in the fibers, as shown by the X-ray diffraction patterns in Figure 2.4. The degree of crystallinity of the cellulose fibers can be controlled by various process conditions; for example, varying the coagulation scheme resulted in a range of crystallinities for the DP 210 cellulose. Table 2.3(a) - (d) summarizes the results of various coagulation schemes on the crystallinity; Figure 2.6(a) - (d) shows the fiber morphologies. Spinning conditions in all cases were as follows unless otherwise indicated: $100\,^{\circ}$C chamber temperature, $65 - 70\,^{\circ}$C needle temperature, 17 kV applied voltage, 15 cm collector distance, ~ 0.005 ml/min infusion rate, and $\sim 10\,^{\circ}$C water bath. The needle temperature was difficult to control precisely, as it was done with a heating gun fitted with a nozzle that was pointed at

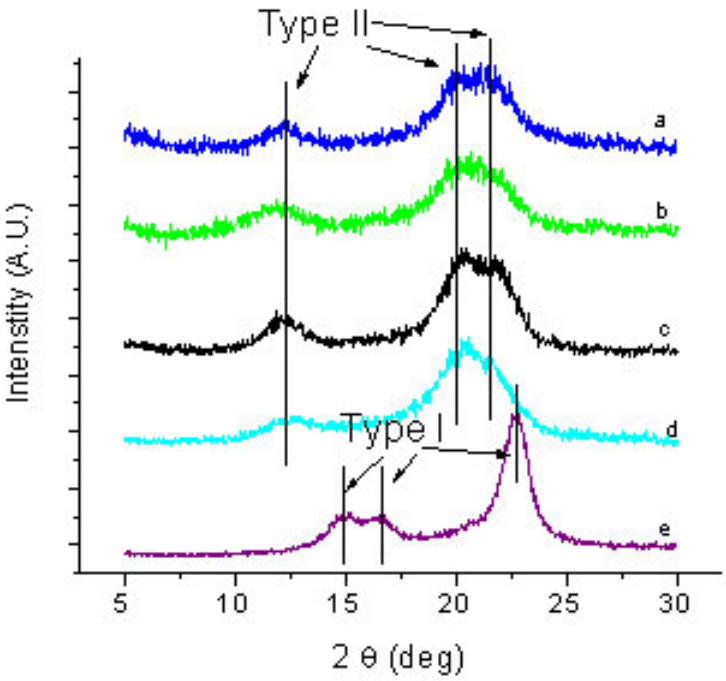

Figure 2.4: X-ray diffraction patterns for cellulose electrospun from NMMO/water solutions. (a) 2 wt% DP 1140, (b) 5 wt% DP 550, (c) 9 wt% DP 210, (d) regenerated cellulose from 9 wt% DP 210 in NMMO/water, (e) raw cellulose (DP 1140)

the needle tip and measured with a temperature probe before and after electrospinning. Due to the high voltages, continuous monitoring of the temperature at the needle tip was not possible. The spinning environment was under ambient conditions, so fluctuations in the ambient temperature and humidity may have affected the fiber morphology in unknown ways. These spinning issues were present during all experiments conducted for this study.

Different coagulation schemes were investigated: heated collector without *in situ* coagulation, hot water coagulation, heated collector with cold water coagulation, and methanol coagulation. Removal of the solvent via *in situ* coag-

Table 2.3: Effect of various coagulation schemes on crystallinity

	Solution Composition	**Coagulation Scheme**	**$T_{collector}$ ($^\circ$C)**	**T_{needle} ($^\circ$C)**	**CrI**	**Fiber Diameter (μm)**
(a)	210 DP cellulose, 9 wt% in NMMO/water	Heated collector, no water bath, coagulated after spinning	80	70	57%	n/a
(b)	210 DP cellulose, 9 wt% in NMMO/water	Hot water collector	80	70	80%	0.2 ± 0.1
(c)	210 DP cellulose, 9 wt% in NMMO/water	Cold water bath, heated collector	80	65	65%	0.6 ± 0.3
(d)	210 DP cellulose, 9 wt% in NMMO/water	Methanol bath at collector	Room Temp	65	61%	0.5 ± 0.2
(e)	550 DP cellulose, 5 wt% in NMMO/water	Hot water collector	80	70	85%	0.8 ± 0.4
(f)	1140 DP cellulose, 2 wt% in NMMO/water	Hot water collector	80	70	80%	0.6 ± 0.2

ulation is very important in maintaining the fiber morphology. Without *in situ* solvent removal the fibers melt together again to form a film (Table 2.3 and Figure 2.5 (a)). NMMO cannot be readily removed by evaporation because it has very low vapor pressure, which makes *in situ* coagulation necessary. Hot water coagulation (T_{water} = $T_{collector}$ = $80\,^\circ$C) produces highly crystalline fibers (80%, Table 2.3 and Figure 2.5 (b)); hot water near the glass transition temperature of cellulose ($T_g \approx 100\,^\circ$C) allows the cellulose to recrystallize even after solvent removal. Heating the collector with cold water coagulation produces a mixture of fibers and film of moderate crystallinity (65%, Table 2.3 and Figure 2.5 (c)). A heating gun was applied to the area of the collector that was not submerged in water as it rotated through the ice-water coagulation bath ($T_{collector}$

= 80 °C, $T_{water} \approx 10$ °C). Heating the collector prevents crystallization of the NMMO/water/cellulose solution as the fibers arrive at the collector and cold water coagulation quenches the fibers, preserving the lower crystallinity. However, some of the fibers melt together before solvent removal can take place due to the elevated temperature at the collector. The use of methanol as a coagulant also results in moderately crystalline fibers (61%, Table 2.3 and Figure 2.5 (d)) but preserves the fiber morphology. Chanzy *et al.* [54] reported that in cooled solutions of NMMO/water/cellulose, amorphous cellulose is present within a crystalline matrix of NMMO/water. Removal of the crystalline NMMO/water by dissolution in anhydrous methanol or by sublimation preserved the amorphous nature of the cellulose, but the recovered cellulose sample could be converted to Type II crystal structure by soaking in water. Biganska *et al.* [59] also found that cellulose remains in the amorphous state in NMMO/water/cellulose crystals. Solvent removal with water washing produced Type II cellulose crystal structure, while removal of the solvent by sublimation produced amorphous cellulose, so it is the presence of water that causes crystallization of cellulose. Use of methanol at the coagulation bath allowed for easy removal of NMMO, and the reduced presence of water allowed for the formation of less crystalline cellulose. The lower needle temperature (65 °C compared to 70 °C) could also have contributed to the lower crystallinity, as previous work has shown that lower needle temperatures result lead to slightly lower crystallinities [46].

Figure 2.5: SEM images of fibers from various coagulation schemes. From 9 wt% DP 210 cellulose/NMMO/water- (a) without water coagulation (scale bar $1\,\mu\mathrm{m}$); (b) hot water coagulation (scale bar $1\,\mu\mathrm{m}$); (c) cold water coagulation (scale bar $10\,\mu\mathrm{m}$); (d) methanol coagulation (scale bar $10\,\mu\mathrm{m}$); (e) Fibers from 2 wt% DP 1140 cellulose/NMMO/water, hot water coagulation (scale bar $3\,\mu\mathrm{m}$); (f) fibers from 5 wt% DP 550 cellulose/NMMO/water, hot water coagulation (scale bar $3\,\mu\mathrm{m}$). Collector and needle temperature and corresponding degree of crystallinity are in Table 2.3

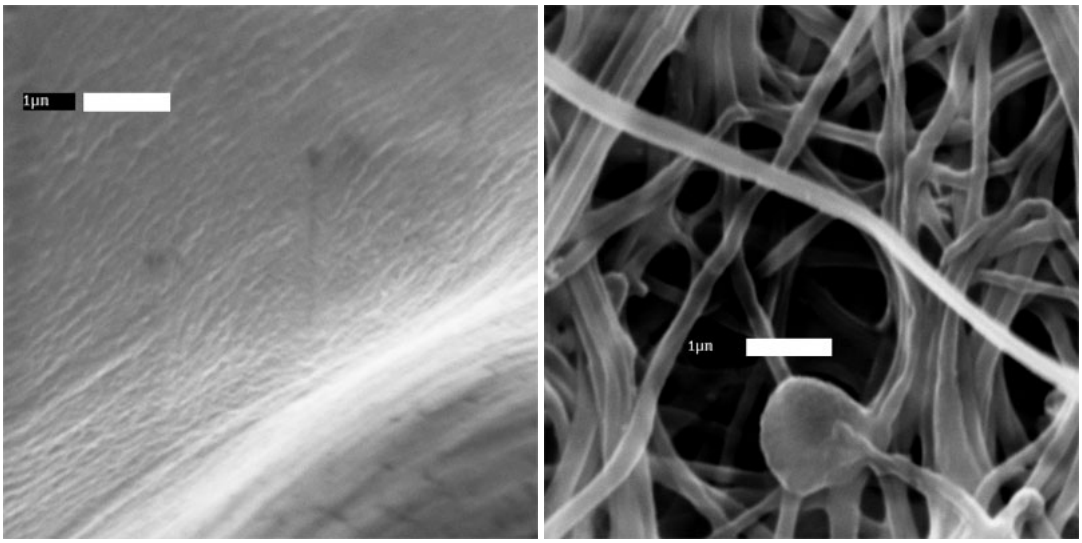

(a) (b)

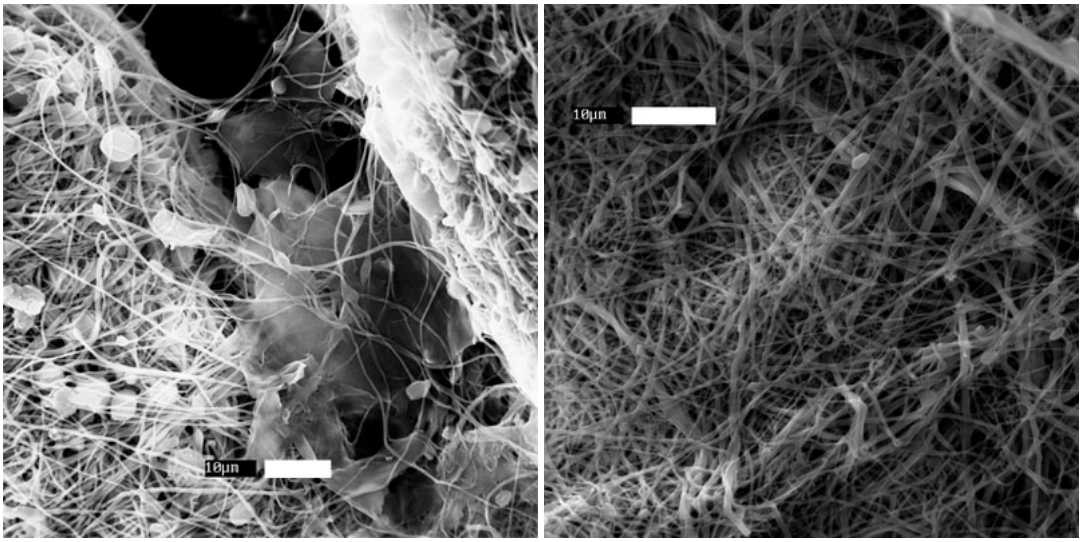

(c) (d)

Figure 2.5: (continued)

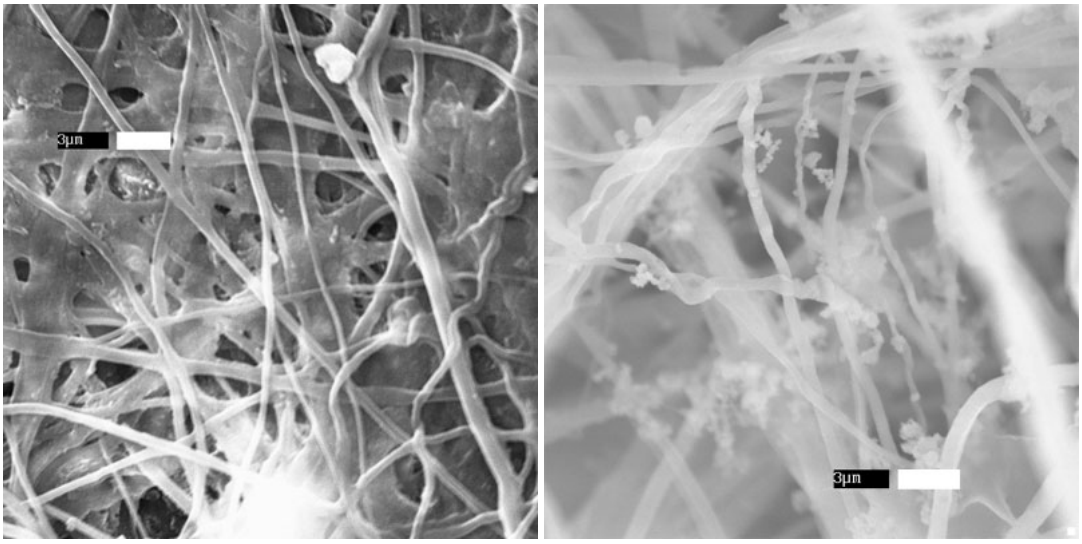

(e) (f)

The effect of the hot water bath on the higher DP substrates is similar. A hot water bath at the collector for both DP 550 and DP 1140 cellulose results in highly crystalline fibers, $\geq 80\%$ (see Table 2.3 and Figure 2.5; (e) - (f)). The fiber morphology is not as uniform as in the case of the DP 210 substrate, which may be caused by the rotation speed of the collector. Although the rotation speeds for the higher-DP substrates were similar to that of the DP 210 substrate (around 1.2 rpm), lower cellulose concentrations may require lower rotation speeds for sufficient solvent removal. This is due to the corresponding higher solvent concentration, which requires longer coagulation time for removal. The effect of other coagulation schemes on the higher-DP substrates is expected to be similar to their effect on the low DP substrate, but other processing conditions may also need to be altered to preserve fiber morphology.

Cellulose Fibers from LiCl/DMAc

The LiCl/DMAc binary solvent produces fibers that are less crystalline. This is because the majority of DMAc is removed by evaporation at the heated collector rather than by coagulation, and DMAc is the primary component of the solvent (92 wt%). The timescale of solvent removal is much shorter than that of crystallization, so the cellulose fiber is still mostly amorphous when the DMAc is removed. This differs from the NMMO/water case, where the solvent is mostly removed by coagulation in water, giving the cellulose time to crystallize. In addition, heating the collector to effectively evaporate DMAc can erase any crystal structure developed during spinning, and subsequent coagulation with water causes quenching which does not favor the re-crystallization of cellulose. Figure 2.6 shows the X-ray diffraction patterns for the various DP cellu-

lose substrates spun in LiCl/DMAc (fibers shown in Figure 2.3, diameters were 0.6 ± 0.5 μm for both substrates), which shows the Type-II polymorph with low crystallinity. The crystallinities of the fibers were 33% and 36% for DP 550 and 1140, respectively. Previous work had obtained almost completely amorphous fibers from the LiCl/DMAc system but utilized *in situ* coagulation of the cellulose fibers at the collector [45]. Here a post-electrospinning coagulation treatment was used, which indicates that changes in the coagulation scheme of the fibers can allow for a range of crystallinities at the lower end of the crystallinity scale with either the LiCl/DMAc or NMMO/water solvent.

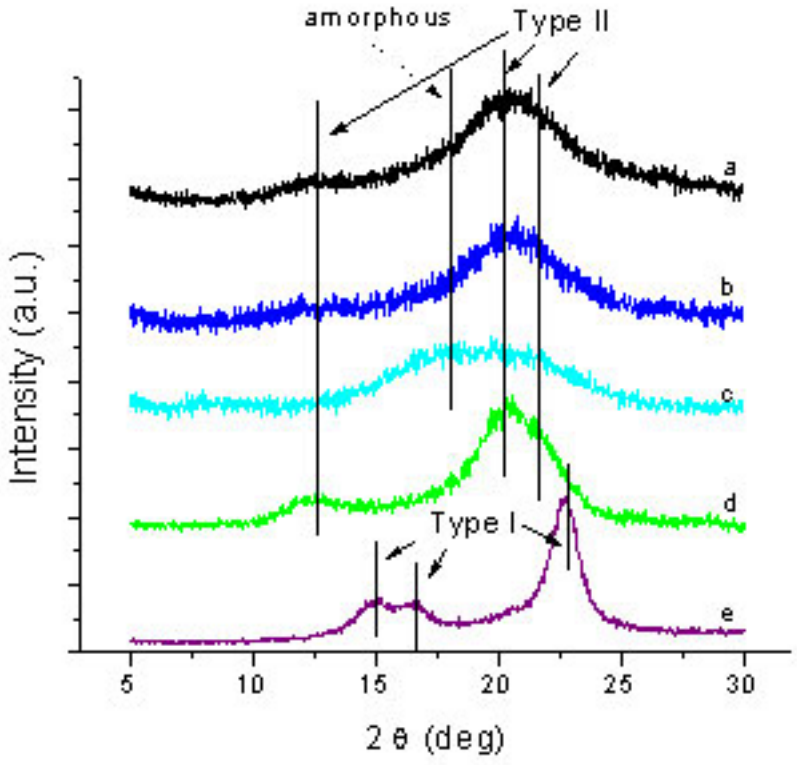

Figure 2.6: X-ray diffraction patterns for cellulose electrospun from LiCl/DMAc solutions. (a) 4 wt% DP 550, (b) 3 wt% DP 1140, (c) amorphous cellulose, (d) regenerated cellulose from 9 wt% DP 210 in NMMO/water, (e) raw cellulose (DP 1140).

2.3.3 Fiber Diameters

Fiber surface area can be altered by changing fiber diameters, which can be controlled by varying the infusion rate and/or collector distance. Infusion rates less than $0.01\ \mathrm{ml/min}$ produce fibers with submicron diameters (see Figure 2.2 and Table 2.2), but an infusion rate of about $0.03\ \mathrm{ml/min}$ can produce fiber diameters on the micron scale ($2.5 \pm 0.8\ \mu\mathrm{m}$, Figure 2.7(a)). Decreasing the collector distance also produces slightly thicker fibers; for example, changing the collector distance from 15 cm to 10 cm increases fiber diameters to $0.4 \pm 0.2\ \mu\mathrm{m}$ (Figure 2.7(b)). The fibers in Figure 2.7(a) and 2.7(b) were from DP 210 cellulose in NMMO/water solutions, and a similar increase in infusion rate of DP 1140 cellulose also results in larger diameter fibers of $0.9 \pm 0.3\ \mu\mathrm{m}$ (Figure 2.7(c)). It is expected that increasing the infusion rate for the DP 550 substrate will also result in larger diameter fibers.

Either increasing the infusion rate or decreasing the collector distance decreases the time that the jet takes to reach the collector, giving the fiber less time to crystallize and lowering the crystallinity [34, 60]. Table 2.4 shows the effects of these process conditions on the fiber diameters and crystallinity. The degree of crystallinity and the fiber diameter have potential to be decoupled by taking advantage of the effects of varying the coagulation scheme of the NMMO/water system or by utilizing the LiCl/DMAc system, which produces more amorphous fibers.

Although the mass percent of cellulose ranges from 2 wt% to 9 wt%, the fiber diameter appears to depend more on the infusion rate and collector distance than the percent solids in solution. This is most likely because the difference in DP of the cellulose substrates required different concentrations in order to be

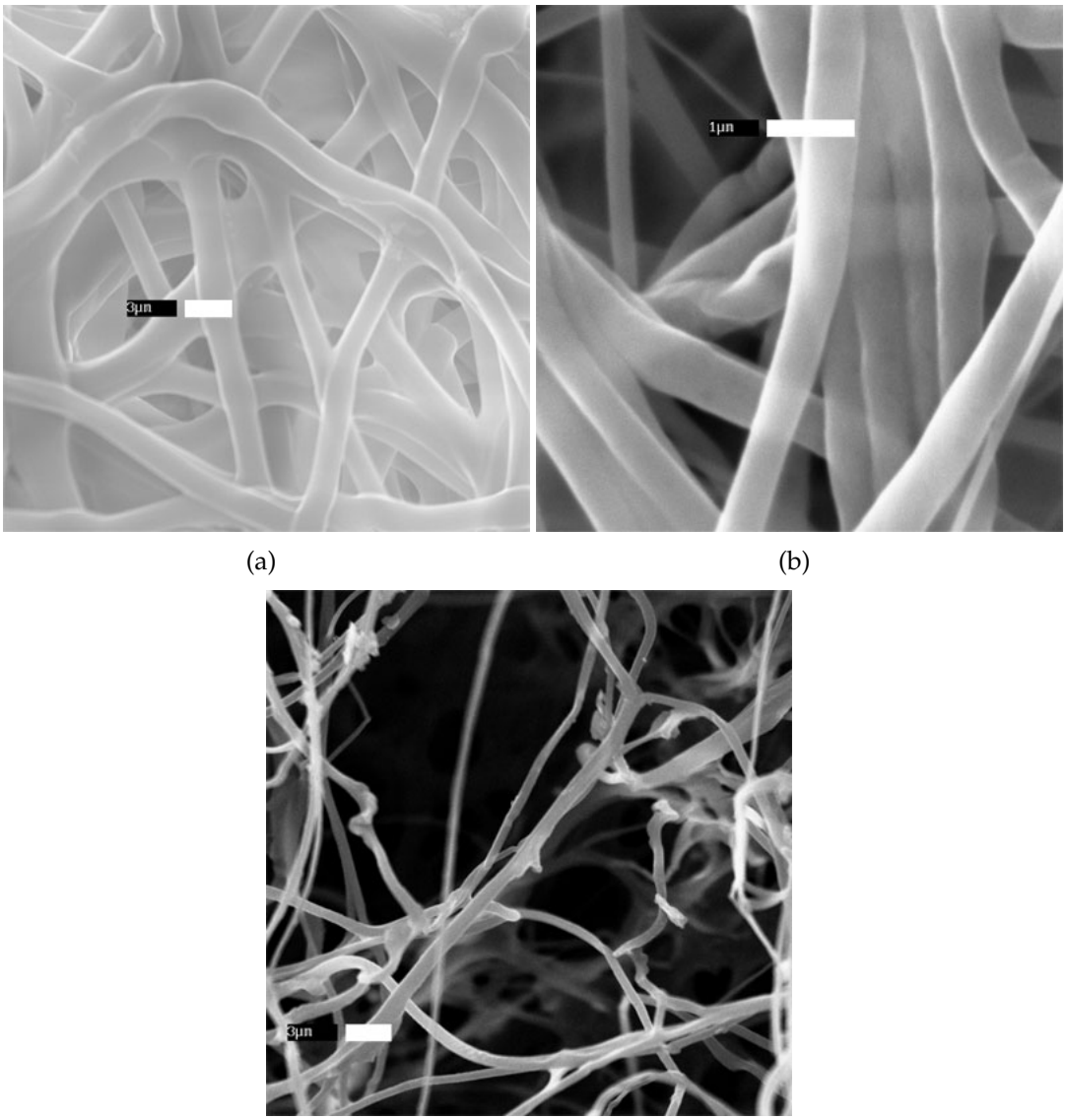

(a) (b)

(c)

Figure 2.7: SEM images of larger diameter fibers from NMMO/water/cellulose solutions. From 9 wt% DP 210 cellulose: (a) infusion rate of $0.03\ \mathrm{ml/min}$, fiber diameters of $2.5 \pm 0.8\ \mu\mathrm{m}$ (scale bar is $3\ \mu\mathrm{m}$); (b) collector distance of 10 cm, fiber diameters of $0.4 \pm 0.2\ \mu\mathrm{m}$ (scale bar is $1\ \mu\mathrm{m}$); (c) From 2 wt% DP 1140 NMMO/water/cellulose solution: infusion rate of $0.02\ \mathrm{ml/min}$, fiber diameters of $0.9 \pm 0.3\ \mu\mathrm{m}$ (scale bar is $3\ \mu\mathrm{m}$)

Table 2.4: Comparison of effect of infusion rates on fiber diameters and crystallinity (all utilizing cold water coagulation with room temperature collector)

Solution Composition	**Infusion rate** $\mathrm{ml/min}$	**Fiber Diameter (μm)**	**Collector Distance (cm)**	**CrI**	**Figure**
DP 1140, 2 wt% in NMMO/water	~ 0.005	0.3 ± 0.1	15	81%	2.2(b)
DP 550, 5 wt% in NMMO/water	~ 0.005	0.4 ± 0.1	15	69%	2.2(c)
DP 210, 9 wt% in NMMO/water	~ 0.005	0.3 ± 0.1	15	78%	2.2(d)
DP 210, 9 wt% in NMMO/water	~ 0.03	2.5 ± 0.8	15	56%	2.7(a)
DP 210, 9 wt% in NMMO/water	~ 0.005	0.4 ± 0.2	10	69%	2.7(b)
DP 1140, 2 wt% in NMMO/water	~ 0.02	0.9 ± 0.3	15	55%	2.7(c)

able to electrospin the solutions. The viscosity of the solution very important in determining the fiber diameter, as higher viscosities result in thicker fibers [33], and all three substrates had qualitatively similar viscosities at the concentrations used, resulting in similar fiber diameters.

2.4 Preliminary Hydrolysis of Electrospun Cellulose

Although electrospun cellulose (ESC) is an attractive model substrate for enzymatic hydrolysis due to its purity and carefully controllable microstructure, it is not a naturally occurring form of cellulose and differs from natural cellulose in some ways that may affect hydrolysis quite significantly. Most obviously, the crystal structure of ESC is Type II, while native cellulose is Type I. ESC may have an unusual reactivity with cellulase enzymes due to unknown effects of

the production processes of dissolution, electrospinning, and regeneration. In order to verify that ESC can be a valid model substrate for cellulose hydrolysis, preliminary hydrolysis studies of ESC with a cellulase enzyme have been conducted. The majority of this work was performed by John W. Dingee (Cornell University, Chemical Engineering PhD 2009) in the lab of Dr. David Wilson, and the details of it are laid out in Appendix A; only the relevant details and results are discussed here.

In order for ESC to be a suitable model substrate for enzymatic hydrolysis, the enzymes must be able to both bind to it and hydrolyze it similarly to other insoluble substrates. Therefore, both binding assays and hydrolysis assays were conducted on ESC using a single cellulase, Cel5A, an endocellulase from *Thermobifidia fusca*. Only a single cellulase was used in order to create the most basic model for cellulose hydrolysis; further layers of complexity can be added at later stages. The ESC used for these first studies were produced from DP 210 cellulose, and had an average fiber diameter of about $0.5\ \mu\mathrm{m}$ and average crystallinity of about 50%.

Binding of Cel5A to ESC was compared to BMCC, a standard model substrate. Binding isotherms measured at $5\ ^{\circ}\mathrm{C}$ represent the maximum binding capacity of the substrate, and can be seen in Figure A.1. The general shape of the binding isotherms was similar, but the maximum binding of Cel5A to ESC was much lower than that of BMCC, $0.3\ \mu\mathrm{mol/g}$ compared to $12\ \mu\mathrm{mol/g}$. However, ESC has a much lower surface area than BMCC ($\sim 5.5\ \mathrm{m^2/g}$ calculated for ESC, $\sim 200\ \mathrm{m^2/g}$ for BMCC [3]), and the maximum binding capacities are roughly proportional to the surface area of each substrate. This indicates that Cel5A binds to ESC as it would bind to other insoluble cellulose substrates. This also suggests

that Cel5A binds only on the surface of ESC and does not penetrate into the core of the fibers, which will allow for a simplified kinetic model for hydrolysis using a moving boundary in a cylindrical coordinate. A moving boundary in the cylindrical coordinate would lead to gradual thinning of the fibers in areas where the enzymes are active. A factor not taken into consideration here was the drying of the cellulose sample, and what effect (if any) that may have on pore size and cellulose accessibility to the enzymes. In general, the fibers used in these studies were air-dried overnight before being hydrolyzed, which may have had the effect of collapsing larger pores in the fibers [30] and preventing the enzymes from accessing more than the fiber surface.

Hydrolysis of ESC by Cel5A was conducted at $50\,^{\circ}\mathrm{C}$, and was characterized with respect to both product formation and substrate structure. Figure A.2 shows both the quantitative and qualitative measures of product formation with time, and the conversion vs. time curve (Figure A.2(a)) looks very much the same as those for other insoluble cellulose substrates. A thin layer chromatography (TLC) assay was done to roughly quantify sugar composition (Figure A.2(b)), and the product composition shown is consistent with previous homologous hydrolysis of cellulose by Cel5A [61], indicating that ESC is hydrolyzed by Cel5A much as other cellulose substrates are.

The evolution of the structure of the remaining insoluble fractions over time was observed with SEM at each time point (Figure A.3), and the physical deterioration of the fibers becomes apparent at about 40% conversion (53 hrs, Figure A.3(c)). This is also consistent with the behavior of other insoluble cellulose substrates such as Avicel [62] and BMCC [63] during enzymatic hydrolysis. SEM analysis of the insoluble fractions show moderate microstructural changes

appearing at 20% hydrolysis (35 hrs, Figure A.3(b)) with increasingly visible deterioration as hydrolysis approaches 100%. The principle visible result of enzyme exposure is fragmentation of the fibers and loss of long-range fiber connectivity. The SEM analysis also suggests that the remaining fibers may have a rough surface texture caused by the enzyme activity. No apparent thinning of the fibers is seen, and a final characteristic segment length of $10\ \mu\mathrm{m}$ is observed. It is possible that these $\sim 10\ \mu\mathrm{m}$ segments are caused by some artifacts introduced during electrospinning. The causes of these observed microstructural changes and their relation to fiber properties such as fiber diameter warrant further study.

A second hydrolysis study was conducted with ESC to observe effects of hydrolysis on the crystallinity and fiber diameters of ESC. This batch of ESC had DP 210, average fiber diameter of $1.0 \pm 0.4\ \mu\mathrm{m}$, and average crystallinity of $62 \pm 11\%$. The effect of enzyme exposure on overall fiber morphology was similar to what was seen in the previous study despite the slightly larger initial fiber diameter (Figure A.4), with similar fiber splicing and fragmentation. At the end of hydrolysis, the ESC was reduced to the non-uniformities created during the electrospinning process such as "plates", films, and merged fibers.

The crystallinity of the fibers increased to about 70% after 4 hours of hydrolysis, but then leveled off (Figure A.5(a)). The change in crystallinity of ESC was caused by exposure to enzymes and not merely by exposure to the buffer solution, and indicates that some amorphous cellulose may initially be more readily hydrolyzed than crystalline cellulose. However, hydrolysis continued although the crystallinity did not continue to change significantly, so it is possible that after a certain point amorphous cellulose and crystalline cellulose are hydrolyzed

at nearly equal rates.

The binding assay indicated that the enzymes do not penetrate into the fibers, leading to the expectation that a thinning of the fibers would be observed. However, analysis of the SEM images indicate that the fiber diameter does not change significantly with hydrolysis time (Figure A.5(b)), and the SEM images again only show fiber splicing and fragmentation (Figure A.4). This apparent stability of the fiber diameters raises questions about the physical mechanism of hydrolysis of ESC fibers. It is possible, however, that the apparent lack of fiber thinning is due to the post-hydrolysis processing, which involves centrifugation to separate the soluble hydrolysis products from the remaining insoluble cellulose fraction. The forces imposed on the fibers during the centrifugation may break apart fiber sections that have been mechanically weakened by the enzymatic action. This possibility also indicates an area where continued study is necessary.

2.5 Conclusions

It has been demonstrated that the microstructural features of cellulosic materials can be varied and controlled via the process of electrospinning. Table 2.5 summarizes the current range of controllable substrate characteristics. Namely, the degree of polymerization, degree of crystallinity, and surface area of the cellulose fibers can be varied nearly independently of each other. The degree of crystallinity and surface area (fiber diameter) are somewhat coupled, but there is potential for uncoupling the two by altering processing conditions, specifically the coagulation scheme. These fibers can then be used in enzymatic hydroly-

sis studies in order to determine which microstructural features of the cellulose substrate are most influential in determining the hydrolysis rate.

Table 2.5: Summary of Current Control of Cellulose Microstructure

Degree of Polymerization	**Degree of Crystallinity**			**Fiber Diameter**	
	Low ($< 40\%$)	*Intermediate* ($40 - 60\%$)	*High* ($> 60\%$)	*Small* (< 0.5 μm)	*Large* (> 0.5 μm)
210	-	✓	✓	✓	✓
550	✓	✓	✓	✓	-
1140	✓	✓	✓	✓	✓

The process of electrospinning will generally allow for the separation of the effects of substrate microstructure on enzymatic hydrolysis. Although ESC is not a natural form of cellulose, an understanding of how cellulases interact with and hydrolyze ESC will help to explain the fundamental hydrolysis mechanisms of individual cellulases, independent of the type of insoluble substrate being hydrolyzed or the presence of additional cellulases. Further work must be done to pinpoint the processing conditions to produce fibers of desired DP, crystallinity, and diameter independently of one another, in order to systematically look at the effects of these substrate characteristics on the rates of enzymatic hydrolysis. In particular, a method to produce DP 210 cellulose of low crystallinity must be investigated. A possibility is utilizing coaxial electrospinning, as the inner jet does not have to be spinnable in order to form fibers [40]. The electrospinning set-up has also been modified to allow for better control over the spinning parameters such as needle temperature and the temperature of the spinning region.

Preliminary binding and hydrolysis studies have also demonstrated that the binding and hydrolysis kinetics of enzymes on ESC are similar to that of other insoluble substrates, validating the use of ESC as a model cellulose substrate.

SEM analysis of the remaining insoluble cellulose fractions revealed fiber splicing, and a characteristic fragment length of about $10\ \mu\mathrm{m}$. A second hydrolysis study that observed the evolution of crystallinity and fiber diameter indicated that while some amorphous cellulose may be more readily hydrolyzed than crystalline cellulose, the degree of crystallinity leveled off quickly although hydrolysis continued to proceed. This study also showed that fiber diameter remained fairly constant over the course of hydrolysis, and again revealed fiber splicing and fragmentation. This may be caused by artifacts introduced by the electrospinning process that cannot be seen via SEM and X-ray diffraction, the effects of post-hydrolysis processing on the fibers, or some combination thereof. These studies show the potential for utilizing ESC as a cellulose hydrolysis substrate, but fiber substrates with smaller deviations in microstructural characteristics are required in order to make any decisive conclusions about the effects of microstructure on cellulose hydrolysis. In addition, the use of coaxial fibers may provide further insight into how the enzymes are working on the fiber substrate. Coaxial fibers with a cellulose shell and a non-hydrolysable, insoluble core may prevent fiber break-up and preserve long-range fiber connectivity throughout hydrolysis. This would allow for better observation of the effect of enzyme activity on the fiber substrate and perhaps aid in elucidating the mechanisms of macroscopic cellulose degradation by cellulase enzymes.

CHAPTER 3

ELECTROSPINNING OF COAXIAL CELLULOSE FIBERS

3.1 Introduction

Coaxial electrospinning is an extension of monoaxial electrospinning, and has been used to create core/shell nanofibers and hollow nanofibers as well to provide encapsulation of certain materials [37–40, 64–67]. Coaxial electrospinning offers an advantage over conventional methods for creating these kinds of microstructured fibers, as processes that formerly took multiple steps can now be done in one or two steps.

In coaxial electrospinning, two capillary liquid-liquid jets of polymeric solutions are attached to a high voltage source and electrospun much in the same manner as monoaxial fibers. Figure 3.1 shows a typical coaxial electrospinning setup. A compound droplet of two layers will form at the tip of the coaxial nozzle, and a compound Taylor cone then leads to a compound jet being electrospun much as a monoaxial jet is electrospun [67]. A variety of solution pairs can be coaxially electrospun, including both miscible and immiscible solutions. When miscible solutions are used, the stretching and solidification of the fibers is generally fast enough that diffusion between the inner and outer jets is negligible [67]. When immiscible solutions are co-electrospun, the boundary between the core and shell of the coaxial nanofiber tends to be sharper than with miscible solutions [66, 68], but in both cases nanofibers with a core/shell morphology can be created.

Coaxial electrospinning allows for electrospinning of solutions that cannot

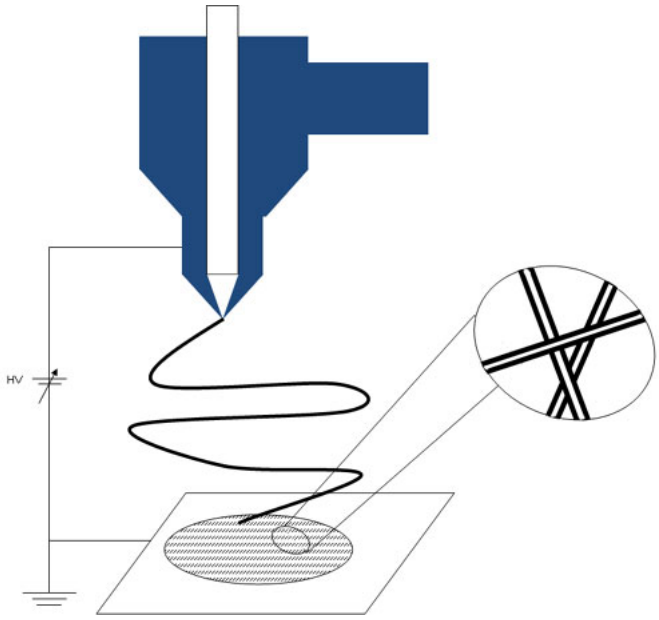

Figure 3.1: Coaxial electrospinning set-up

be electrospun on their own due to low viscosity or low conductivity, such as aqueous solutions of bioactive agents [39, 69, 70] or hydrophobic liquids [65]. Hollow fibers can be created by utilizing mineral oil as the inner jet in coaxial electrospinning followed by thermal treatment to remove the mineral oil core [37, 40, 66, 69, 70]. In these situations, the inner jet is encapsulated in the outer solution as the outer solution undergoes electrospinning, allowing for fibers to be made from solutions that cannot be formed into fibers otherwise.

A concern with coaxial electrospinning is in ensuring that the inner solution is entrained within the outer jet to obtain truly coaxial fibers. Analysis of as-spun fibers has shown that in several cases not all fibers contain the desired core/shell structure [39, 64]. Although a compound droplet is formed at the nozzle tip, the jet that is electrospun only contains the outer solution. Reznik *et al.* [39] produced a solution to this problem, in which the core nozzle protrudes from the shell nozzle by about half the radius of the latter.

Although most coaxial electrospinning is done at room temperature, there have been some examples of melt or heated solution coaxial electrospinning. Melt coaxial electrospinning was utilized by McCann *et al.* [38] to encapsulate phase change materials inside a composite or polymer matrix. Their setup included a glass syringe heated by a heating mantle that was connected to a silica capillary, which was then placed concentrically inside a metal needle connected to a plastic syringe. The heated glass syringe allowed for electrospinning of materials that are solid at room temperature, and the coaxial nature of the setup allowed for solutions that cannot be electrospun on their own to be encapsulated inside fibers.

These studies utilize the process of coaxial electrospinning to form cellulose fibers with unique microstructure to address the following issues seen in monoaxial fiber spinning and hydrolysis in described Chapter 2.

One major issue seen in monoaxial electrospinning of cellulose was the inability to spin monaxial fibers from low DP cellulose/LiCl/DMAc solutions due to jet break-up. Polymeric solutions that electrospin well, such as cellulose acetate, polylactic acid, or polyacrylonitrile, are used to entrain low DP cellulose/LiCl/DMAc solutions. The non-cellulose shell is then removed by chemical means in order to obtain low DP, low crystallinity fibers of pure cellulose.

An issue seen during the hydrolysis of monoaxial cellulose fibers was fiber break-up and loss of long-range fiber connectivity over the course of hydrolysis. This may have been caused by unknown artifacts introduced by the electrospinning process or the post-hydrolysis treatment of the remaining insoluble fraction. The centrifugation step may have broken apart areas of the fibers that have been weakened by the action of the enzymes. In order to investigate

this further, insoluble, non-hydrolysable strong polymeric cores are introduced into cellulose fibers made from both LiCl/DMAc and NMMO/water solutions. Fiber cores made from cellulose acetate, polystyrene, polylactic acid, and polyacrylonitrile are investigated. Those fibers that are successfully coaxially electrospun are then used in enzyme hydrolysis studies to determine if the non-hydrolysable core will enable new insights into the mechanism of macroscopic cellulose degradation.

3.2 Experimental Methods

3.2.1 Materials

For this study, only low DP cellulose was investigated. DP 210 cellulose (Whatman fibrous cellulose CF-11 powder) was used as is. All other chemicals were analytical grade from commercial sources. Anhydrous dimethylacetamide (DMAc), 97% N-methylmorpholine-N-oxide (NMMO) powder, 50% aqueous N-methylmorpholine-N-oxide solution, n-propyl gallate, cellulose acetate (30,000 average MW), and polyacrylonitrile were obtained from Sigma-Aldrich; lithium chloride (LiCl, granular), N-N- dimethylformamide (DMF), acetone, and chloroform were obtained from Mallinckrodt; polystyrene resin was obtained from Alfa Aesar (100,000 MW); polylactic acid resin was obtained from Natureworks (6251D); and Pluronic F88 Prill surfactant was obtained from BASF.

3.2.2 Solution Preparation

Solution preparation of cellulose solutions are described in Chapter 2. For the LiCl/DMAc solutions, cellulose concentrations of 4 - 8 wt% were used; for the NMMO/water solutions, cellulose concentrations of 8 - 9 wt% were used. Where surfactant was added to the cellulose/NMMO/water solutions, surfactant was added at 5% of the cellulose mass.

Cellulose acetate (CA) of MW ∼30,000 was prepared in solutions of acetone/DMAc since acetone alone was too volatile for electrospinning. CA was also dissolved in pure DMAc, which is not spinnable on its own [71] but may be suitable for an inner jet. The procedure described by Kim [36] was followed. The solvent ratio used was 1:2 v/v acetone/DMAc. Concentrations of CA were 16 - 28 wt% for acetone/DMAc solutions and 9 - 21 wt% for pure DMAc solutions. After the solvents were mixed thoroughly, the CA powder was added slowly to prevent clump formation. The solutions were stirred at room temperature for an additional hour to ensure complete dissolution, and were left unstirred for another hour to allow any air bubbles trapped in the solution to dissipate.

Polystyrene (PS) of MW ∼100,000 was dissolved in solutions of DMF or DMAc. PS pellets were added to the solvent and allowed to stir overnight until complete dissolution was achieved. Solution concentrations were 22 wt% polystyrene in DMF, and 23 wt% in DMAc (0.273 g/mL in both). This concentration was determined such that the Barry number, $[\eta]C$, was around 9, where $[\eta]$ is the intrinsic viscosity and C is the concentration. Intrinsic viscosity was calculated based on Mark-Houwink constants for PS in DMF and the molecular weight of the polymer [72]. As Mark-Houwink data for PS in DMAc was unavailable, the same concentration was used for both solvents. PS was also

dissolved in solutions of 1:2 v/v acetone/DMAc, at 14.5 to 18 wt% concentrations (0.15 - 0.20 g/ml).

Polylactic acid (PLA) of MW ∼200,000 was dissolved in chloroform/acetone, or pure DMF. The solutions were 3:1 v/v chloroform/acetone, and the binary solvent was first mixed before adding the PLA pellets and allowing the solutions to stir overnight until complete dissolution was achieved. PLA was added at a concentration of 8 - 10 wt%, following the procedure of Li *et al.* [73]. Solutions of 22wt% PLA in DMF were also made. PLA does not dissolve in DMF at room temperature, so solutions were made by combining the desired amounts of PLA and DMF and allowing the mixture to stir heated ($\sim 70 - 100\ ^{\circ}\mathrm{C}$) overnight [74].

Polyacrylonitrile (PAN) of MW ∼150,000 was prepared in solutions of DMF. PAN and DMF were combined in the desired proportions (10-14 wt% PAN) and stirred for at least one hour to allow the PAN to be homogenously dispersed. Heat was then applied while stirring for an additional hour to achieve complete dissolution. Once the PAN was dissolved in DMF, the solutions were stable and did not need to be heated while electrospinning.

3.2.3 Electrospinning Conditions

The electrospinning setup used is shown in Figure 3.2. For any monoaxial electrospinning done for these studies, the same setup was used as shown in Figure 2.1. For coaxial electrospinning with cellulose/NMMO/water, the syringe containing the cellulose solution was heated to $90 - 110\ ^{\circ}\mathrm{C}$, and the needle tip was heated to $70 - 100\ ^{\circ}\mathrm{C}$. Temperatures were controlled with heating guns fit-

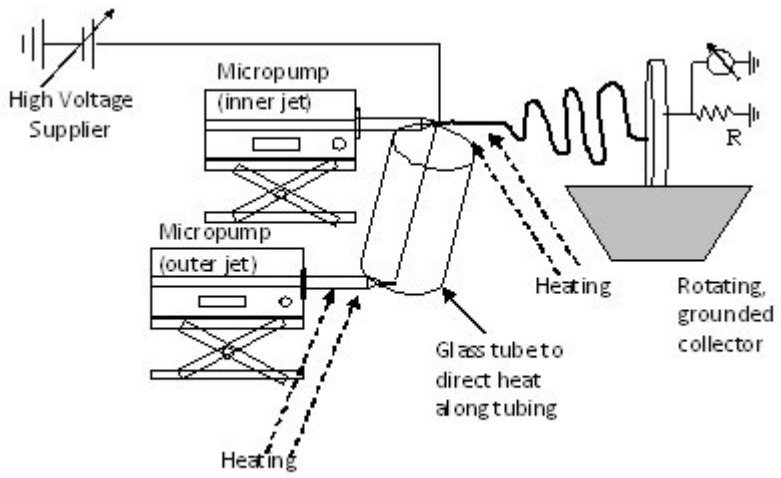

Figure 3.2: Experimental coaxial electrospinning setup. For solutions requiring high temperatures such as cellulose/NMMO/water, heating guns were used where dashed lines are present.

ted with glass nozzles. The temperature of the syringe containing the inner jet solution was typically around $60 - 80\,^{\circ}\mathrm{C}$ when heating was applied to the outer solution. Any coaxial fibers spun from cellulose/LiCl/DMAc solutions were electrospun at room temperature, so no heating was applied and the glass tube was not utilized. Needle tip to collector distances were typically 15 cm, and voltages ranged from 15-20 kV. Infusion rates varied depending on the polymer solutions used and whether the cellulose solution made up the core material or the shell material, but typically ranged from 0.001 - 0.02 ml/min. The rotating water bath was used when cellulose/NMMO/water solutions were electrospun, rotation speeds ranged from 1.2 - 1.5 rpm and the water bath was at room temperature. Samples where cellulose/LiCl/DMAc solutions were used did not utilize the *in situ* coagulation, and typically the collector was heated to facilitate DMAc evaporation. All samples made from cellulose/NMMO/water were coagulated overnight before drying; samples made from cellulose/LiCl/

DMAc were rinsed with water and typically dried immediately. Conditions used for electrospinning are summarized in Table 3.1 and Table 3.2.

Table 3.1: Coaxial Electrospinning Conditions: Fibers with cellulose core

Coaxial system (shell; core) wt%	Solution Temp	Needle Temp	Collector Temp	Electric Field	Typical Infusion Rates (shell; core) ml/min
CA (28%); cellulose/ LiCl/DMAc (6%)	RT	RT	$\sim$100 °C	20 kV /15 cm	0.01-0.02; 0.005- 0.007
PLA (8%); cellulose/ LiCl/DMAc (4 - 6%)	RT	RT	RT or $\sim$100 °C	20 - 22 kV /15 cm	0.005-0.01; 0.001-0.007
PAN (12%); cellulose/ LiCl/DMAc (6%)	RT	RT	$\sim$100 °C	25 kV /10 cm	0.0073; 0.001

3.2.4 Structural characterization of electrospun cellulose

The morphology of the fibers was observed with a scanning electron microscope (LEICA 440 SEM), and wide-angle X-ray scattering (WAXS, Scintag, Inc. Theta-Theta Diffractometer) was used to determine crystal structure, degree of crystallinity, and to get a measure of fiber composition. Degree of crystallinity was determined by an area ratio of the crystalline phase to the total area of the diffraction pattern, which was obtained after peak deconvolution. Fiber compositions were estimated by considering the mass percents of polymer in solution and the flowrates used. A transmission electron microscope (FEI Tecnai T12 Spirit Twin TEM/STEM) was used to look at cross-sections of some of the coax-

Table 3.2: Coaxial Electrospinning Conditions: Fibers with cellulose shell

Coaxial system (shell; core) wt%	Solution Temp	Needle Temp	Collector Temp	Electric Field	Typical Infusion Rates (shell; core) ml/min
cellulose/ LiCl/DMAc (6 - 7.5%); CA (28%)	RT	RT	$\sim$100 °C	20 kV /15 cm	0.005; 0.01
cellulose/ LiCl/DMAc (4 - 7%); PS (14.5 - 18, 22%)	RT	RT	$\sim$100 °C	15-20 kV /15 cm	0.005 - 0.01; 0.005 - 0.007
cellulose/ NMMO/water (9%); CA (16-28%)	$\sim$90$-$ 100 °C	$\sim$70$-$ 100 °C	RT	15 kV /12 cm	0.015 - 0.02; 0.005
cellulose/ NMMO/water (9%); CA (9-21%)	$\sim$90$-$ 100 °C	$\sim$70$-$ 100 °C	RT	17 kV /14 cm	0.01; 0.007
cellulose/ NMMO/water (9%); PS (14.5-18%)	$\sim$70$-$ 100 °C	$\sim$50$-$ 70 °C	RT	20 kV /10 cm	0.02; 0.005 - 0.01
cellulose/ NMMO/water (9%); PLA (22%)	$\sim$80$-$ 110 °C	$\sim$50$-$ 70 °C	RT	15-20 kV /12-14 cm	0.007-0.01; 0.003-0.005
cellulose/ NMMO/water (8%); PAN (12-14%)	$\sim$80$-$ 110 °C	$\sim$60$-$ 100 °C	RT	15-20 kV /12-15 cm	0.004-0.01; 0.001 - 0.005

ially spun fibers to verify the coaxial nature of the fibers. Fibers analyzed via TEM were first fixed with glutaraldehyde and stained with osmium tetroxide, then embedded in epoxy and microtomed in order to obtain thin cross-sections of material.

3.3 Results and Discussion

3.3.1 Coaxial Fibers with a Cellulose Core

Three different polymer materials were used in an attempt to entrain DP 210 cellulose solutions in LiCl/DMAc in order to form continuous fibers of low DP and low crystallinity. Cellulose acetate, polylactic acid, and polyacrylonitrile formed the shells of coaxial fibers with a cellulose core made from cellulose/LiCl/DMAc solutions of various concentrations. The non-cellulose shell was then removed by selective dissolution of the shell. This was particularly straightforward since cellulose does not dissolve readily in most solvents.

Figure 3.3(a) shows the fibers formed with a cellulose acetate shell and cellulose core. These fibers are fairly uniform and have an average diameter of $190 \pm 95\,\mathrm{nm}$. The cellulose acetate shell was removed by washing the fibers with acetone, which can be seen in Figure 3.3(b). The overall fiber morphology is greatly lost as fibers are merged together and large sheets and films are formed, and the average fiber diameter is reduced to $81 \pm 40\,\mathrm{nm}$. This indicates that the cellulose acetate shell is relatively thick, comprising approximately half of the as-spun fiber radius. This was probably due to the high concentration of cellulose acetate as compared to cellulose (26 wt% vs. 6 wt%). The actual com-

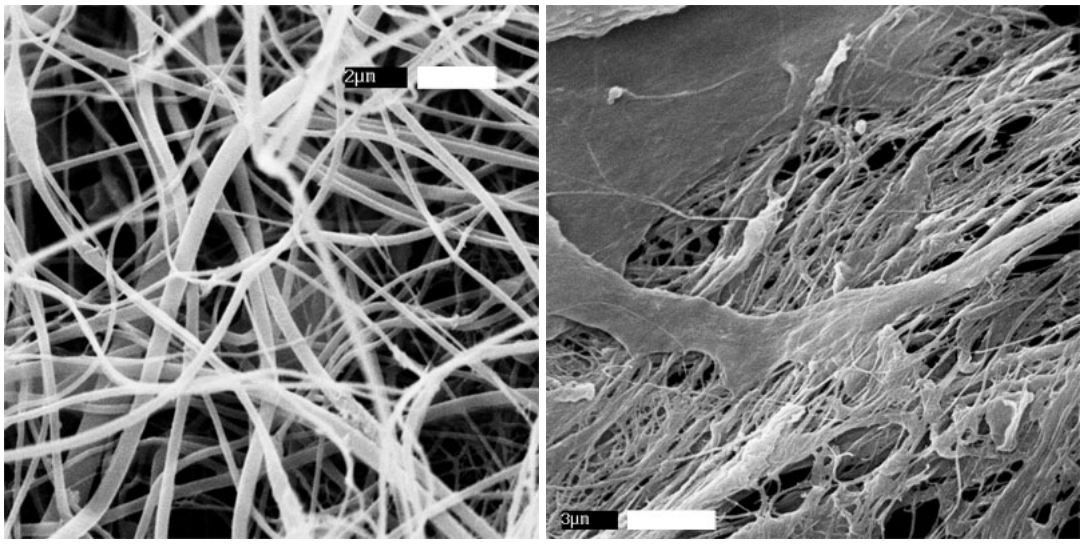

(a) (b)

Figure 3.3: SEM images of CA/DMAc/acetone-cellulose/LiCl/DMAc fibers, 93/7 CA/cellulose: (a) as-spun fibers (scale bar = $2\ \mu\mathrm{m}$); (b) fibers after washing with acetone (scale bar = $3\ \mu\mathrm{m}$)

position of the fibers was not measured, but Figure 3.4 shows the X-ray diffraction pattern for both the as-spun fibers and the fibers washed with acetone. As the peaks of pure cellulose acetate overlap the amorphous peak of cellulose, it was difficult to deconvolute the XRD pattern to determine relative amounts of cellulose acetate to cellulose. Also, it is possible that the XRD pattern shows primarily the material on the shell of the fibers and not both the shell and the core. However, the diffraction pattern for the washed fibers reveals some Type I crystal structure in addition to the amorphous cellulose normally present with fibers from cellulose/LiCl/DMAc solutions. This is probably due to incomplete dissolution of cellulose in the binary solvent, which would preserve some Type I crystal structure. This is an important discovery, as it could point the way to production of electrospun cellulose fibers with Type I crystal structure. However, the fiber morphology must be preserved once the cellulose acetate shell is removed.

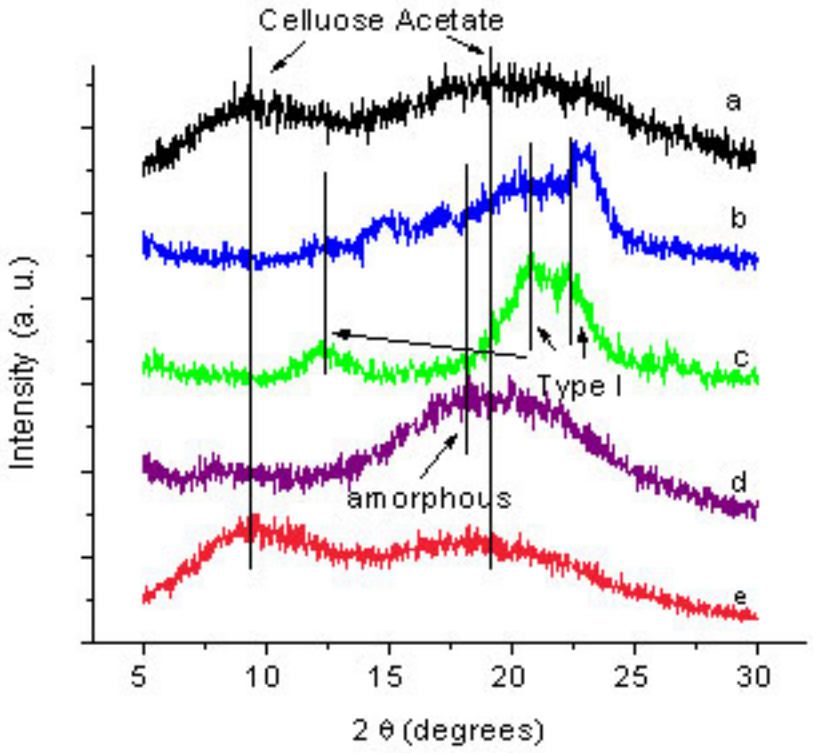

Figure 3.4: X-ray diffraction pattern for CA/DMAc/acetone-cellulose/LiCl/DMAc fibers: (a) as-spun fibers; (b) acetone-washed fibers; (c) Type I cellulose; (d) amorphous cellulose; (e) pure cellulose acetate.

Polylactic acid in chloroform/acetone was also used as a shell material to encapsulate cellulose/LiCl/DMAc solutions. Figure 3.5(a) shows the as-spun fibers, Figure 3.5(b) shows the fibers after washing with chloroform. By mass, the fibers were almost entirely PLA as there were only residual amounts of the non-woven fiber mat remaining after PLA removal. There was a skeleton of a fiber mat left on the aluminum foil after washing with chloroform; this is probably residual PLA that had no cellulose entrained within the fibers. The average fiber diameter before washing was $0.20 \pm 0.12\,\mu\mathrm{m}$, although there were occasional fibers that were much wider (up to $1.5\,\mu\mathrm{m}$ diameter). It is likely that

these wider fibers had cellulose entrained in the core, and the large, scrunched-looking segments that were also left after washing the as-spun fibers are probably cellulose fragments. Due to the small sample size after removal of PLA, X-ray analysis was not possible. The average diameter of the fiber skeleton in Figure 3.5(b) was 0.28 ± 0.10 μm, which correspond reasonably well to the fiber diameters of the majority of the fiber mat. The average diameter of the large scrunched segments was 2.1 ± 0.7 μm, which also corresponds reasonably with the largest fiber diameters in the as-spun fiber mat. These observations further support the conclusion that cellulose was not well-entrained into the core of the PLA fibers.

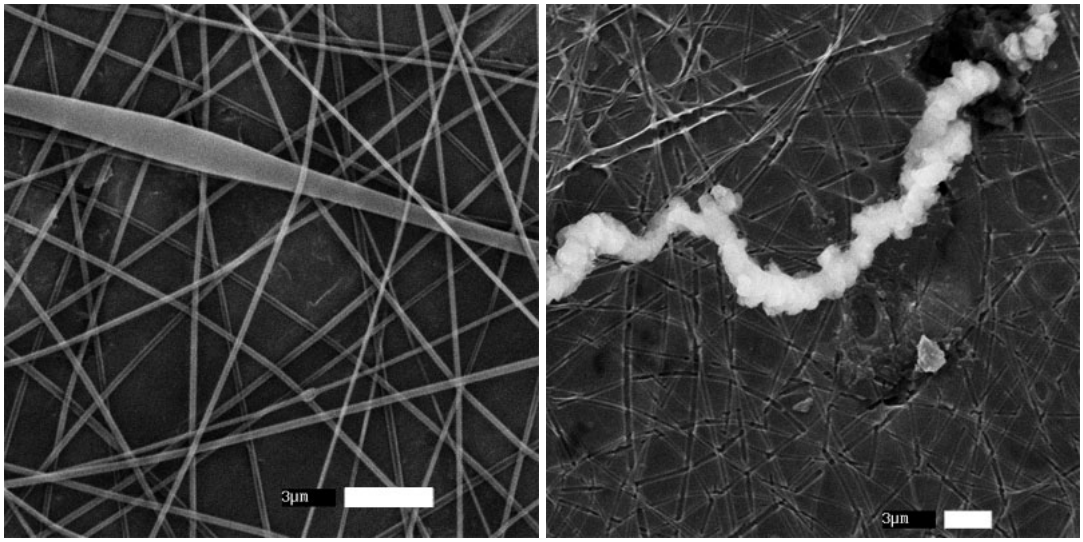

(a) (b)

Figure 3.5: SEM images of PLA/chloroform/acetone-cellulose/LiCl/DMAc fibers, 95/5 PLA/cellulose: (a) as spun; (b) washed with chloroform (scale bars are 3 μm

A third material that was used to entrain cellulose was polyacrylonitrile. 12 wt% PAN was used as the shell material to encapsulate 8 wt% cellulose. The cellulose was not completely dissolved in LiCl/DMAc, as the concentration of cellulose was higher than usual and the resulting solution was very cloudy. The

PAN was removed by placing the electrospun sample in a vial with 5 mL DMF and heating and stirring for one hour. The DMF was filtered off and the residual fibers were washed with additional DMF before being dried and analyzed under the SEM. However, as in the case with the PLA-cellulose fibers, there was a negligible mass of residual fibers after the hot DMF treatment, indicating that these fibers are primarily composed of PAN. Figure 3.6(a) shows the as-spun PAN-cellulose fibers, Figure 3.6(b) shows the fibers after the hot DMF treatment. Fiber diameters were 1.5 ± 1.7 μm before and 0.43 ± 0.81 μm after the hot DMF treatment, indicating that these fibers had more than half the as-spun fiber radius as PAN. Again, due to the small sample size remaining after removal of the PAN shell, these fibers were also not analyzed via X-ray diffraction. The small mass of fibers left after PAN removal suggests that in these fibers, as in the PLA-cellulose fibers, cellulose has not been entrained as the core material for most of the fibers that have been electrospun.

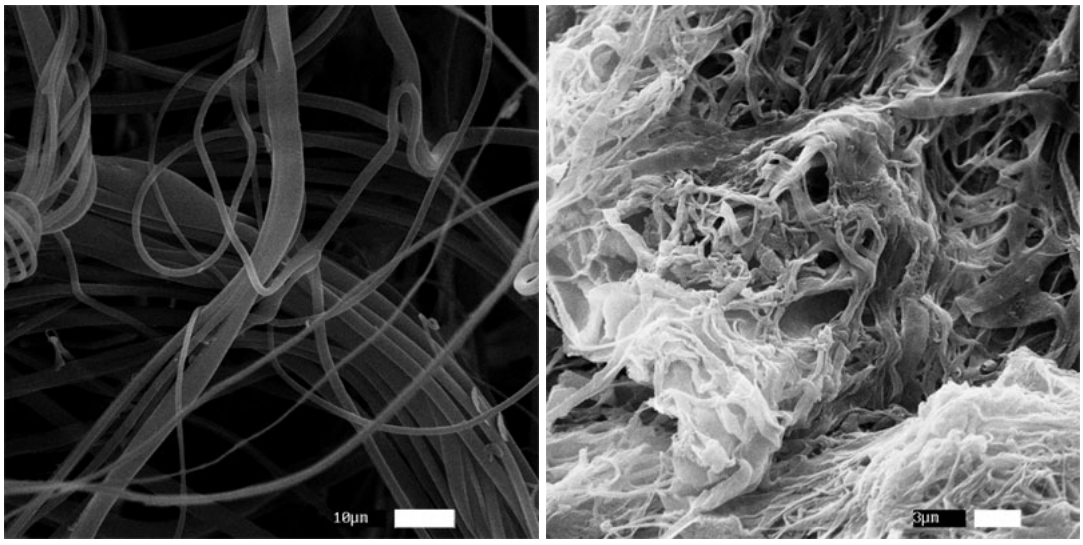

(a) (b)

Figure 3.6: SEM images of PAN/DMF-cellulose/LiCl/DMAc fibers, 93/7 PAN/cellulose: (a) as-spun (scale bar = 10 μm); (b) treated with hot DMF (scale bar = 3 μm)

3.3.2 Coaxial Fibers with a Cellulose Shell

Coaxial fibers with cellulose/LiCl/DMAc solutions

Although low DP cellulose/LiCl/DMAc solutions are not spinnable on their own, it was thought that incorporating a well-spinning solution as the core material would allow for the core to be coated with the cellulose solution, and thus provide a cellulose shell on these coaxial fibers. Two different core materials, cellulose acetate and polystyrene, were investigated.

Figure 3.7 shows both the SEM and TEM images of cellulose-cellulose acetate fibers. Cellulose concentrations of 6 - 7.5 wt% and cellulose acetate concentrations of 28 wt% were electrospun coaxially. The SEM images show nicely uniform fibers, but it is difficult to tell whether the fibers have been coated with cellulose or not. The samples analyzed under the TEM have been stained such that the cellulose should be selectively fixed with glutaraldehyde and stained with osmium tetroxide; however, few TEM images show clearly coaxial fibers. The images shown in Figure 3.7(b) and (d) indicating evidence of coaxial fibers were rare. Glutaraldehyde will react with the hydroxyl groups available on the cellulose chain, and osmium tetroxide will react with the C-C double bonds created by the attachment of glutaraldehyde with cellulose. Cellulose acetate has less hydroxyl groups available, so should be stained considerably less than the cellulose. The lack of clearly coaxial fibers could be due to either insufficient staining or too much staining (longer contact time with glutaraldehyde and osmium tetroxide would allow the few hydroxyl groups present in cellulose acetate to react), or due to insufficient coating of the cellulose acetate fibers with cellulose.

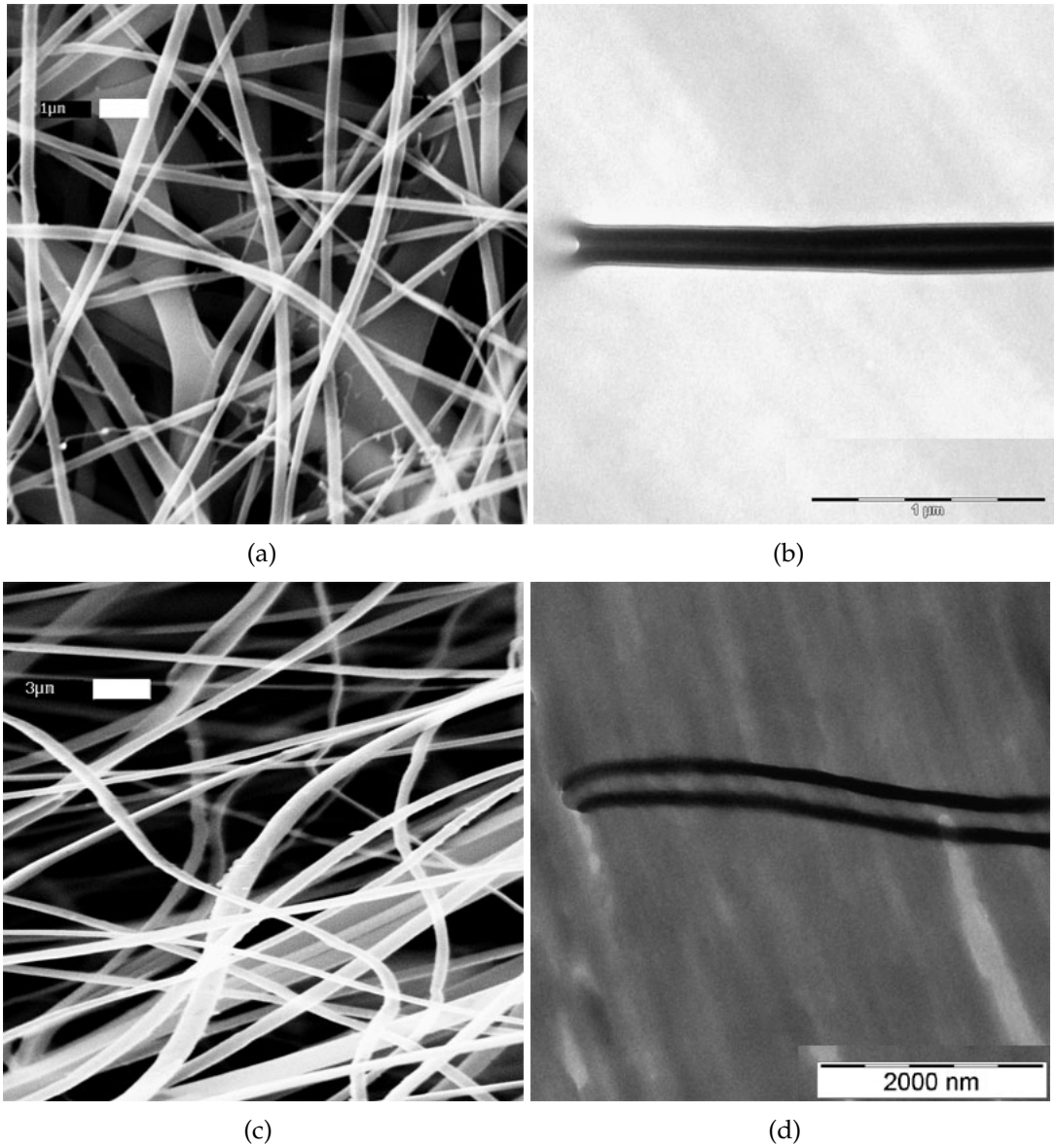

Figure 3.7: SEM images of cellulose/LiCl/DMAc-cellulose acetate/ DMAc/acetone fibers: 6 wt% cellulose, 28 wt% CA [8/92 cellulose/CA] (a) SEM (scale bar = $1\ \mu m$), (b) TEM (scale bar = $1\ \mu m$); 7.5 wt% cellulose, 28 wt% CA [10/90 cellulose/CA] (c) SEM (scale bar = $3\ \mu m$), (d) TEM (scale bar = $2\ \mu m$).

Figure 3.8 shows the X-ray diffraction pattern commonly seen with these coaxial fibers. As with the cellulose acetate-cellulose coaxial fibers, the XRD patterns show primarily cellulose acetate with little clear evidence of the presence of cellulose. The overlap between the cellulose amorphous peak and one of the cellulose acetate peaks makes it difficult to determine the composition of the fibers, but the prominence of the CA peak at $2\theta \approx 9.5^\circ$ indicates a high percentage of cellulose acetate.

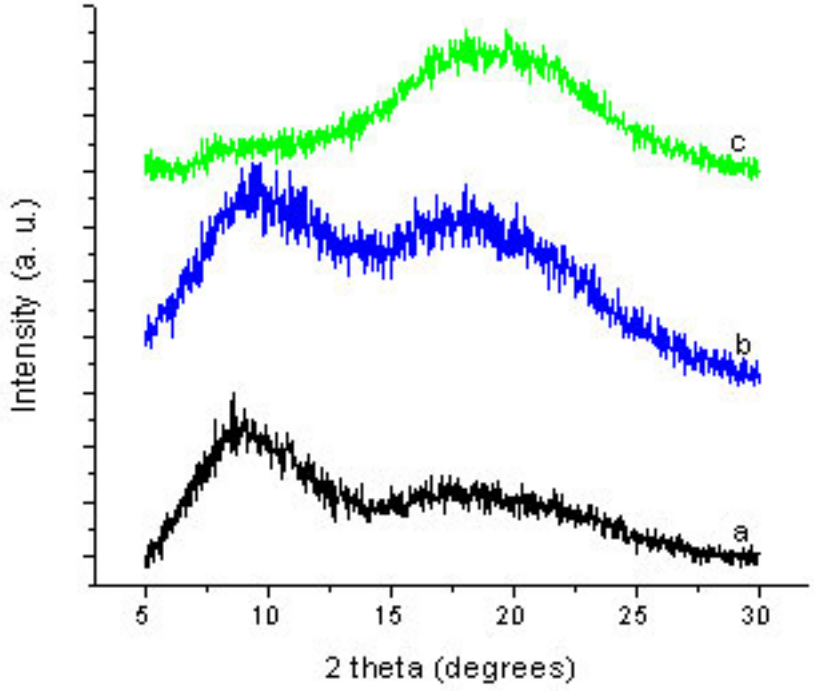

Figure 3.8: X-ray diffraction pattern for coaxially spun cellulose-cellulose acetate fibers: (a) coaxial cellulose-cellulose acetate fibers; (b) pure CA fibers; (c) pure amorphous cellulose

Polystyrene was also studied as a potential core material, and Figure 3.9 shows the SEM images of these fibers. These fibers also appear to be relatively uniform, but fiber production was difficult. For fibers formed from PS

in DMF as a single solvent (Figure 3.9(a)), the needle clogged often so producing a reasonable mass of fibers was not possible. PS in DMAc was not used as a core material, as the monoaxial fibers did not dry well during electrospinning and the fibers on the collector appeared wet despite heating. The jet formed when using PS in DMAc/acetone was very erratic, and also did not spin well. Coaxial fibers formed with 18 wt% PS in DMAc/acetone were not very uniform (Figure 3.9(b)). Monoaxial fibers formed from 14.5 wt% PS in DMAc/acetone also tended to be beaded (Figure 3.9(c)), resulting in beaded fibers in the coaxially spun fibers as well (Figure 3.9(d)). Due to the difficulty of forming fibers, polystyrene was rejected as a core material.

Although the cellulose content of these fibers was unknown, a batch of coaxial cellulose-cellulose acetate fibers was hydrolyzed with Cel5A as described in Appendix B.3.1. These fibers had average diameter of $0.4 \pm 0.3\ \mu\mathrm{m}$, and were composed of amorphous cellulose and cellulose acetate. The exact composition of the fibers was unknown. Over the course of hydrolysis, the average fiber diameter did not change significantly (Figure B.1), the X-ray diffraction pattern of the fibers did not change (Figure B.3), and negligible amounts of soluble sugars were produced, suggesting that the fibers were primarily cellulose acetate. However, SEM analysis of the fibers after hydrolysis showed some evidence of possible enzyme activity in the form of pits and surface roughness. These can be seen in Figure B.2. The pitting seen in Figure B.2(a) and B.2(c) were not seen in previous monoaxial cellulose hydrolysis. This evidence of enzyme activity on the coaxial fibers indicates that these fibers may be able to provide new insight into the physical mechanism of cellulose hydrolysis by cellulase enzymes, once more cellulose is placed on the shell-side of the fibers.

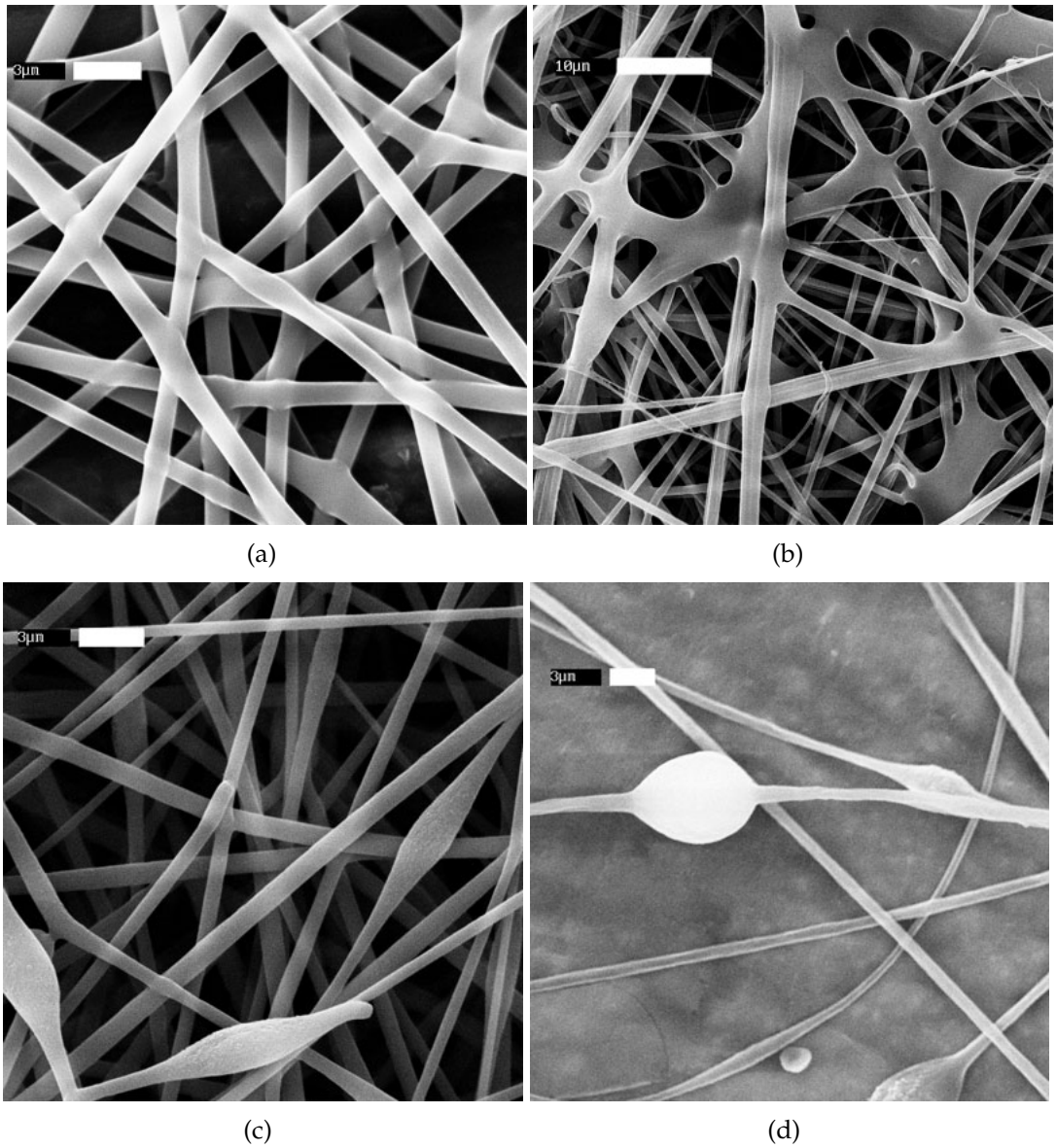

Figure 3.9: SEM images of fibers from cellulose/LiCl/DMAc-polystyrene: (a) 7 wt% cellulose, 22 wt% PS in DMF [28/72 cellulose/PS] (scale bar = $3\,\mu m$); (b) 7 wt% cellulose, 18 wt% PS in DMAc/acetone [28/72 cellulose/PS] (scale bar = $10\,\mu m$); (c) 14.5 wt% PS in DMAc/acetone (monoaxial) (scale bar = $3\,\mu m$); (d) 4 wt% cellulose, 14.5 wt% PS in DMAc/acetone [36/64 cellulose/PS] (scale bar = $3\,\mu m$)

Coaxial fibers with cellulose/NMMO/water solutions

A literature search revealed no other work on producing coaxial fibers with a non-spinnable solution placed on the shell-side of the fibers. According to Yarin *et al.* [40], in coaxial electrospinning the electric charges are practically located only at the outer surface, so the inner droplet in the coaxial Taylor cone is not charged at all. This must be true only of solutions where the outer jet spins well on its own; otherwise the above studies utilizing a non-spinnable solution on the shell-side of the fibers would have produced no fibers whatsoever. However, with this information in mind, it was desirable to place a solution that spins well on the shell side of the fibers, so coaxial systems utilizing the cellulose/NMMO/water fibers were investigated. Due to the necessity of heating the NMMO/water solutions, heating guns were employed at the cellulose solution syringe and at the needle tip, and a glass tube was used to direct the heat along the tubing carrying the cellulose/NMMO/water solutions. This was a very imprecise method of heating, and temperatures varied as much as $\pm 15\,^{\circ}\mathrm{C}$ during the course of electrospinning (temperatures were monitored before and after electrospinning, as the high voltages involved prevented real-time temperature observations). Solutions of cellulose acetate in DMAc/acetone and pure DMAc, polystyrene in DMAc/acetone, PLA in DMF, and PAN in DMF were investigated as possible inner jets.

Coaxial fibers made with a cellulose/NMMO/water shell and cellulose acetate/DMAc/acetone core were electrospun using the setup shown in Figure 3.2. Proper heating of the syringe containing the cellulose solution and the needle tip were essential in keeping the viscosity of the cellulose solution low enough for electrospinning and to prevent solution re-solidification. However,

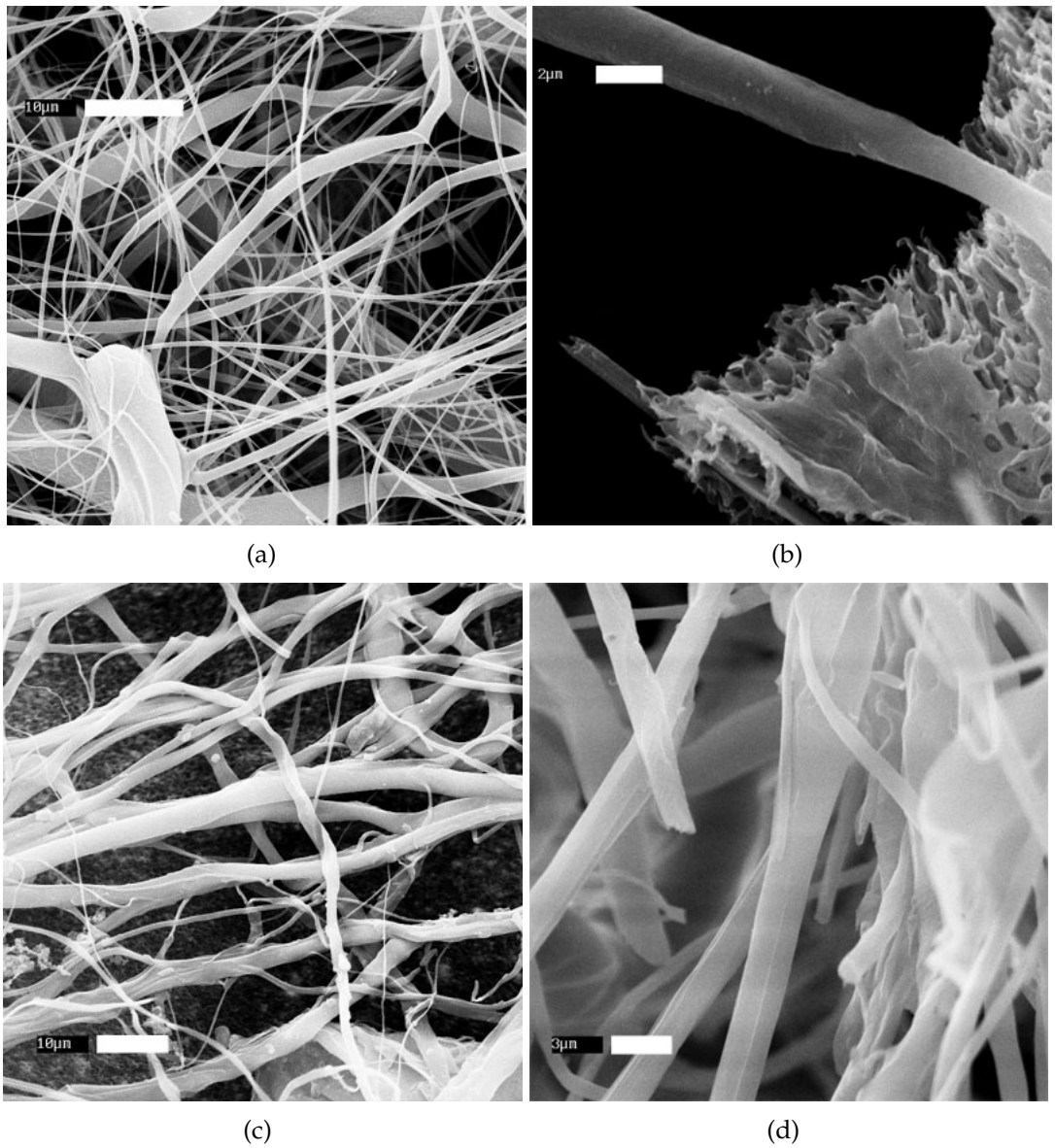

Figure 3.10: SEM images of cellulose/NMMO/water - CA/DMAc/acetone: (a) as-spun, 9 wt% cellulose, 26 wt% CA [26/74 cellulose/CA] (scale bar = $10\ \mu m$); (b) fibers in (a) treated with acetone (scale bar = $2\ \mu m$); (c) as-spun, 9 wt% cellulose, 24 wt% CA [45/55 cellulose/CA] (scale bar = $10\ \mu m$); (d) fibers in (c) treated with acetone (scale bar = $3\ \mu m$).

the high temperatures required to heat the cellulose solution caused a visible lowering of viscosity of the cellulose acetate solutions. The cellulose acetate/ DMAc/acetone solutions had flowrates that were visibly higher than the set infusion rate, and enclosure of the syringe containing the cellulose acetate solution in a ceramic shell to inhibit heat transfer did not solve this issue. This resulted in multiple jets being seen at the needle tip, and very non-uniform fibers were seen (Figure 3.10(a)). It was suspected that the thinner fibers were pure cellulose acetate and the thicker fibers were pure cellulose, instead of producing coaxial fibers as desired. The as-spun fibers were washed in acetone to selectively dissolve the cellulose acetate. While there was some evidence of hollow fibers (Figure 3.10(b), presumably cellulose fibers with the cellulose acetate core removed), the fiber morphology was largely lost and the fibers were about 89 wt% cellulose acetate, indicating that most of the fibers were not coaxial. Fibers shown in Figure 3.10 (c) (as-spun) and (d) (acetone-washed for CA removal) were analyzed for fiber diameters, and Figure 3.11 shows a shift in the histogram of fiber diameters after the acetone treatment. This indicates that the thinner fibers were predominantly cellulose acetate, also indicating that many of the fibers were not coaxial. This shift in fiber diameter distribution after acetone treatment was common for cellulose-cellulose acetate fibers.

Cellulose acetate in pure DMAc was next investigated as a potential core material. Although cellulose acetate does not form continuous fibers when dissolved in pure DMAc [71], it was hoped that the cellulose solution would be able to entrain the cellulose acetate solution, and that the cellulose acetate solution would be more stable at higher temperatures due to the higher boiling point of DMAc as compared to acetone (T_b = $164\,^{\circ}\mathrm{C}$ for DMAc, $56.2\,^{\circ}\mathrm{C}$ for acetone [71]). However, Figure 3.12 shows that these fibers were a mixture of fibers

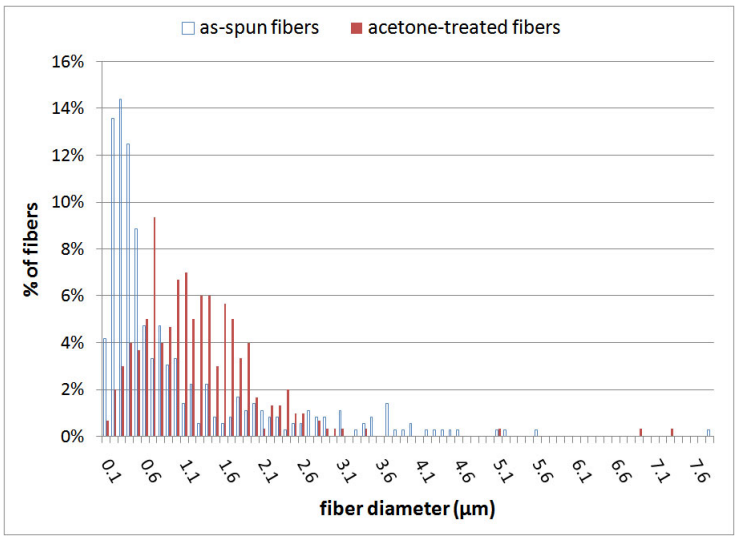

Figure 3.11: Diameter distributions of cellulose/NMMO/water-CA/DMAc/acetone fibers: as-spun and after acetone treatment (fibers shown in Figure 3.10(c) and (d)).

and beads; the beads are probably pure cellulose acetate. It can be seen that for the various concentrations of cellulose acetate used as the inner jet, coaxial fibers were not formed but rather beads of cellulose acetate trapped in cellulose fiber shells. This is most likely due to the higher surface tension of pure DMAc compared to pure acetone (γ = 32.4 dyne/cm for DMAc, 23.7 dyne/cm for acetone [71]), as higher surface tension causes beading of fibers [33]. Because of these issues with forming coaxial cellulose-cellulose acetate fibers with a heated set-up, cellulose acetate was rejected as a core material for fibers formed from cellulose/NMMO/water solutions.

Polystyrene was again considered as a potential core material, this time only investigating PS/DMAc/acetone solutions since previous work with PS and cellulose/LiCl/DMAc solutions showed that PS in pure DMAc or pure DMF did not electrospin well. The heating required for the cellulose/NMMO/water solutions caused similar viscosity issues with PS/DMAc/acetone as a core ma-

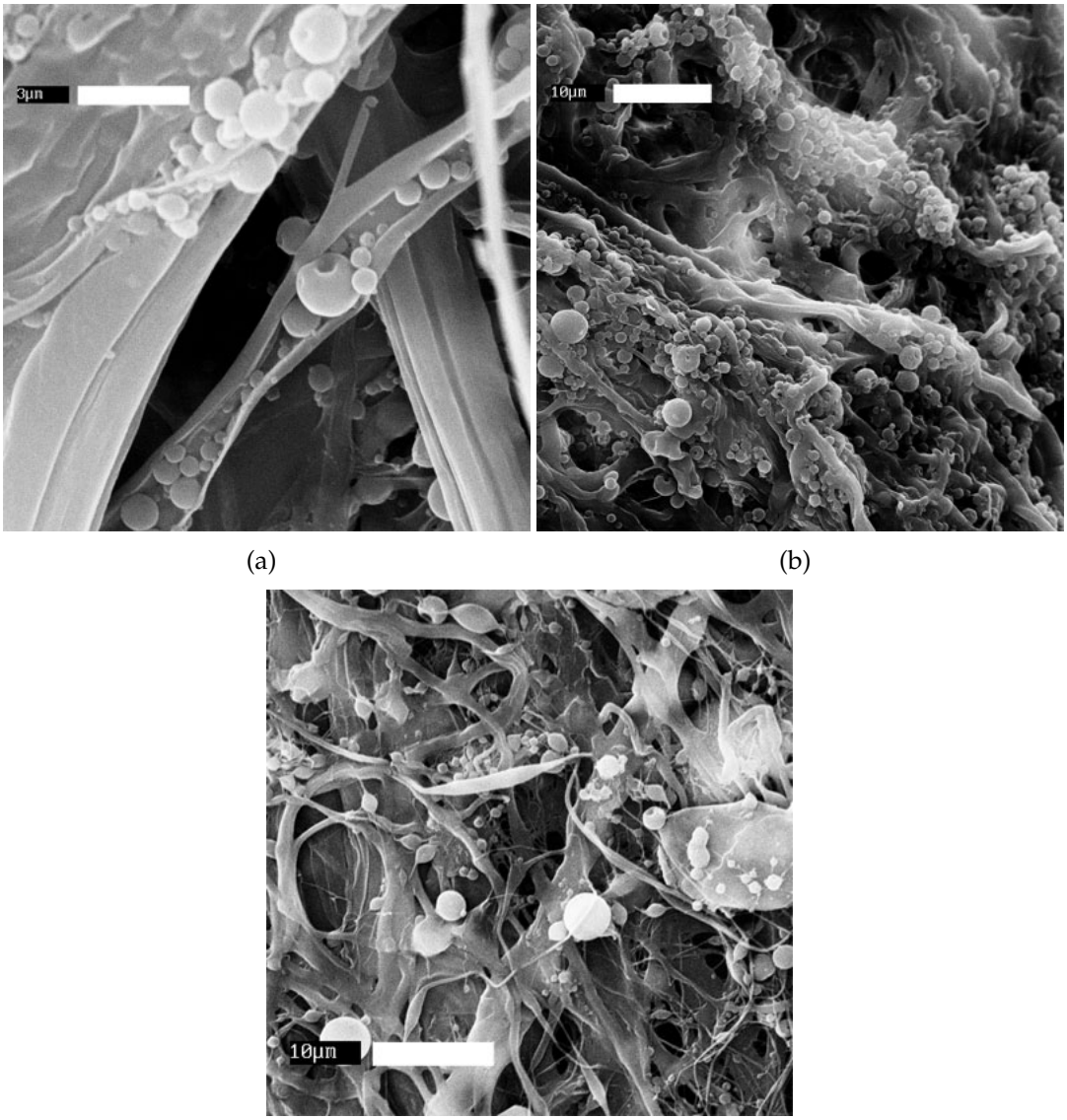

(a) (b)

(c)

Figure 3.12: SEM images of cellulose/NMMO/water-CA/DMAc fibers: (a) 9 wt% cellulose, 9 wt% CA [63/37 cellulose/CA] (scale bar = 3 µm); (b) 9 wt% cellulose, 16 wt% CA [62/38 cellulose/CA] (scale bar = 10 µm); (c) 9 wt% cellulose, 21 wt% CA [54/46 cellulose/CA] (scale bar = 10 µm)

terial as with CA/DMAc/acetone solutions. Figure 3.13 shows SEM images of fibers formed with 14.5 and 18 wt% PS, but fiber formation was again difficult due to the erratic nature of the polystyrene jet. Often, multiple jets were formed at the needle tip, and it appeared as though the cellulose and PS solutions were electrospinning separately. Fibers formed appeared very non-uniform, and a mixture of small diameter and large diameter fibers suggests the formation of thin PS fibers with thick cellulose fibers rather than the desired coaxial fibers. Fiber production was also extremely slow, as the PS solution often clogged the needle tip. Due to these difficulties in fiber production, PS was also rejected as a core material.

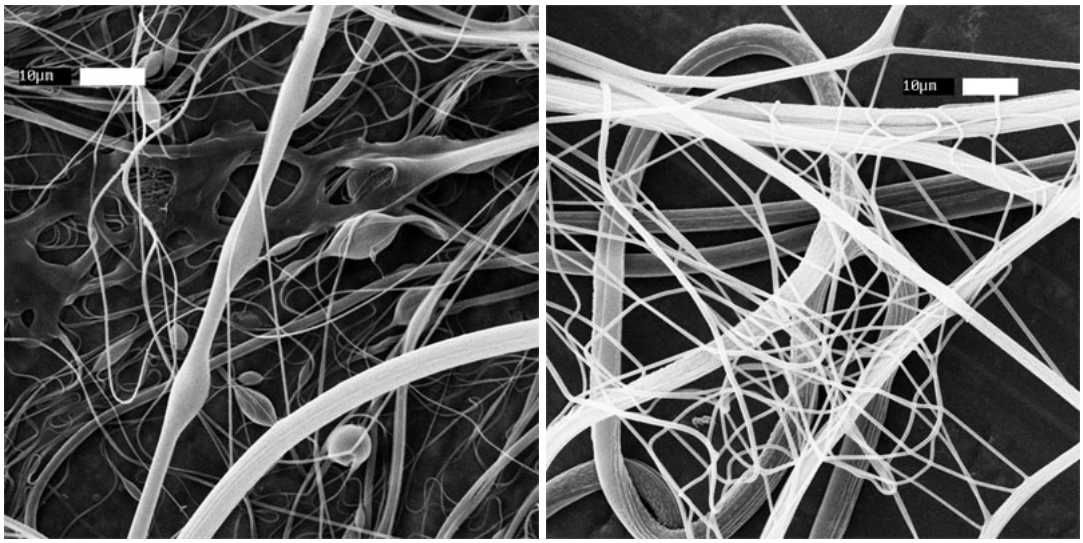

(a) (b)

Figure 3.13: SEM images of cellulose/NMMO/water-PS/DMAc/acetone fibers: (a) 9 wt% cellulose, 14.5 wt% PS [80/20 cellulose/PS]; (b) 9 wt% cellulose, 18 wt% PS [74/26 cellulose/PS] (scale bars = 10 µm)

The solutions of cellulose acetate and polystyrene posed problems in coaxial electrospinning with cellulose/NMMO/water solutions because of the high temperatures required to successfully electrospin the cellulose solution. In order

to overcome this hurdle, inner jet solutions that can be electrospun at elevated temperatures were investigated.

PLA in DMF requires temperatures of around $70\,^{\circ}\mathrm{C}$ in order to be successfully electrospun [74]. Monoaxial fibers were spun from 22 wt% PLA in DMF, and it was observed that the whipping motion commenced very close to the needle tip. With the heated solution setup in Figure 3.2, the temperature at the syringe containing the PLA solution was about $50 - 80\,^{\circ}\mathrm{C}$ when the cellulose/NMMO/water solution was heated to $80 - 110\,^{\circ}\mathrm{C}$. This allowed for reasonable ease of electrospinning the coaxial fibers, but analysis of the as-spun fibers shows that the fibers were not very uniform (Figure 3.14(a)), and average fiber diameters were $0.51 \pm 0.39\ \mu\mathrm{m}$. PLA was selectively removed by washing the fibers in chloroform, and the fibers were only approximately 3% PLA by mass. SEM analysis of the chloroform-treated fibers showed that the average diameter increased to $0.58 \pm 0.26\ \mu\mathrm{m}$ (Figure 3.14(b)), and a histogram of fiber diameters the overall shift of diameters (Figure 3.15), similar to what was seen with cellulose/NMMO/water-cellulose acetate/DMAc/acetone fibers (Figure 3.11). This, coupled with the small mass percentage of fiber that is PLA, indicates that many of the fibers are not coaxial and many of the smaller fibers are pure PLA. Due to the apparent lack of coaxial fibers, PLA was also rejected as a potential core material for fibers with a cellulose/NMMO/water shell.

An issue with using PLA/DMF as the core material was the difference in the monoaxial jet formation between cellulose/NMMO/water solutions and PLA/DMF solutions. It was observed that jets of cellulose/NMMO/water solutions have a very long stable jet region, while PLA/DMF solutions underwent whipping very close to the needle tip. It was suspected that the use of an inner jet

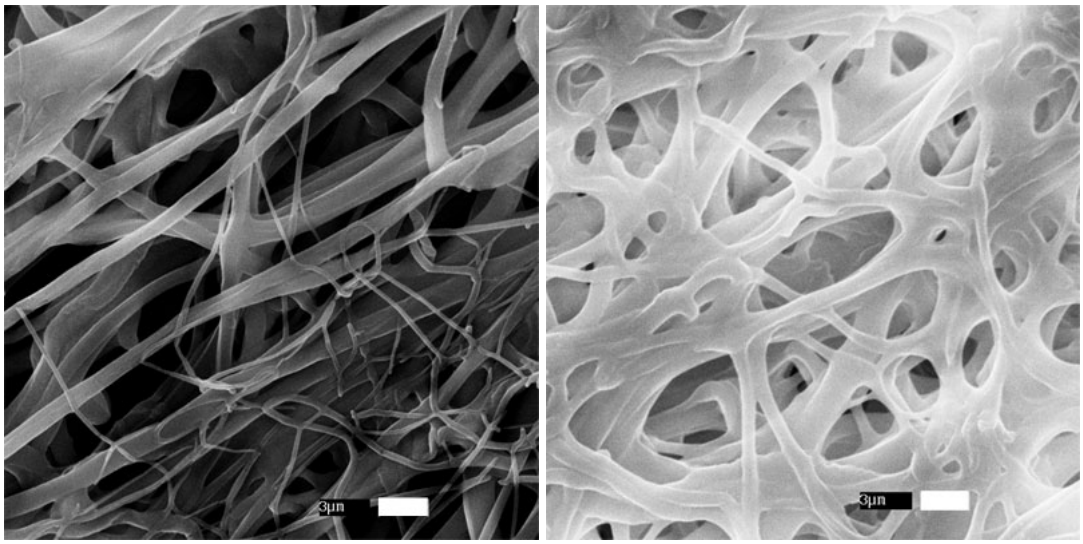

(a) (b)

Figure 3.14: SEM images of cellulose/NMMO/water-PLA/DMF fibers (9wt% cellulose, 22 wt% PLA, 30/70 cellulose/PLA): (a) as-spun; (b) treated with chloroform (scale bars = 3 µm)

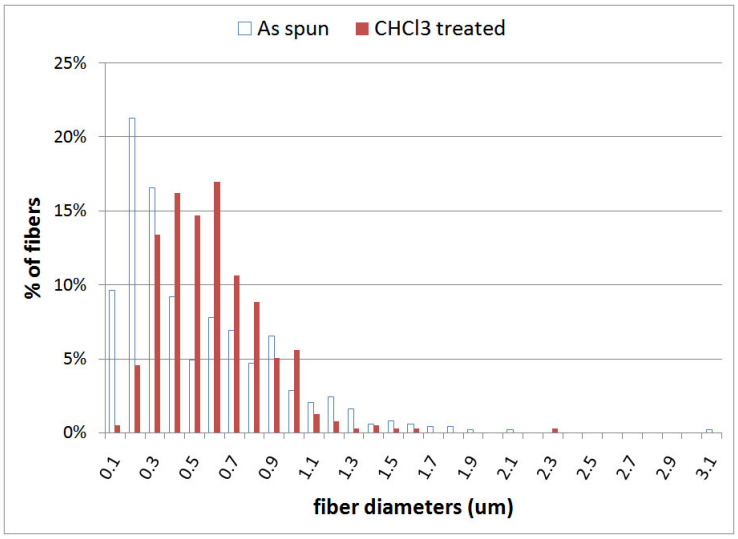

Figure 3.15: Diameter distributions of cellulose/NMMO/water-PLA/DMF fibers: as-spun and after chloroform treatment (fibers shown in Figure 3.14(a) and (b)).

that behaves similarly to the cellulose outer jet (i.e. has reasonably long stable jet region) would have more success in creating coaxial fibers.

Polyacrylonitrile in DMF has been successfully monoaxially electrospun at temperatures ranging from ambient to $88.7\,^{\circ}\mathrm{C}$ [75]. Solution concentrations used for this monoaxial spinning ranged from 5 to 12 wt%, and higher PAN concentrations resulted in a longer stable jet length at elevated temperatures. Accordingly, PAN solutions of 12 - 14 wt% were prepared for coaxial electrospinning.

For these fibers, a slightly lower concentration of cellulose in NMMO/water (8 wt% as compared to the previously used 9 wt%) was used in order to decrease the viscosity of the cellulose/NMMO/water solution and allow for easier electrospinning. In addition to this, the use of a surfactant was investigated. Surfactants have been found to decrease the surface tension of polymeric fluids and produce more uniform fibers [33]. Monoaxial fibers of cellulose were electrospun under these new conditions to first verify that uniform fibers would be obtained.

Figure 3.16 shows monoaxial cellulose fibers electrospun from solutions with and without surfactant added. Fibers were electrospun from 8 wt% cellulose in NMMO/water (Figure 3.16(a)) and 8 wt% cellulose + F88 surfactant (Figure 3.16(b)). The fibers produced with surfactant added were thinner and more uniform; fiber diameters in Figure 3.16(a) were $0.23 \pm 0.15\ \mu\mathrm{m}$ while diameters in Figure 3.16(b) were $0.17 \pm 0.07\ \mu\mathrm{m}$. The solution with the surfactant added was also much easier to electrospin, so surfactant was added in 0.5% mass proportions to cellulose in all following solutions. The F88 Prill surfactant is a polyethylene glycol-polypropylene glycol block copolymer with MW $\sim$11,400

and is water soluble, so should be removed with the NMMO during coagulation. There was no evidence of residual surfactant in the XRD patterns (data not shown).

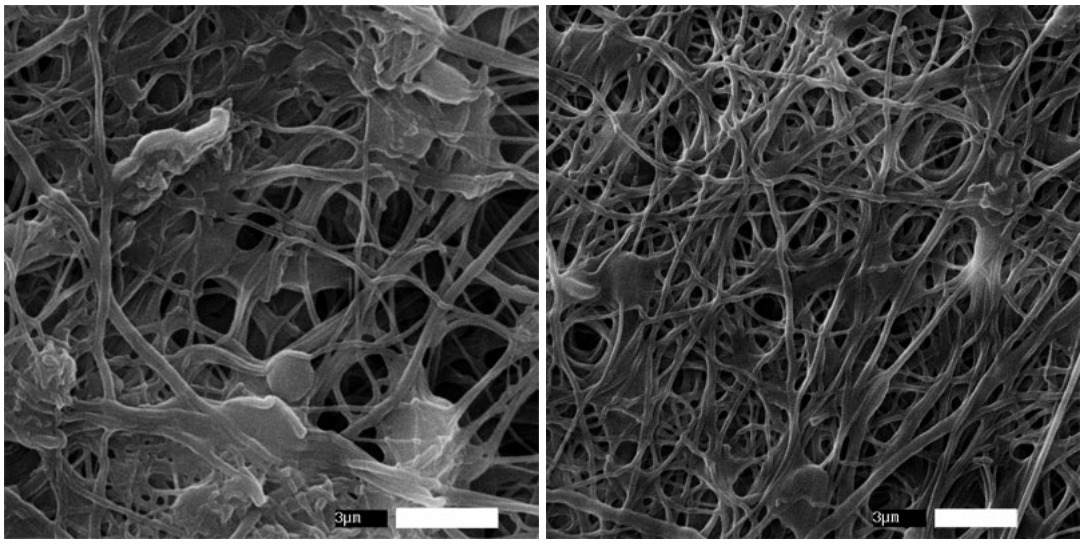

(a) (b)

Figure 3.16: SEM images of 8 wt% cellulose/NMMO/water (monoaxial): (a) without surfactant; (b) with surfactant

Fibers coaxially electrospun from cellulose/NMMO/water and PAN/DMF solutions are shown in Figure 3.17. There are regions of non-uniformity, but this was true of all coaxially electrospun fibers with cellulose/NMMO/water solutions. Fibers were treated with hot DMF in order to selectively remove the PAN from the cores, and SEM images reveal hollow fibers after hot DMF treatment, indicating formation of coaxial fibers (Figure 3.17(b), (d)). By mass, the fibers were about 52% PAN, indicating even fiber compositions. These fibers were spun without the same sort of issues seen with other coaxial systems (such as needle clogging), and a batch of fibers made from this coaxial system were produced for use in an enzymatic hydrolysis study. However, further work must be done to investigate the necessary processing conditions to produce consistently

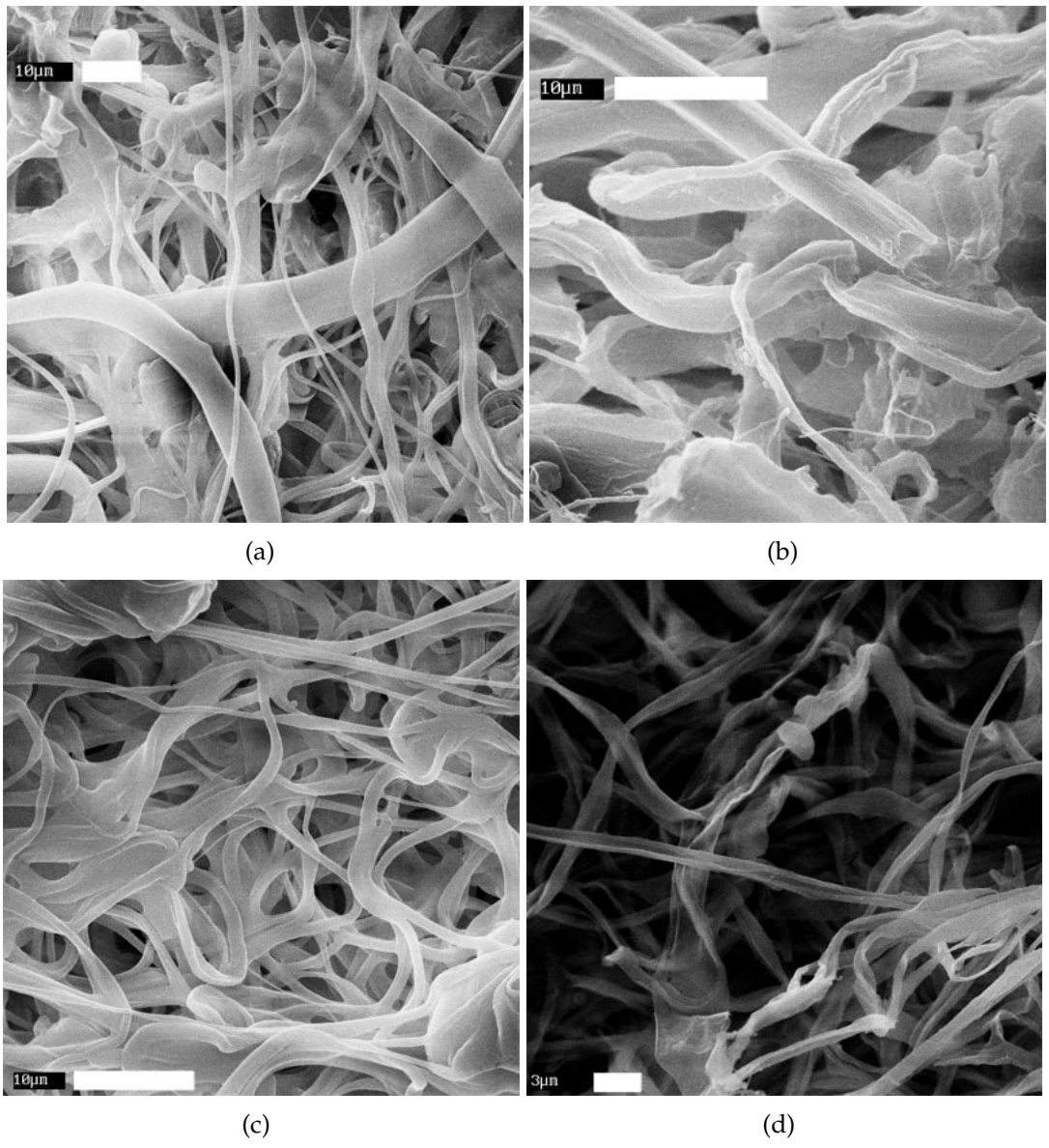

Figure 3.17: SEM images of cellulose/NMMO/water-PAN/DMF fibers: 8% cellulose (+ surfactant), 12 wt% PAN [64/36 cellulose/ PAN] (a) as-spun (scale bar = $10\ \mu m$); (b) treated with hot DMF (scale bar = $10\ \mu m$); 8% cellulose (+ surfactant), 14 wt% PAN [59/41 cellulose/PAN] (c) as-spun (scale bar = $10\ \mu m$ m); (d) treated with hot DMF (scale bar = $3\ \mu m$)

uniform fibers from this coaxial system.

The details of this enzymatic hydrolysis study are presented in Appendix B.3.2. The cellulose-PAN fibers produced appreciable amounts of soluble sugars, unlike the cellulose-CA fibers used in the previous coaxial fiber hydrolysis. Hydrolysis was performed over 48 hrs, and maximum conversion was approximately 30% (Figure B.4), assuming a fairly uniform cellulose composition of 52 wt% in the original fibers. Fiber diameters decreased slightly, but not significantly. Starting fiber diameters were about $0.65 \pm 0.35\ \mu\mathrm{m}$, while fiber diameters after hydrolysis were $0.55 \pm 0.29\ \mu\mathrm{m}$. However, X-ray diffraction patterns of the fibers before and after hydrolysis reveal a more prominent PAN peak after 48 hrs of hydrolysis, indicating that more PAN has been exposed by enzymatic activity (Figure B.5).

The most interesting results from this hydrolysis study came from the SEM analysis. SEM imaging of fibers after 48 hrs of hydrolysis revealed areas where the fibers appeared to be stripped of the cellulose shell (Figure B.6 (a) - (c)), regions of fiber thinning (Figure B.6(d)), and areas where the cellulose shell appeared to be peeling off (Figure B.6 (e) - (g)). The remaining insoluble fractions from earlier conversion data collection points were not kept for SEM analysis so the evolution of the fibers was not documented, but the stripping, thinning, and peeling of the coaxial fibers and the retention of long-range fiber connectivity and fiber morphology indicate that these coaxial fibers may be able to provide new insights into macroscopic degradation of ESC. However, for meaningful results to be obtained, coaxial electrospinning of cellulose-shelled fibers needs to be extended to enable variation of microstructure, and uniformity of coaxial ESC fibers must be ensured.

3.4 Conclusions

Coaxial electrospinning is a method of producing uniquely structured nanofibers with core/shell morphology. It was attempted to entrain low DP cellulose/LiCl/DMAc solutions in various polymeric shells, in order to produce cellulose fibers from an otherwise unspinnable cellulose solution. Cellulose acetate, polylactic acid, and polyacrylonitrile were used as the shell materials. Removal of the shell by selective dissolution indicates that in order to most effectively entrain cellulose/LiCl/DMAc solutions as the core of a coaxial fiber, cellulose acetate should be used as the shell material. However, the use of cellulose acetate as a shell material must be studied further, in order to determine the right cellulose acetate and cellulose solution concentrations that will produce uniform fibers but also retain fiber morphology after removal of the cellulose acetate shell.

Low DP cellulose/LiCl/DMAc was also utilized as a shell material, with a non-hydrolysable polymer placed in the core of the fibers. However, there was limited success obtained with using a non-spinnable solution on the shell-side of coaxial fibers, even though well-spinning solutions such as cellulose acetate and polystyrene were investigated. TEM images showed some evidence of coaxial fibers, but selective dissolution of the core material showed that the fibers were primarily made up of the core materials. A preliminary hydrolysis of fibers made with a cellulose shell and cellulose acetate core showed negligible soluble sugar production, but SEM analysis of the hydrolyzed fibers suggested that some enzyme activity had taken place. The observed pits and surface roughening had not been seen in hydrolysis of monoaxial cellulose fibers, and led to the expectation that coaxial fibers with thicker, more consistent cellu-

lose shells may be able to provide new insights into the physical mechanism of macroscopic cellulose degradation.

Accordingly, cellulose/NMMO/water solutions were also investigated as shell-side materials for coaxial fibers. However, due to the heating required to electrospin this solution, several different potential core materials were rejected. Solutions of cellulose acetate and polystyrene were rejected as core materials because the high temperatures caused drastic lowering of solution viscosity and made the core jet behave very erratically, making coaxial electrospinning difficult and slow. Polylactic acid was also rejected as a core material even though it can be electrospun at elevated temperatures, because selective removal of PLA indicated that the fibers were predominately made of cellulose, and were probably not coaxial. Polyacrylonitrile was utilized as a core material, and could be electrospun successfully at elevated temperatures. The additional changes of using a slightly lower concentration of cellulose and adding a small amount of surfactant to the cellulose solution allowed for easier electrospinning of cellulose both monoaxially and coaxially with the PAN core. These coaxially spun fibers showed reasonable conversion when exposed to cellulase enzymes, and show opportunity for further insight into the mechanisms of cellulose hydrolysis.

There is still much work to be done to produce uniformly coaxial fibers from cellulose solutions. Use of a well-spinning shell material to entrain low DP cellulose in LiCl/DMAc solutions has had some success, but more work must be done to retain the fiber morphology after removal of the non-cellulose shell by selective dissolution. Placement of cellulose/NMMO/water solutions on the shell-side of coaxial fibers has also been demonstrated, but the fiber uniformity

needs to be optimized. Also, it would be ideal to extend the current work on fibers with shells made from cellulose/NMMO/water solutions to include variations in cellulose microstructure as shown in Chapter 2. Much work must be done to find the proper electrospinning conditions to vary the DP and crystallinity of the cellulose and to vary the fiber diameters in coaxial electrospinning. However, once this is accomplished, it is likely that these coaxial cellulose fibers will be able to provide new insights into cellulose degradation by cellulase enzymes and how the cellulose microstructure affects this process.

APPENDIX A

HYDROLYSIS OF MONAXIAL FIBERS

The following hydrolysis experiments were primarily conducted by John W. Dingee (Cornell University, Chemical Engineering PhD 2009), in the lab of Dr. David Wilson, Microbiology, Cornell University.

A.1 Introduction

These studies utilize the electrospun cellulose (ESC) fibers in enzymatic hydrolysis studies, as a proof-of-concept for the viability of ESC as a model cellulose substrate. Important in these considerations are the binding of cellulase enzymes to the ESC fibers and the hydrolysis kinetics. In order for ESC to be a suitable model substrate for enzymatic hydrolysis, cellulase enzymes must be able to bind to and hydrolyze it in a similar manner to other insoluble cellulose substrates. Binding of cellulases to cellulose is considered to be a critical step in cellulose hydrolysis [76, 77]. Binding to and hydrolysis of ESC by cellulase enzymes may not proceed as for more typical cellulose substrates, due to both the carefully controlled microstructure and the change in crystal structure of the fibers upon electrospinning.

These preliminary studies utilize a single cellulase enzyme, Cel5A, for binding and hydrolysis. Cel5A is an endocellulase from *Thermobifidia fusca* (formerly known as E5), with molecular weight of 46.3 kDa and isoelectric point of 4.5 [78, 79]. *Thermobifidia fusca* is a thermophilic actinomycete that has a high level of cellulase activity when grown on cellulose [79], and Cel5A has a high activity

on carboxymethylcellulose (CMC), which is an indication of a highly active endocellulase [62]. The advantage of using a bacterial cellulase versus a generally more active fungal cellulase is in ease of purification. The bacterial cellulase gene can be placed on a plasmid and expressed in a bacterial species such as *Streptomyces lividans* [78], allowing for harvesting of pure protein species. These studies aim at creating a very basic model for cellulose hydrolysis, upon which further layers of complexity can be added gradually; therefore a single cellulase enzyme is utilized rather than the mixture of enzymes that is commonly required to completely hydrolyze a cellulose substrate.

A.2 Experimental Methods

A.2.1 Protien Production and Purification

S. lividans strain PGG74 expressing Cel5A was grown as described by Jung *et al.* [77] in a 10 liter culture for 2-3 days at dissolved oxygen levels no less than 30%, impeller speeds of 300-320 rpm, pH of 7.0 and 7.5, and aeration rates of $12\,\mathrm{l/min}$. The production culture was harvested by centrifugation at 4,000 rpm for 30 min at $5\,^{\circ}\mathrm{C}$. The supernatant was collected and poured over glass wool, and ammonium sulfate (AS) and PMSF were added to 1.2 M and 0.1 mM, respectively. The supernatant was then clarified by centrifugation at 8,000 rpm for 30 min at $5\,^{\circ}\mathrm{C}$. This supernatant was collected and clarified by depth microfitration using a $2\,\mu\mathrm{m}$ Cuno BetaPure polyolefin cartridge, item number AU09Z13NG020 (Cuno Inc, Meriden CT).

The filtrate was further purified at $5\,^{\circ}\mathrm{C}$ as described by Irwin *et al.* [80] us-

ing a P-Sepharose hydrophobicity column followed by a Q-Sepharose anion-exchange column with the following modifications. The loaded P-Sepharose column was washed with 1-column volume of 1.2 M AS, 2-column volumes of 0.6 M AS, 10 mM NaCl, and 5 mM Kpi, pH 6.0, followed by 3-column volumes of 0.3 M AS, 5 mM NaCl, and 5 mM Kpi, pH 6.0, and eluted with 3-column volumes of 5 mM Kpi, pH 6.0. The loaded Q-Sepharose column was eluted with a 6-column volume gradient of 0-0.3 M NaCl, 1-10 mmho, in 10 mM BisTris of pH 5.5, followed by a 2-column volume wash with 0.5 M NaCl and 10 mM BisTris, 20 mmho, pH 5.5.

Purified Cel5A was exchanged into standard buffer (50 mM NaAc and 0.02% NaAz, pH 5.5) and concentrated to roughly 60 μM using a stirred cell ultrafiltration chamber with a polyethersulfone 10 kDa MWCO ultrafiltration membrane (Millipore, Billerica, MA). All purified cellulase concentrations were determined spectrophometrically with published extinction coefficients [78]. The resulting protein was stored at -$70\ ^{\circ}\mathrm{C}$.

A.2.2 ESC Production and Characterization

Cellulose was electrospun from solutions of cellulose/N-methylmorpholine-N-oxide(NMMO)/water as described in Chapter 2. Degree of polymerization (DP) 210 cellulose (Whatman CF-11 powder) was dissolved in 85/15 NMMO/water (w/w) at concentrations of 9 wt%.

ESC was characterized before and after hydrolysis for fiber diameter, crystallinity, and crystal structure. Fiber diameter and morphology was observed via scanning electron microscope (LEICA 440 SEM). Wide angle X-ray scatter-

ing (WAXS, Scintag, Inc. Theta-Theta Diffractometer) was used to determine the crystal structure and degree of crystallinity of the samples. The degree of crystallinity was obtained by taking the area ratio of the crystalline phase to the sum of the crystalline plus amorphous phases, which was obtained after deconvolution of each peak in the WAXS patterns [46].

A.2.3 Binding Assays

Cel5A was bound to electrospun cellulose in 2-ml screw-cap centrifuge tubes and rotated end-over-end at $5\,^{\circ}\mathrm{C}$ with $10\,\mathrm{mg/ml}$ ESC or $1\,\mathrm{mg/ml}$ BMCC and varying amounts of Cel5A in standard buffer. All materials were pre-chilled for 24 hrs at $5\,^{\circ}\mathrm{C}$, and all reactions were carried out in triplicate. Duplicate enzyme and buffer blanks and single substrate blanks were made for each concentration. After binding for 2 hrs, the tubes were centrifuged at $5\,^{\circ}\mathrm{C}$ and 13,000 rpm for 10 min to form pellets. The supernatant was removed from the pellet, centrifuged again, and a second supernatant collected. These supernatants were analyzed for protein concentration by A280 and the extinction coefficient for Cel5A, 97,100 M^{-1}.

A.2.4 Hydrolysis Assays

ESC was hydrolyzed at $50\,^{\circ}\mathrm{C}$ in 2-ml screw-cap centrifuge tubes rotated end-over-end, each with a total volume of 1.6 ml containing $4\,\mathrm{mg/ml}$ ESC and $1\,\mu\mathrm{M}$ Cel5A in standard buffer. Substrate was pre-suspended in buffer for 24 hrs prior to hydrolysis, and all reactions were carried out in triplicate. Duplicate enzyme

and buffer blanks and single substrate blanks were made for each time point. At each time point, triplicate sample tubes along with their respective blanks were centrifuged at room temperature at 13,000 rpm for 5 min to form pellets. The supernatant was removed, centrifuged again, and a second supernatant was then collected. The second supernatant was then analyzed for reducing end concentration using the p-hydroxybenzoic acid hydrazide (PAHBAH) assay and for sugar composition using the thin layer chromatography (TLC) assay, both described by Irwin *et al.*[80]. The remaining pellets were resuspended in distilled water, vortexed, and centrifuged again at 13,000 rpm for 5 min. This washing procedure was repeated 3 times. The wet pellets were frozen with dry ice and lyophilized for 3 days before being analyzed with SEM.

A.3 Results and Discussion

In spite of electrospun cellulose's purity and apparent microstructural homogeneity, it is not a naturally occurring form of cellulose. The intricate production history of ESC fibers, including cellulose dissolution and electrospinning, may produce a form of cellulose with unusual reactivity for hydrolysis, either increasing or decreasing it relative to other substrates. Here, the binding and hydrolysis of ESC is investigated using a purified cellulase, Cel5A, from the thermophilic soil bacteria *Thermobifida fusca* [81]. These initial studies have validated the applicability of ESC as an insoluble substrate for cellulases and shown that it is sufficiently hydrolyzed by *T. fusca* Cel5A at rates and yields comparable to other non-electrospun insoluble substrates such as BMCC and Avicel. Thus, ESC offers a uniquely controlled insoluble substrate for kinetic study. The ESC used for these preliminary studies was made from DP 210 cellulose dissolved

in NMMO/water, and had an average diameter of $0.5\ \mu m$ and crystallinity of about 50%.

A.3.1 Binding of Cel5A to ESC

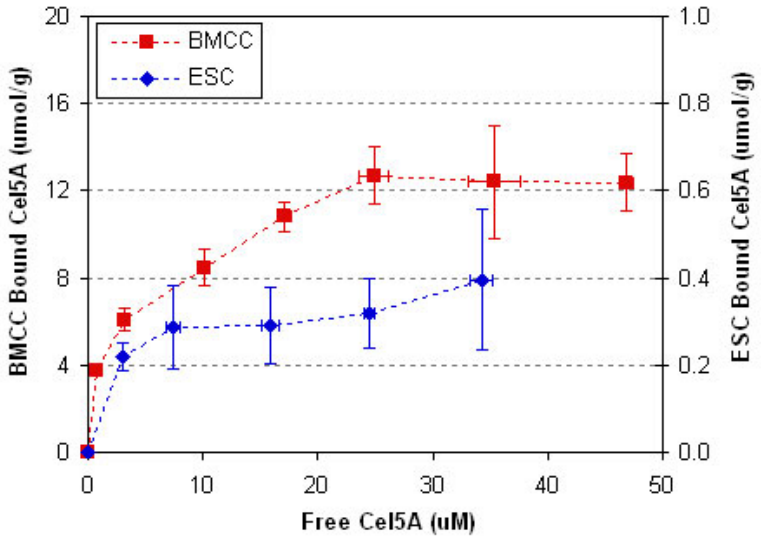

Figure A.1: Binding isotherms for electrospun cellulose (ESC) as compared to BMCC.

This study, along with other preliminary hydrolysis experiments, indicates that ESC is hydrolyzed at a rate comparable to, if not greater than, BMCC under equal substrate mass concentrations, but with much less Cel5A bound. Binding isotherms for Cel5A adsorbing to ESC and BMCC at $5\ ^{\circ}C$ were measured in order to better understand this behavior. Although these isotherms are not applicable in kinetic descriptions of binding at hydrolysis temperatures of $50\ ^{\circ}C$, they are representative of the maximum binding capacity of each substrate. The resulting isotherms (Figure A.1) indicate a much lower binding capacity for the ESC substrate ($0.3\ \mu mol/g$) compared to BMCC ($12\ \mu mol/g$). For the electrospun

fibers, this explains, in part, the lower concentration of bound enzymes during hydrolysis. Furthermore, if it is assumed that the these ESC fibers are on average $0.5\ \mu\mathrm{m}$ in diameter with a density comparable to microcrystalline cellulose [82] and that cellulases have an average footprint of $30\ \mathrm{nm}^2$, then the saturation binding of Cel5A observed here at $0.3\ \mu\mathrm{mol/g}$ corresponds roughly to a complete coverage of the superficial outer area of the cylindrical ESC fibers. ESC has a surface area of about $5.5\ \mathrm{m}^2/\mathrm{g}$, while BMCC has a surface area of about $200\ \mathrm{m}^2/\mathrm{g}$ [3]. The binding capacity of Cel5A for each of the substrates is roughly proportional to the specific surface area for the substrate, which indicates that Cel5A binds to ESC much as it binds to other, more typical insoluble cellulose substrates. This suggests that Cel5A may not be able to penetrate the fiber surface, allowing for the use of a simplified kinetic model for hydrolysis involving a moving boundary in a cylindrical coordinate. A factor not taken into consideration here was the drying of the cellulose sample, and what effect (if any) that may have on pore size and cellulose accessibility to the enzymes. In general, the fibers used in these studies were air-dried overnight before being hydrolyzed, which may have had the effect of collapsing larger pores in the fibers [30] and preventing the enzymes from accessing more than the fiber surface. However, as will be shown in the following section, the drying did not seem to drastically reduce the hydrolysability of the electrospun fibers. It would be worthwhile to investigate what effects drying ESC has on the enzymatic hydrolysis, and to investigate various drying schemes. These could include air drying, freeze drying, oven drying, and also hydrolysis of never-dried fibers.

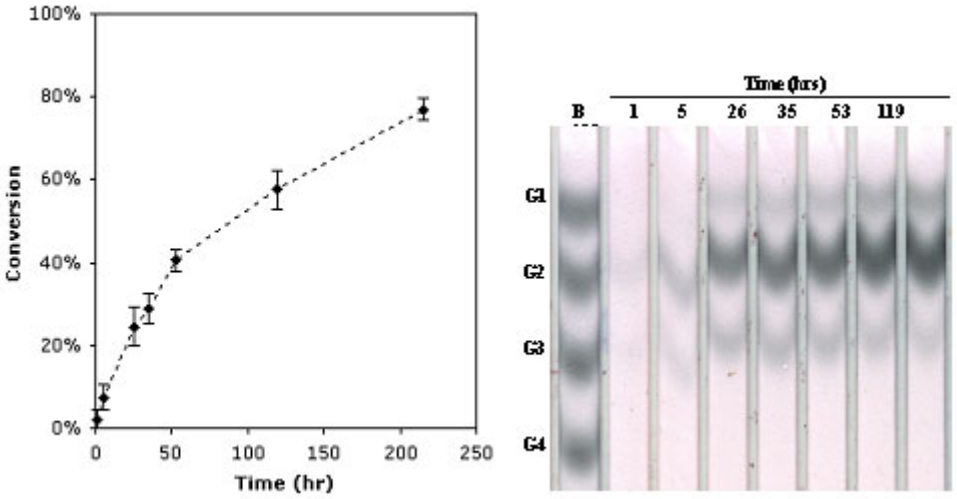

(a) (b)

Figure A.2: ESC Hydrolysis by *T. fusca* Cel5A: (a) Conversion of ESC (4 mg/ml) to soluble products with a total of $1\ \mu$ M Cel5A present at $50\ ^{\circ}\mathrm{C}$. (b) Hydrolysis product compositions as determined by TLC. A bench (B) on the left indicates cello-oligosaccharides G1-G4. Product compositions with increasing time are shown left to right. The band intensities are approximate by proportion to the amount of product mass present.

A.3.2 ESC Hydrolysis by Cel5A

ESC hydrolysis by *T. fusca* Cel5A at $50\ ^{\circ}\mathrm{C}$ was characterized regarding product formation and substrate microstructure with an initial enzyme concentration of $1\ \mu$M and initial substrate concentration of 4 mg/ml. Hydrolysis proceeds in much the same way as hydrolysis of other insoluble substrates; soluble products are released quickly on a short timescale, followed by a gradual decrease in the hydrolysis rate with an appreciable amount of substrate still remaining (Figure A.2(a)). Soluble sugar composition was roughly quantified using a TLC assay. As shown in Figure A.2(b), the initial products of hydrolysis are cellobiose

(G2) and cellotriose (G3), with little or no glucose (G1). Product composition gradually shifts to a G2-dominated product with an increasing fraction of G1 and decreasing fraction of G3. These findings suggest G2 and G3 are the dominant products of Cel5A hydrolysis, with G3 hydrolysis to G2 and G1 proceeding at a slower rate than the overall process. This is consistent with homogeneous Cel5A cellooligosaccharide hydrolysis data reported previously by Barr [61]. Soluble sugar products were quantified by their reducing ends using a PAH-BAH assay and a mass balance was approximately completed by assuming an average 1:8:1 ratio of G1:G2:G3 products.

At the macroscopic level, a gradual deterioration or fragmentation of the substrate is observed over time, consistent with other insoluble substrates such as Avicel [62], BMCC [63], and filter paper. In the current study, this deterioration becomes apparent at around 40% conversion. At about the same time, the remaining substrate begins to precipitate into two phases after washing and lyophilization. While some of the substrate remains in its original filter paper-like consistency, a second portion of the substrate begins to aggregate in a separate phase, with a considerably lower density. This later phase begins to dominate the remaining insoluble substrate fractions as hydrolysis approaches 100%.

SEM analysis of the remaining insoluble fractions at various degrees of hydrolysis reveals moderate microstructural changes after 20% hydrolysis with increasingly visible deterioration as hydrolysis approaches 100% (Figure A.3). The principle result of enzyme exposure is the fragmentation of cellulose fibers and a loss of long-range fiber connectivity. This fiber-cutting process leads to the sedimentation of a secondary pellet during centrifugation, apart from the initial ESC pellet, that is a combination of short fiber segments and more recalcitrant

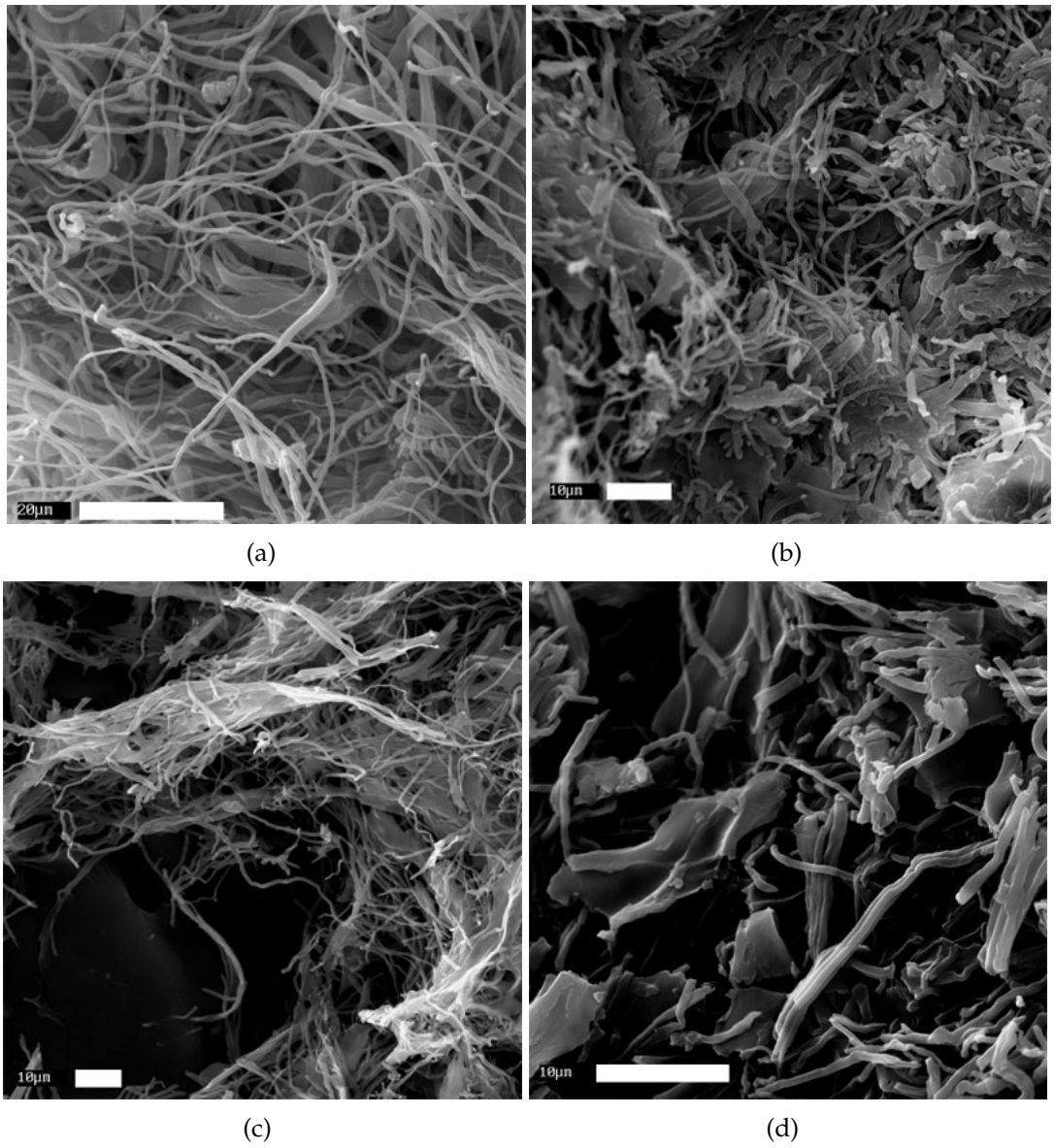

(a) (b)

(c) (d)

Figure A.3: SEM images of electrospun fibers after exposure to *T. fusca* Cel5A, experiment 1: (a) 1 hr with 2% conversion (scale bar = $20\ \mu\mathrm{m}$); (b) 35 hrs with 29% conversion (scale bar = $10\ \mu\mathrm{m}$); (c) 53 hrs with 40% conversion (scale bar = $10\ \mu\mathrm{m}$); (d) 215 hrs with 77% conversion (scale bar = $10\ \mu\mathrm{m}$). Hydrolysis data corresponding to these images is shown in Figure A.2.

cellulose structures present as spinning defects that have been freed from the fiber matrix. Furthermore, increased surface charging of the secondary pellet by the SEM suggests that these precipitates may have a rough surface texture caused by enzyme activity. The kinetics of the cutting process and its relation to fiber diameter, in addition to other fiber properties, and the cause of the observed characteristic segment length of $10\ \mu\mathrm{m}$ warrant further study.

A.3.3 Effect on Crystallinity and Fiber Diameter

A second set of ESC hydrolyzed by *T. fusca* Cel5A at $50\ ^{\circ}\mathrm{C}$ was characterized with respect to changes in crystallinity and fiber diameter. Hydrolysis was performed in the same manner as the previous ESC hydrolysis study. The degree of polymerization of these fibers was 210, average fiber diameter was $1.0 \pm 0.4\ \mu\mathrm{m}$, and average crystallinity was $62 \pm 11\%$. The effect of hydrolysis on overall fiber morphology was similar to the previous study despite the larger fiber diameter. Figure A.4 shows the evolution of fiber morphology as hydrolysis progressed. One sample of ESC was allowed to remain in contact with enzymes for > 7 days, and Figure A.5(f) shows how the ESC sample has been reduced to the non-uniformities created by defects during the electrospinning process such as films, "plates", and merged fibers. Again, a loss of long-range fiber connectivity is seen as hydrolysis proceeds, and fibers are cut rather than thinned as might be expected if hydrolysis is proceeding as a moving boundary along a cylindrical coordinate as was suggested by the binding assay.

Figure A.4: SEM images of electrospun fibers after exposure to *T. fusca* Cel5A, experiment 2. (a) before hydrolysis; (b) 1 hr; (c) 4 hrs; (d) 24 hrs; (e) 48 hrs; (f) > 7 d. Scale bars are $10\ \mu\mathrm{m}$.

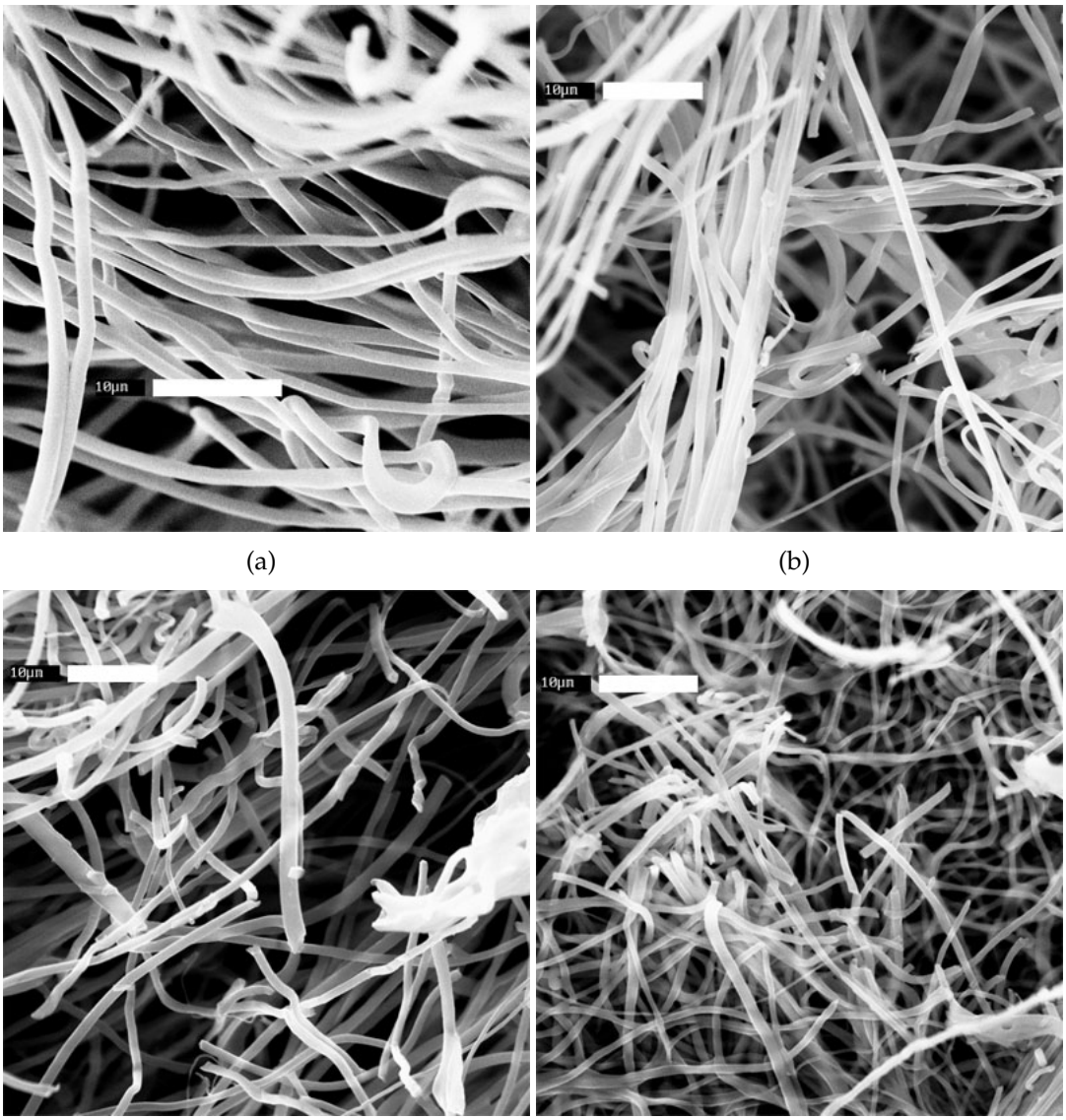

(a) (b)

(c) (d)

Figure A.4: (continued)

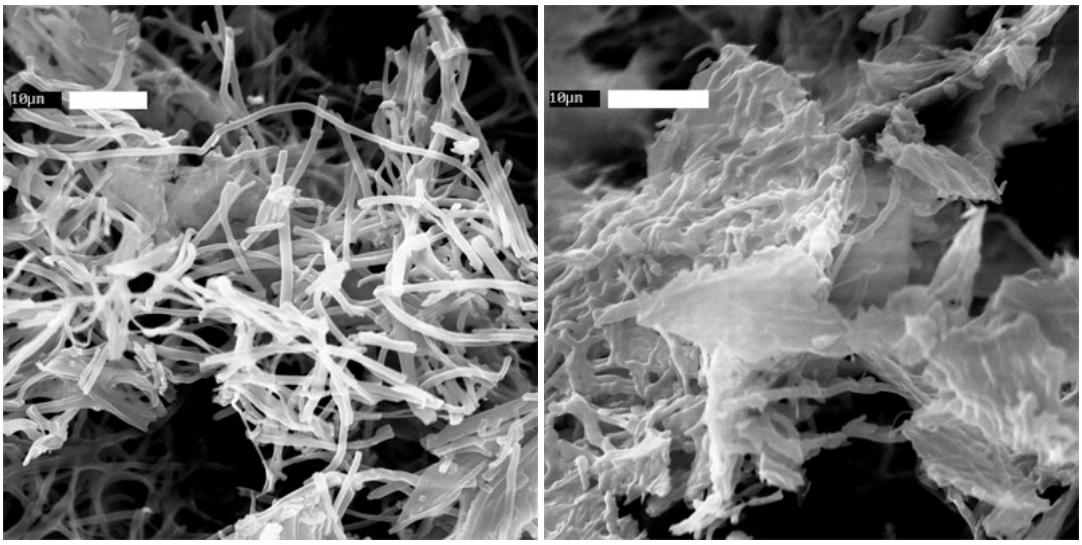

(e) (f)

The crystallinity of the fibers over the course of hydrolysis is mapped out in Figure A.5(a). Fiber crystallinity increases rapidly after the start of hydrolysis, but levels off to about 70% after 4 hours. This increase in crystallinity is caused by the enzyme activity and not merely by exposure to the buffer solution, as shown by the crystallinity of the substrate blanks in Figure A.5(a). There is a slight but insignificant increase in crystallinity of the ESC that was used as substrate blanks. This indicates that some amorphous cellulose may be more readily hydrolyzed than crystalline cellulose. However, since hydrolysis continues even though the crystallinity does not continue to change significantly, it is likely that after a certain point amorphous and crystalline cellulose are hydrolyzed at nearly equal rates. The drop in crystallinity at time points 3 and 4 are probable due to inhomogeneities of the cellulose samples, and it is likely that the starting cellulose samples were less crystalline than those evaluated at different time points.

The diameter of the fibers over the course of hydrolysis is shown in Figure A.5(b), and does not change as hydrolysis proceeds. This was expected from a qualitative inspection of the SEM images shown in Figure A.4. The stability of fiber diameter raises questions about the physical mechanism of cellulose hydrolysis, as the enzymes appear to cut in the middle of fibers, and then shorten the fiber segments created. Figure A.5(e) is similar to Figure A.3(d), and it is possible that the presence of the $\sim 10\ \mu\mathrm{m}$ long recalcitrant fragments is due to some artifact introduced by the electrospinning process. It is also possible that the apparent lack of fiber thinning is a result of the post-hydrolysis processing, where sections of fiber that have been attacked by the cellulase enzymes are mechanically weaker and thus break apart during the centrifugation that is done to separate the insoluble cellulose from the soluble sugar products.

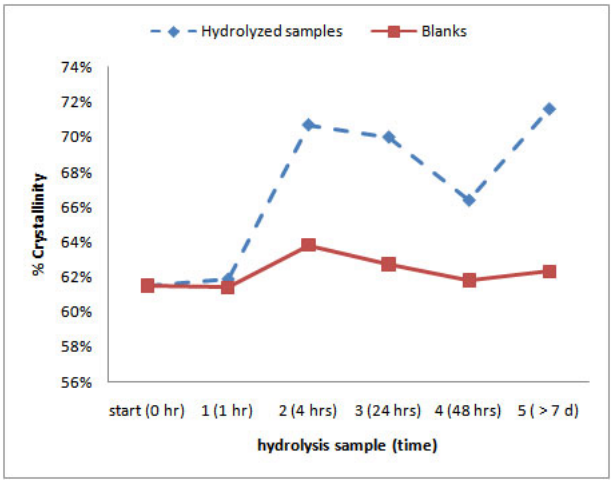

(a)

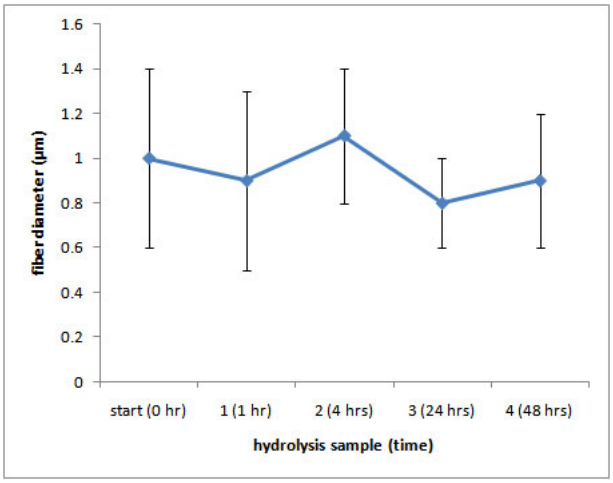

(b)

Figure A.5: Progression of (a) crystallinity and (b) fiber diameter as hydrolysis proceeds; fiber morphologies can be seen in Figure A.4.

A.4 Conclusions

Although ESC is not a natural form of cellulose, it can be successfully hydrolyzed by cellulase enzymes. The binding of Cel5A to ESC is much lower than to BMCC, but it appears that Cel5A completely covers the outer surface of the cellulose fibers. In general, BMCC has a much higher surface area than ESC,

and the binding capacity of Cel5A for each of the substrates is roughly proportional to the surface area of the substrate, indicating that Cel5A binds to ESC at least as well as it binds to natural insoluble cellulose substrates, if not better. However, the effect of drying the ESC substrate on binding and subsequent hydrolysis should also be investigated. Specifically, the effects of different drying schemes (such as using never-dried fibers, air-dried, oven-dried, or freeze-dried fibers) on enzyme binding and hydrolysis should be looked into to determine if the drying scheme of ESC had any significant impact on the hydrolysis kinetics.

The hydrolysis of ESC by Cel5A also proceeds similarly to more typical insoluble substrates, which indicates that ESC is a valid substrate for modeling cellulose hydrolysis. This was important to validate, as the carefully controlled microstructure of ESC and the processing it undergoes in electrospinning may give ESC an unusual reactivity for hydrolysis. However, some interesting observations of the macroscopic fiber morphology warrant further investigation. The binding of Cel5A indicates that the cellulase does not penetrate into the cellulose fibers, and supports the idea of a moving boundary of hydrolysis along the cylindrical coordinate of the fibers. Despite this, a thinning of the fibers is never seen. Instead, loss of long-range fiber morphology by fiber splicing is seen as hydrolysis progresses. It is possible that some of the post-hydrolysis processing required to separate the soluble products from the insoluble cellulose remaining is causing breakup of the fibers, and it is also possible that electrospinning introduces some artifacts into the fiber microstructure that cannot be observed via SEM or X-ray diffraction.

The hydrolysis study that looked at the evolution of crystallinity and fiber diameter indicated that some amorphous cellulose is more readily hydrolyzed

than crystalline cellulose, but crystallinity leveled off quickly as hydrolysis proceeded. A more in-depth crystallinity study is desired, with ESC that has a smaller deviation of crystallinity. This will require overcoming some of the electrospinning processing conditions that were described previously. Fiber diameter does not change over the course of hydrolysis, although some thinning was expected from the binding assay. Two fiber diameters were looked at, $0.5\ \mu\mathrm{m}$ and $1.0\ \mu\mathrm{m}$, and both sets of fibers showed similar changes in morphology as hydrolysis progressed. These studies show the potential of utilizing ESC as a model cellulose substrate, but ESC must be produced in batches that are distinctly different in microstructural features in order to be able to make any substantial conclusions about the effect of such microstructural features on cellulose hydrolysis.

APPENDIX B

HYDROLYSIS OF COAXIAL FIBERS

The following hydrolysis experiments were primarily conducted by John W. Dingee (Cornell University, Chemical Engineering PhD 2009), in the lab of Dr. David Wilson, Microbiology, Cornell University.

B.1 Introduction

These studies utilize coaxially electrospun cellulose (ESC) fibers in enzymatic hydrolysis studies, to determine the advantages, if any, of utilizing coaxial fibers over monoaxial fibers as a model substrate for enzymatic hydrolysis. The viability of using monaxially electrospun cellulose has already been demonstrated in the work described in Appendix A. These studies also use a single endocellulase enzyme, Cel5A, for hydrolysis.

Previous work with monoaxial ESC demonstrated that while the kinetics of ESC hydrolysis are similar to that of other insoluble substrates, the macroscopic changes to the cellulose substrate cannot be easily explained. In particular, loss of long-range fiber connectivity and fragmentation were present in hydrolyzed monoaxial ESC (Figure A.3(d), Figure A.5(e) and (f)). It is possible that the presence of $\sim 10\ \mu\mathrm{m}$ segments at the end of hydrolysis may be caused by artifacts created by the electrospinning process, but fiber thinning is never observed during the course of hydrolysis as fiber diameters remain essentially constant (Figure A.5(b)). However, binding studies indicated that the cellulase enzymes cover only the superficial surface area of the ESC fibers (Figure A.1),

suggesting that the enzymes cannot penetrate the fiber surface and should work from the outside in. This should lead to thinning of the fibers over the course of hydrolysis. One possibility is that the fibers are mechanically weakened due to the enzymatic action, and during the post-hydrolysis treatment (centrifugation to separate the supernatant with products from the remaining insoluble cellulose fraction and washing) these weakened parts of the fibers are broken apart. If this is the case, then coaxial fibers with a cellulose shell and a strong, non-hydrolysable core should retain the long-range fiber connectivity throughout hydrolysis and may provide the means for obtaining new insights into the physical mechanisms of cellulose degradation on a more macroscopic level.

These studies take coaxial fibers created with a cellulose shell as described in Chapter 3.3.2 and uses them in hydrolysis studies, in order to obtain a first look at how cellulose is degraded.

B.2 Experimental Methods

Protein production and purification, and hydrolysis assays were carried out as described in Appendix A; coaxial ESC was produced as described in Chapter 3. Coaxial ESC produced from cellulose/lithium chloride (LiCl)/ dimethylacetamide (DMAc) - cellulose acetate (CA)/DMAc/acetone and cellulose/N-methylmorpholine-N-oxide (NMMO)/water-polyacrylonitrile (PAN)/ dimethylformamide (DMF) were used for these studies. ESC was characterized via scanning electron microscope (LEICA 440 SEM) and wide angle X-ray scattering (WAXS, Scintag, Inc. Theta-Theta Diffractometer).

B.3 Results and Discussion

B.3.1 Hydrolysis of ESC made from cellulose/ LiCl/ DMAc and CA/ DMAc/ acetone

ESC was electrospun using 6 wt% cellulose in LiCl/DMAc as a shell material and 28 wt% CA in DMAc/acetone as a core material. The fibers had an average diameter of 0.4 ± 0.3 μm, and the exact composition of the fibers was unknown, but the fibers were suspected to be predominately cellulose acetate (see Chapter 3.3.2).

Hydrolysis was conducted over 48 hrs, and the PAHBAH assay was used to determine the reducing end concentration. PAHBAH relies on a spectrophotometric method to determine reducing end concentration [80], but the reducing end concentration in the supernatant was too small to be detected by this method, and fiber diameters did not change significantly over the course of hydrolysis (Figure B.1). However, SEM analysis of the hydrolyzed fibers revealed some instances of interesting pitting and surface roughening that was not observed with monoaxial cellulose fibers (compare Figure B.2 to Figures A.3 and A.4).

It is possible that some of the uneven surfaces seen in Figure B.2 (especially in the almost bead-like appearance of fibers in Figure B.2(d)) are due to artifacts introduced by the coaxial electrospinning process. However, the kind of pitting seen in Figure B.2 (a) and (c) have not been seen previously with monoaxial cellulose fiber hydrolysis, and may be due to enzyme activity on a fiber substrate that will not lose its overall fiber connectivity as hydrolysis proceeds. Despite

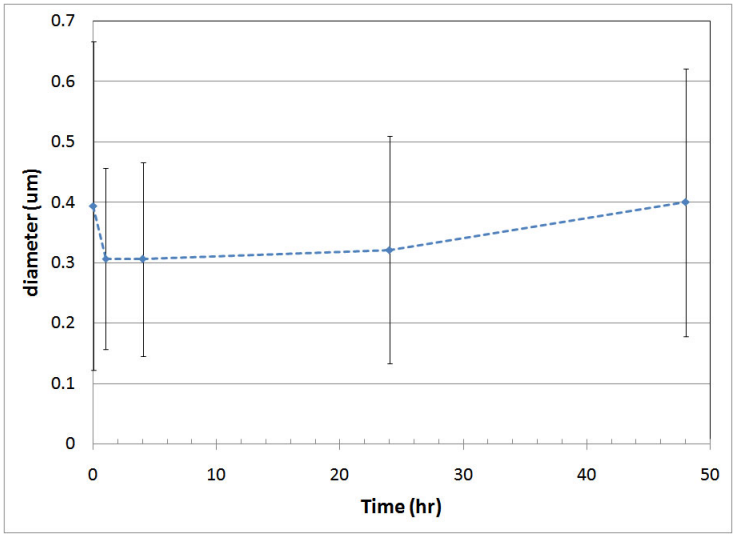

Figure B.1: Fiber diameters of hydrolyzed cellulose-CA fibers as hydrolysis proceeded.

this possibility, pitting was not commonly seen in the hydrolyzed fibers.

The crystallinity of the remaining insoluble fiber pellets was also analyzed over the course of hydrolysis, and the X-ray diffraction patterns are shown in Figure B.3 Actual crystallinity of the fibers was difficult to determine, as the CA peaks overlap the amorphous cellulose peak. However, there was little evolution of the X-ray diffraction patterns with time, and the combination of neglible change in X-ray diffraction pattern with hydrolysis time, scarcity of pitting, negligible decrease in fiber diameter over the course of hydrolysis, and negligible sugar production confirms the lack of cellulose present on the fiber surface. This lack of evidence of enzymatic activity made it difficult to make any definitive conclusions on how the cellulase enzymes behave with the fibers.

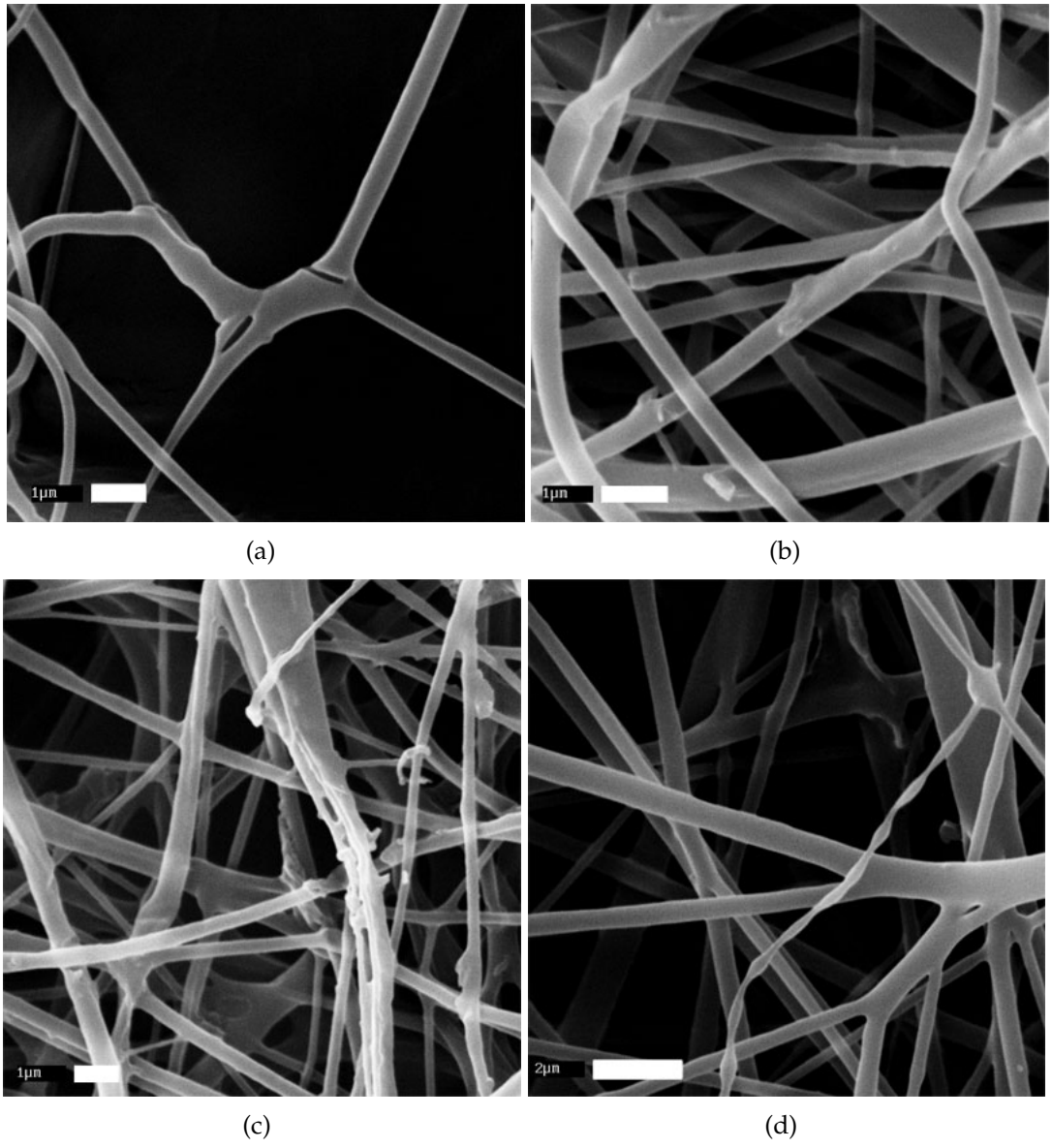

(a) (b)

(c) (d)

Figure B.2: SEM images of hydrolyzed cellulose-cellulose acetate coaxial fibers: (a) after 1 hr of hydrolysis (scale bar = $1\ \mu\mathrm{m}$); (b) after 4 hrs of hydrolysis (scale bar = $1\ \mu\mathrm{m}$); (c) after 24 hrs of hydrolysis (scale bar = $1\ \mu\mathrm{m}$); (d) after 48 hrs of hydrolysis (scale bar = $2\ \mu\mathrm{m}$)

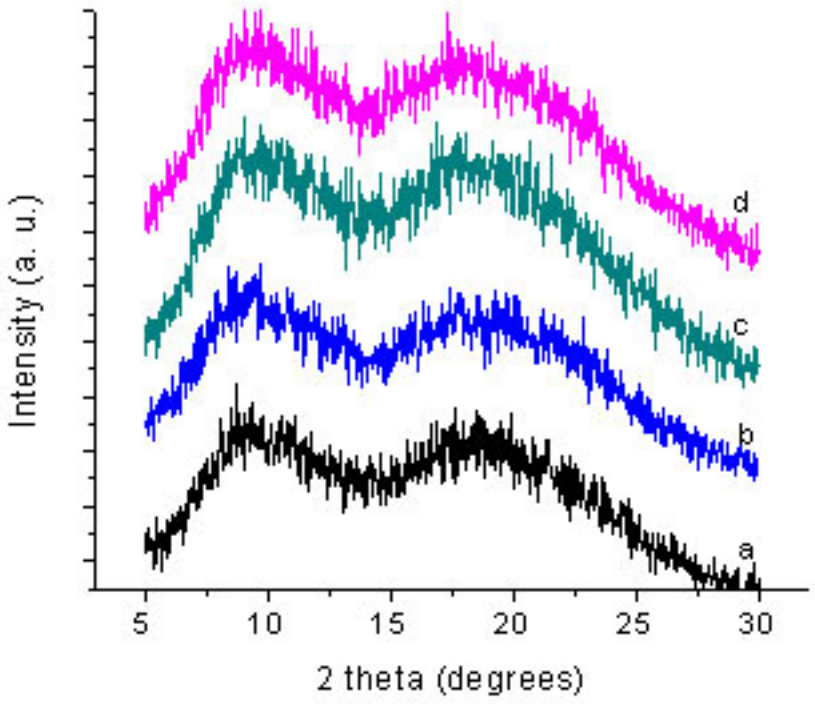

Figure B.3: X-ray diffraction patterns for hydrolyzed cellulose-CA fibers: (a) after 1 hr; (b) after 4 hrs; (c) after 24 hrs; (d) after 48 hrs.

B.3.2 Hydrolysis of ESC made from cellulose/ NMMO/ water and PAN/ DMF

ESC was electrospun using 8 wt% cellulose in NMMO/water with F88 Prill surfactant as a shell material and 14 wt% PAN in DMF as a core material. The fibers had an average diameter of $0.65 \pm 0.35\ \mu\mathrm{m}$, and the exact composition of the fibers was unknown, but removal of the core with hot DMF treatment suggested the fibers were about 50% by mass (see Chapter 3.3.2).

Hydrolysis was conducted over 48 hrs, and the PAHBAH assay was again used to determine the reducing end concentrations. Figure B.4 shows the con-

version as a function of time, and is very similar to the conversion plot seen in Figure A.2(a). The conversion after 48 hrs had only reached 29%, but this is comparable to the 40% conversion reached after 53 hrs in the monoaxial hydrolysis (Appendix A). The detectable and reasonable amounts of product production with these coaxial fibers were encouraging as to the use of these coaxial fibers as a new model substrate for cellulose hydrolysis.

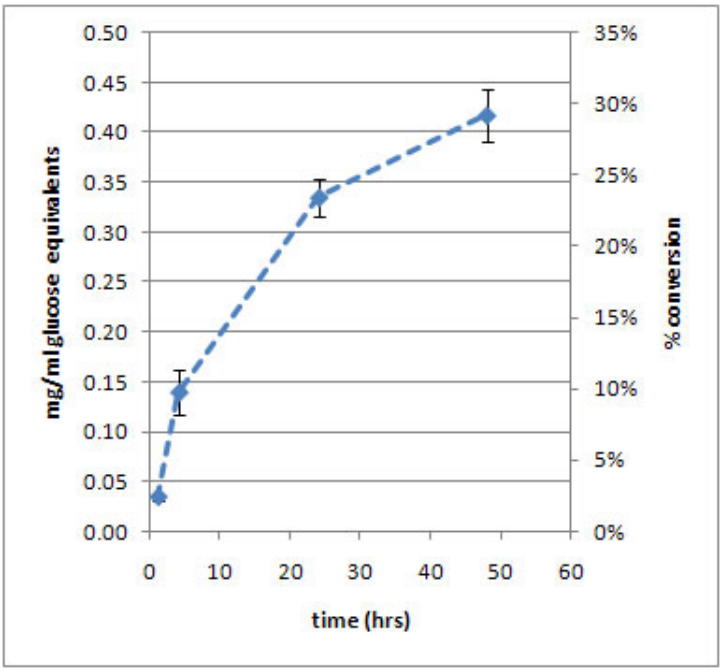

Figure B.4: Coaxial ESC/PAN hydrolysis by *T. fusca* Cel5A. Conversion of coaxial ESC (4 mg/ml) to soluble products with a total of 1 μM Cel5A present at 50 °C

X-ray diffraction analysis indicated that more PAN was exposed after hydrolysis, as the PAN peak at $2\theta \approx 16.8°$ became stronger after 48 hrs of hydrolysis (Figure B.5). The X-ray diffraction pattern of the substrate blank (ESC in buffer with no enzyme added) showed a PAN peak similar to the as-spun fibers, indicating that enzyme activity was the cause of the more prominent PAN peak.

SEM analysis of the fibers after 48 hrs of hydrolysis showed interesting ev-

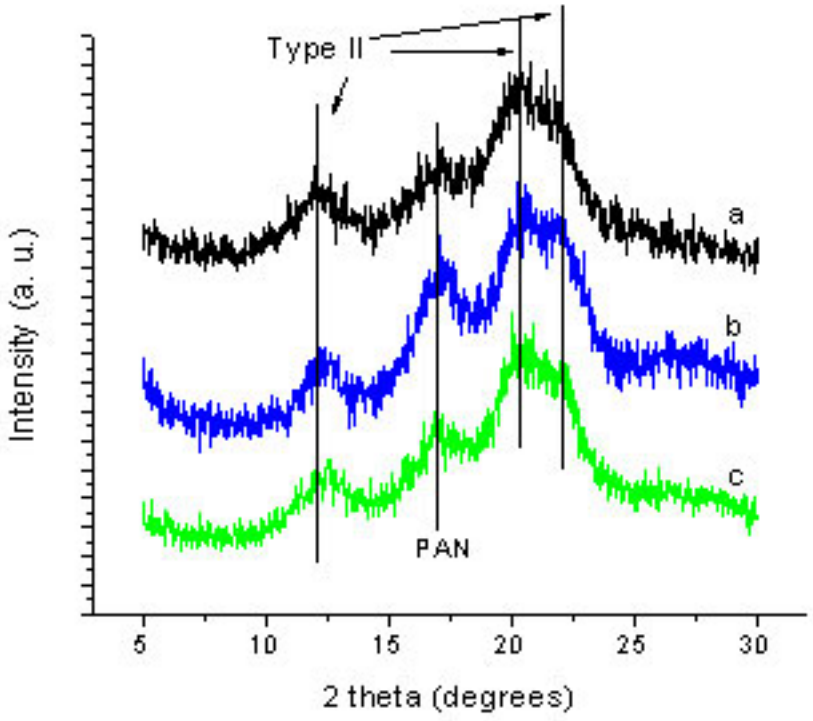

Figure B.5: X-ray diffraction patterns for hydrolyzed cellulose-PAN fibers: (a) as-spun (before hydrolysis); (b) after 48 hrs of hydrolysis; (c) substrate blank after 48 hrs

idence of enzymatic activity that was not seen with either monoaxial fibers or coaxial cellulose-CA fibers. Average fiber diameters did not decrease significantly, as the as-spun fibers had an average diameter of 0.65 ± 0.35 μm and the fibers after 48 hrs of hydrolysis had an average diameter of 0.55 ± 0.29 μm. However, SEM analysis revealed some fiber peeling, and there was some evidence of the fibers being stripped of the cellulose shell in certain regions (Figure B.6). Figure B.7(a) - (c)are particularly intriguing, as they appear to show an area of fiber where the cellulose shell has been removed along a certain portion of the fiber. Figure B.7(b) shows the shell as being unattached from the core, suggesting that the boundary between the cellulose shell and PAN core is sharp as might be

expected from coaxial electrospinning of two immiscible fluids [66, 68]. Figure B.7(d) - (g) show other examples of evidence for cellulase activity, such as the thinning (Figure B.7(d)) and peeling (Figure B.7(e) - (g)) of the fibers. As the remaining insoluble fractions for the earlier hydrolysis times were not kept, the evolution of fibers over the course of hydrolysis has not been documented, but it would be useful to observe the evolution of the fiber morphology with hydrolysis to draw some conclusions about the kinetics of these morphological changes. These images show that coaxial ESC will retain long-range fiber connectivity over the course of hydrolysis, and there is potential for an in-depth hydrolysis study with cellulose-PAN coaxial fibers to reveal new insights into how *T. fusca* Cel5A degrades ESC.

B.4 Conclusions

Coaxial ESC shows potential to be used as a model substrate for enzymatic hydrolysis. Although coaxial ESC made from low DP cellulose/LiCl/DMAc and cellulose acetate/DMAc/acetone solutions did not have any detectable soluble sugar production, SEM analysis revealed fiber pitting that was not seen with monoaxial fibers. It is possible that higher DP cellulose in LiCl/DMAc solutions will be able to make a thicker and more uniform cellulose shell in coaxial fibers, as these solutions will electrospin monaxially. This possibility should be addressed in future studies.

Figure B.6: SEM images of hydrolyzed cellulose-PAN fibers after 48 hrs: (a) evidence of a portion of fiber stripped of cellulose, boxed inserts shown in (b) and (c); (d) areas of fiber thinning; (e), (f), and (g) fiber peeling and surface roughening

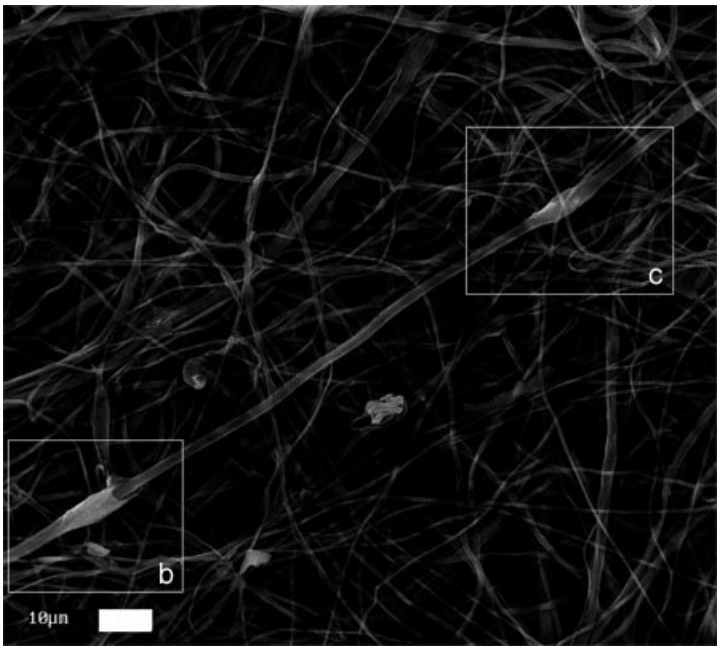

(a)

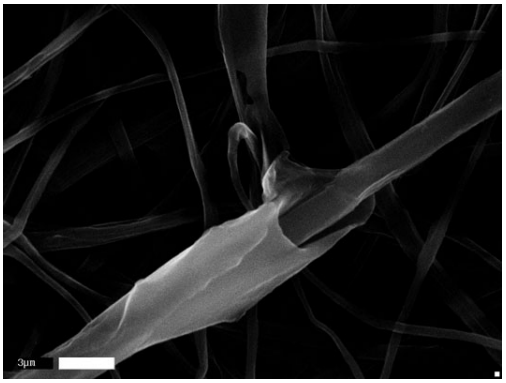

(b)

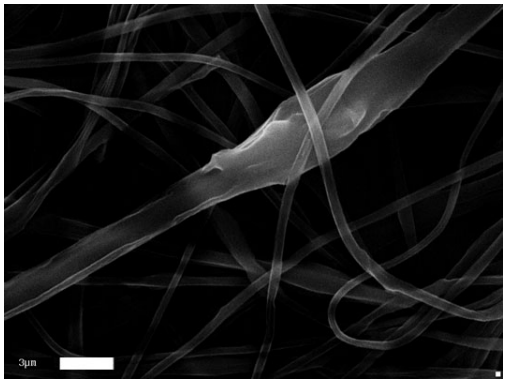

(c)

Figure B.6: (continued)

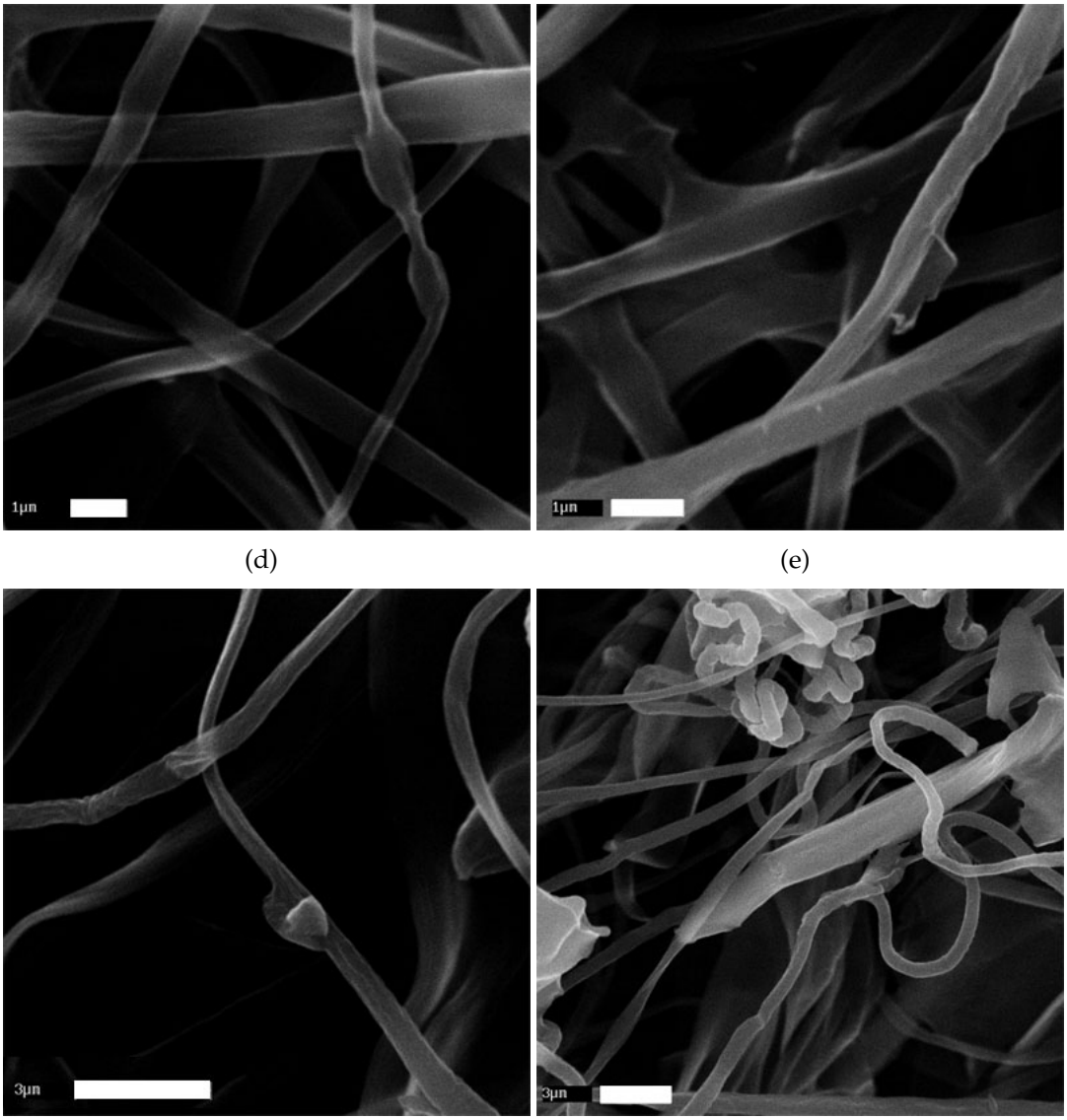

(d) (e)

(f) (g)

Coaxial ESC made from low DP cellulose/NMMO/water and PAN/DMF solutions produced reasonable conversion curves, and SEM analysis showed fiber thinning and peeling/stripping that was not seen in previous hydrolysis studies. These fibers also retained long-range fiber connectivity that was not preserved in monoaxial ESC hydrolysis. Coaxial ESC may be able to show how the cellulose microstructure (degree of polymerization, degree of crystallinity, and surface area) affects the macroscopic degradation of cellulose by revealing variations in rates and extents of fiber thinning and peeling/stripping if the evolution of the fiber morphology is recorded with the extent of hydrolysis. This will require being able to extend the work in varying the microstructure of monoaxial cellulose fibers to coaxial cellulose fibers, and will require production of ESC with distinctly different microstructural features. While the challenges to achieving this are many, the work presented here shows the potential for ESC to be useful as a new model substrate for cellulose hydrolysis.

REFERENCES

[1] L.R. Lynd, C.E. Wyman, and T.U. Gerngross. Biocommodity engineering. *Biotechnology Progress*, 15(5):777–793, 1999.

[2] P. McKendry. Energy production from biomass (part 1): Overview of biomass. *Bioresource Technology*, 83(1):37–46, 2002.

[3] Y-H.P. Zhang and L.R. Lynd. Toward an aggregated understanding of enzymatic hydrolysis of cellulose: Noncomplexed cellulase systems. *Biotechnology and Bioengineering*, 88(7):797–824, 2004.

[4] R Hammerschlag. Ethanol's energy return on investment: A survey of the literature 1990–Present. *Environmental Science and Technology*, 40(6):1744–1750, 2006.

[5] P. McKendry. Energy production from biomass (part 2): Conversion technologies. *Bioresource Technology*, 83(1):47–54, 2002.

[6] D. Pimentel and T.W. Patzek. Ethanol Production Using Corn, Switchgrass, and Wood; Biodiesel Production Using Soybean and Sunflower. *Natural Resources Research*, 14(1):65–76, 2005.

[7] J. Sheehan, A. Aden, K. Paustian, K. Killian, J. Brenner, M. Walsh, and R. Nelson. Energy and environmental aspects of using corn stover for fuel ethanol. *Journal of Industrial Ecology*, 7(3–4):117–146, 2004.

[8] A.O. Converse. Substrate Factors Limiting Enzymatic Hydrolysis. In J.N. Saddler, editor, *Bioconversion of forest and agricultural plant residues*, pages 93–106. CAB International, Wallingford, Oxon, U.K., 1993.

[9] L.T. Fan, Y-H. Lee, and D.R Beardmore. The influence of major structural features of cellulose on rate of enzymatic hydrolysis. *Biotechnology and Bioengineering*, 23(2):419–424, 1981.

[10] S.D. Mansfield, C. Mooney, and J.N. Saddler. Substrate and enzyme characteristics that limit cellulose hydrolysis. *Biotechnology Progress*, 15(5):804–816, 1999.

[11] V.P. Puri. Effect of crystallinity and degree of polymerization of cellulose on enzymatic saccharification. *Biotechnology and Bioengineering*, 26(10):1219–1222, 1984.

[12] L.P. Ramos, M.M. Nazhad, and J.N. Saddler. Effect of enzymatic hydrolysis on the morphology and fine structure of pretreated cellulosic residues. *Enzyme and Microbial Technology*, 15(10):821–831, 1993.

[13] E.T. Reese, L. Segal, and V.W. Tripp. The Effect of Cellulase on the Degree of Polymerization of Cellulose and Hydrocellulose. *Textile Research Journal*, 27(8):626–632, 1957.

[14] D.B. Rivers and G.H. Emert. Factors affecting the enzymatic hydrolysis of municipal-solid-waste components. *Biotechnology and Bioengineering*, 31(3): 278–281, 1988.

[15] T. Sasaki, T. Tanaka, N. Nanbu, Y. Sato, and K. Kainuma. Correlation between X-ray diffraction measurements of cellulose crystalline structure and the susceptibility to microbial cellulase. *Biotechnology and Bioengineering*, 21 (6):1031–1042, 1979.

[16] C.S. Walseth. The Influence of the Fine Structure of Cellulose on the Action of Cellulases. *TAPPI*, 35(5):233–238, 1952.

[17] N.S. Mosier, P. Hall, C.M. Ladisch, and M.R. Ladisch. Reaction Kinetics, Molecular Action, and Mechanisms of Cellulolytic Proteins. In *Recent Progress in Bioconversion of Lignocellulosics*, volume 65 of *Advances in Biochemical Engineering/Biotechnology*, pages 23–40. Springer Berlin / Heidelberg, 1999.

[18] M. Spezio, D.B. Wilson, and P.A. Karplus. Crystal structure of the catalytic domain of a thermophilic endocellulase. *Biochemistry*, 32(38):9906–9916, 1993.

[19] J-Y. Zou, G.J. Kleywegt, J. Ståhlberg, H. Driguez, W. Nerinckx, M. Claeyssens, A. Koivula, T.T. Teeri, and T.A. Jones. Crystallographic evidence for substrate ring distortion and protein conformational changes during catalysis in cellobiohydrolase Ce16A from Trichoderma reesei. *Structure*, 7(9):1035–1045, 1999.

[20] L.T. Fan, Y-H. Lee, and D.H. Beardmore. Mechanism of the enzymatic hydrolysis of cellulose: Effects of major structural features of cellulose on enzymatic hydrolysis. *Biotechnology and Bioengineering*, 22(1):177–199, 1980.

[21] T. Ghose. Cellulase biosynthesis and hydrolysis of cellulosic substances. *Advances in Biochemical Engineering*, 6:39–76, 1977.

[22] M. Chang, T. Chou, and G. Tsao. Structure, pretreatment and hydrolysis of cellulose. *Bioenergy*, pages 15–42, 1981.

[23] E.B. Cowling and W. Brown. Structural Features of Cellulosic Materials in Relation to Enzymatic Hydrolysis. In G.J. Hajny and E.T. Reese, editors, *Cellulases and Their Applications. A symposium sponsored by the Division of Cellulose, Wood, and Fiber Chemistry at the 156th meeting of the American*

Chemical Society, Atlantic City, N.J., pages 152–187, Washington, Sept. 11-12, 1968 1969.

[24] C. Divne, J. Stahlberg, T. Reinikainen, L. Ruohonen, G. Pettersson, J.K. Knowles, T.T. Teeri, and T.A. Jones. The three-dimensional crystal structure of the catalytic core of cellobiohydrolase I from Trichoderma reesei. *Science*, 265(5171):524–528, 1994.

[25] H.E. Grethlein, D.C. Allen, and A.O. Converse. A comparative study of the enzymatic hydrolysis of acid-pretreated white pine and mixed hardwood. *Biotechnology and Bioengineering*, 26(12):1498–1505, 1984.

[26] D.N. Thompson, H-C. Chen, and H.E. Grethlein. Comparison of pretreatment methods on the basis of available surface area. *Bioresource Technology*, 39(2):155–163, 1992.

[27] J.G. Shewale and J.C. Sadana. Enzymatic hydrolysis of cellulosic materials by Sclerotium rolfsii culture filtrate for sugar production. *Canadian Journal of Microbiology*, 25:773–783, 1979.

[28] Y. Akishima, A. Isogai, S. Kuga, F. Onabe, and M. Usada. Kinetic studies on enzymatic hydrolysis of celluloses for evaluation of amorphous structures. *Carbohydrate Polymers*, 19(1):11–15, 1992.

[29] A.R. Esteghlalian, M. Bilodeau, S.D. Mansfield, and J.N. Saddler. Do enzymatic hydrolyzability and simons' stain reflect the changes in the accessibility of lignocellulosic substrates to cellulase enzymes? *Biotechnology Progress*, 17(6):1049–1054, 2001.

[30] S. Park, R.A. Venditti, H. Jameel, and J.J. Pawlak. 2006.

[31] S.D. Mansfield and R. Meder. Cellulose hydrolysis-the role of monocomponent cellulases in crystalline cellulose degradation. *Cellulose*, 10(2):159–169, 2003.

[32] H. Fong and D.H Reneker. Electrospinning and the formation of nanofibers. In D.R. Salem, editor, *Structure Formation of Polymeric Fibers*, chapter 6, pages 225–246. Hanser Gardner Publications, Munich: Hanser; Cincinatti, 2001.

[33] S. Ramakrishna, K. Fujihara, W-E. Teo, T-C. Lim, and Z. Ma. *An Introduction to Electrospinning and Nanofibers*, page 382. World Scientific Publishing Co, Pte. Ltd., Singapore, 2005.

[34] T. Subbiah, G.S. Bhat, R.W. Tock, S. Parameswaran, and S.S. Ramkumar. Electrospinning of nanofibers. *Journal of Applied Polymer Science*, 96(2):557–69, 2005.

[35] A. Formhals. Process and apparatus for preparing artificial threads, October 2 1934. United States patent 1975504.

[36] C-W. Kim. Preparation of cellulose and oxidized cellulose via electrospinning. Master's thesis, Cornell University, 2006.

[37] J.T. McCann, D. Li, and Y. Xia. Electrospinning core-sheath, hollow, porous and surface-functionalized nanofibers as aligned arrays and utile architectures. In *Joint INDA-TAPPI Conference - INTC 2005: International Nonwovens Technical Conference*, pages 567–571, Cary, NC 27512, United States, 2005. Association Nonwoven Fabrics Industry. St. Louis, MO, United States.

[38] J.T. McCann, M. Marquez, and Y. Xia. Melt coaxial electrospinning: A ver-

satile method for the encapsulation of solid materials and fabrication of phase change nanofibers. *Nano Letters*, 6(12):2868–2872, 2006.

[39] S.N. Reznik, A.L. Yarin, E. Zussman, and L. Bercovici. Evolution of a compound droplet attached to a core-shell nozzle under the action of a strong electric field. *Physics of Fluids*, 18(6):062101, 2006.

[40] A.L. Yarin, E. Zussman, J.H. Wendorff, and A. Greiner. Material encapsulation and transport in core-shell micro/nanofibers, polymer and carbon nanotubes and micro/nanochannels. *Journal of Materials Chemistry*, 17(25): 2585–2599, 2007.

[41] J.A. Cuculo, N. Aminuddin, and M.W. Frey. Solvent spun cellulose fibers. In D.R. Salem, editor, *Structure Formation in Polymeric Fibers*, chapter 8, pages 296–327. Hans Gardner Publications, Munich: Hanser; Cincinatti, 2001.

[42] D. Klemm, H-P. Schmauder, and T. Heinze. Cellulose. In E.J. Vandamme, A. De Baets, and A. Steinb´uchel, editors, *Polysaccharides II*, volume 6 of *Biopolymers*, chapter 10, pages 275–319. Wiley-VCH, Inc., Weinheim, 2001. Series Editor: A. Steinb´uchel.

[43] D. Dollimore and B. Holt. Thermal degradation of cellulose in nitrogen. *Journal of Polymer Science: Polymer Physics Edition*, 11(9):1703–1711, 1973.

[44] A. Frenot, M.W. Henriksson, and P. Walkenstrom. Electrospinning of cellulose-based nanofibers. *Journal of Applied Polymer Science*, 103(3):1473–1482, 2007.

[45] C-W. Kim, M.W. Frey, M. Marquez, and Y.L. Joo. Preparation of submicron-

scale, electrospun cellulose fibers via direct dissolution. *Journal of Polymer Science, Part B: Polymer Physics*, 43(13):1673–1683, 2005.

[46] C-W. Kim, D-S. Kim, S-Y. Kang, M. Marquez, and Y.L. Joo. Structural studies of electrospun cellulose nanofibers. *Polymer*, 47(14):5097–5107, 2006.

[47] P. Kulpinski. Cellulose nanofibers prepared by the N-methylmorpholine-N-oxide method. *Journal of Applied Polymer Science*, 98(4):1855–1859, 2005.

[48] S. Chrapava, D. Touraud, T. Rosenau, A. Potthast, and W. Kunz. The investigation of the influence of water and temperature on the LiCl/DMAc/cellulose system. *Physical Chemistry Chemical Physics*, 5(9): 1842–1847, 2003.

[49] Dupont A-L. Cellulose in lithium chloride/N,N-dimethylacetamide, optimisation of a dissolution method using paper substrates and stability of the solutions. *Polymer*, 44(15):4117–4126, 2003.

[50] W. Gindl, T. Schoberl, and J. Keckes. Structure and properties of a pulp fibre-reinforced composite with regenerated cellulose matrix. *Applied Physics A: Materials Science and Processing*, 83(1):19–22, 2006.

[51] T. Matsumoto, D. Tatsumi, N. Tamai, and T. Takaki. Solution properties of celluloses from different biological origins in LiCl - DMAc. *Cellulose*, 8(4): 275–282, 2002.

[52] T. Rosenau, A. Potthast, A. Hofinger, H. Sixta, and P. Kosma. Hydrolytic processes and condensation reactions in the cellulose solvent system n,n-dimethylacetamide/lithium chloride. part 1. *Holzforschung*, 55(6):661–666, 2001.

[53] A. Potthast, T. Rosenau, J. Sartori, H. Sixta, and P. Kosma. Hydrolytic processes and condensation reactions in the cellulose solvent system n,n-dimethylacetamide/lithium chloride. part 2: Degradation of cellulose. *Polymer*, 44(1):7–17, 2003.

[54] H. Chanzy, S. Nawrot, A. Peguy, P. Smith, and J. Chevalier. Phase behavior of the quasiternary system N-methylmorpholine-N-oxide, water, and cellulose. *Journal of Polymer Science: Polymer Physics Edition*, 20(10):1909–1924, 1982.

[55] O. Biganska and P Navard. Kinetics of precipitation of cellulose from cellulose-NMMO-water solutions. *Biomacromolecules*, 6(4):1948–1953, 2005.

[56] C. Cuissinat and P. Navard. Swelling and dissolution of cellulose. Part 1. Free floating cotton and wood fibres in N-methylmorpholine-N-oxide-water mixtures. In *New Cellulose Products and Composites*, pages 1–18, Wiesbaden, Germany, 2006. Wiley.

[57] D.B. Kim, S.M. Jo, W.S. Lee, and J.J. Pak. Physical agglomeration behavior in preparation of cellulose-N-methyl morpholine N-oxide hydrate solutions by simple mixing. *Journal of Applied Polymer Science*, 93(4):1687–1697, 2004.

[58] ASTM Standard D4242. "Standard Test Method for Measurement of Average Viscometric Degree of Polymerization of New and Aged Electrical Papers and Boards". ASTM International, West Conshohocken, PA, 1999. www.astm.org.

[59] O. Biganska, P. Navard, and O Bedue. Crystallisation of cellulose/n-

methylmorpholine-n-oxide hydrate solutions. *Polymer*, 43(23):6139–6145, 2002.

[60] A. Ziabicki. *Fundamentals of fibre formation : the science of fibre spinning and drawing*. Wiley, London ; New York, 1976.

[61] B.K. Barr. *Hydrolysis, specificity and active-site binding of glycosides by Thermomonospora fusca cellulases.* PhD thesis, Cornell University, Ithaca, NY, 1997.

[62] L.P. Walker, D.B. Wilson, D.C. Irvin, C. McQuire, and M. Price. Fragmentation of cellulose by the major Thermomonospora fusca cellulases, Trichoderma reesei CBHI, and their mixtures. *Biotechnology and Bioengineering*, 40 (9):1019–1026, 1992.

[63] K.M. Kleman-Leyer, N.R. Gilkes, R.C. Miller, and T.K. Kirk. Changes in the molecular-size distribution of insoluble celluloses by the action of recombinant Cellulomonas fimi cellulases. *The Biochemical Journal*, 302(2):463–469, 1994.

[64] A.V. Bazilevsky, A.L. Yarin, and C.M. Megaridis. Co-electrospinning of core-shell fibers using a single-nozzle technique. *Langmuir*, 23(5):2311–2314, 2007.

[65] J.E. Díaz, A. Barrero, M. Márquez, and I.G. Loscertales. Controlled encapsulation of hydrophobic liquids in hydrophilic polymer nanofibers by co-electrospinning. *Advanced Functional Materials*, 16(16):2110–2116, 2006.

[66] D. Li and Y. Xia. Direct fabrication of composite and ceramic hollow nanofibers by electrospinning. *Nano Letters*, 4(5):933–938, 2004.

[67] Z. Sun, E. Zussman, A.L. Yarin, J.H. Wendorff, and A. Greiner. Compound core-shell polymer nanofibers by co-electrospinning. *Advanced Materials*, 15(22):1929–1932, 2003.

[68] I.G. Loscertales, A. Barrero, M. Marquez, R. Spretz, R. Velarde-Ortiz, and G. Larsen. Electrically forced coaxial nanojets for one-step hollow nanofiber design. *Journal of the American Chemical Society*, 126(17):5376–5377, 2004.

[69] H. Jiang, Y. Hu, Y. Li, P. Zhao, K. Zhu, and W. Chen. A facile technique to prepare biodegradable coaxial electrospun nanofibers for controlled release of bioactive agents. *Journal of Controlled Release*, 108(2–3):237–243, 2005.

[70] T. Song, Y. Zhang, T. Zhou, C.T. Lim, S. Ramakrishna, and B. Liu. Encapsulation of self-assembled fept magnetic nanoparticles in pcl nanofibers by coaxial electrospinning. *Chemical Physics Letters*, 415(4–6):317–322, 2005.

[71] H. Liu and Y-L. Hsieh. Ultrafine fibrous cellulose membranes from electrospinning of cellulose acetate. *Journal of Polymer Science Part B: Polymer Physics*, 40(18):2119–2129, 2002.

[72] G. Eda, J. Liu, and S. Shivkumar. Solvent effects on jet evolution during electrospinning of semi-dilute polystyrene solutions. *European Polymer Journal*, 43(4):1154–1167, 2007.

[73] D. Li, M.W. Frey, and A.J. Baeumner. Electrospun polylactic acid nanofiber membranes as substrates for biosensor assemblies. *Journal of Membrane Science*, 279(1–2):354–363, 2006.

[74] D. Li, M.W. Frey, D. Vynias, and A.J. Baeumner. Availability of biotin incorporated in electrospun pla fibers for streptavidin binding. *Polymer*, 48 (21):6340–6347, 2007.

[75] C. Wang, H-S. Chien, C-H. Hsu, Y-C. Wang, C-T. Wang, and H-A. Lu. Electrospinning of polyacrylonitrile solutions at elevated temperatures. *Macromolecules*, 40(22):7973–7983, 2007.

[76] H. Jung, D.B. Wilson, and L.P. Walker. Binding of Thermobifida fusca CDCel5A, CDCel6B and CDCel48A to easily hydrolysable and recalcitrant cellulose fractions on BMCC. *Enzyme and Microbial Technology*, 31(7):941–948, 2002.

[77] Jung. H., D.B. Wilson, and L.P. Walker. Binding and reversibility of Thermobifida fusca Cel5A, Cel6B, and Cel48A and their respective catalytic domains to bacterial microcrystalline cellulose. *Biotechnology and Bioengineering*, 84(2):151–159, 2003.

[78] D.C. Irwin, M. Spezio, L.P. Walker, and D.B. Wilson. Activity studies of eight purified cellulases: Specificity, synergism, and binding domain effects. *Biotechnology and Bioengineering*, 42(8):1002–1013, 1993.

[79] D.B. Wilson. Cellulases of Thermomonospora fusca. In A.W. Willis and S.T. Kellogg, editors, *Biomass Part A: Cellulose and Hemicellulose*, pages 314–323. Academic Press, 1988.

[80] D.C Irwin, M. Cheng, B. Xiang, J.K.C. Rose, and D.B. Wilson. Cloning, expression and characterization of a family-74 xyloglucanase from Thermobifida fusca. *European Journal of Biochemistry*, 270(14):3083–3091, 2003.

[81] D.B. Wilson. Studies of Thermobifida fusca plant cell wall degrading enzymes. *The Chemical Record*, 4(2):72–82, 2004.

[82] C. Sun. True density of microcrystalline cellulose. *Journal of Pharmaceutical Sciences*, 94(10):2132–2134, 2005.